2015-07-30

Steam Injection Strategies for Bitumen Recovery from an Element of the Grosmont Carbonate Reservoir

Song, Qiuyue

UNIVERSITY OF CALGARY

Steam Injection Strategies for Bitumen Recovery from an Element of the Grosmont Carbonate Reservoir

by

Qiuyue Song

A THESIS

SUBMITTED TO THE FACULTY OF GRADUATE STUDIES

IN PARTIAL FULFILMENT OF THE REQUIREMENTS FOR THE

DEGREE OF MASTER OF SCIENCE

GRADUATE PROGRAM IN CHEMICAL AND PETROLEUM ENGINEERING

CALGARY, ALBERTA

JULY, 2015

Abstract

The bitumen resource in the Grosmont carbonate deposits in Alberta is over 400 billion barrels, but hitherto a commercial recovery scheme remains elusive. This study employs numerical simulation for several steam-based recovery schemes and proposes steam injection strategies. Selected simulation results were analyzed using analytical methods.

A representative geological model of Grosmont was used to examine numerically several steam injection schemes, which included: vertical or horizontal well cyclic, SAGD, and conventional pattern steamfloods. Steamflooding, using vertical steam injectors and a horizontal producer, is proposed for the Grosmont carbonate reservoir to overcome shortcomings of other schemes.

The vertical well injector-horizontal well producer steamflood gave the same recovery performance 21 months earlier than the horizontal well cyclic. Analytical methods were used to interpret physical mechanisms operating in steam injection processes for this reservoir, including the steam over-injection, steam override, condensate formation at the steam front and water flashing.

Acknowledgements

I would like to convey my deepest gratitude to my supervisor Dr. Zhangxing (John) Chen and co-supervisor Dr. S. M. Farouq Ali for their excellent guidance, insightful advice and continued support.

I am thankful to Dr. Sudarshan A. Mehta, Dr. Hemanta Sarma and Dr. Ron Chik-Kwong Wong for serving on my examining committee.

I gratefully acknowledge the generous donation of the Grosmont elemental model by Osum Oil Sands Corporation for the specific use in this work. In particular, I wish to thank Dr. Qi Jiang, Dr. Jian-Yang Yuan, Dr. Jen Russel-Houston, Ms. Kelli Fraser and Ms. Jinxiu Qi for their time and valuable suggestions.

I appreciate Computer Modelling Group Ltd. (CMG) for providing the CMG software package for this study.

Last but not least, I would like to thank my friends in the University of Calgary and the Reservoir Simulation Group.

Dedication

I dedicate this work to my parents for their unconditional love.

Table of Contents

List of Tables

List of Figures and Illustrations

Nomenclature

Notations

a, b, or x	arbitrary independent variables
A	area of the top of the simulation model, m^2
A_n, (n=1, 2, 3, …)	area of the steam zone at time t_n during a steam-injection oil recovery process, m^2
A(t)	area of the steam zone at time t during a steam-injection oil recovery process, m^2
$\bar{A}(s)$	transformed format of A(s) through Laplace transfer
$\bar{A}(t)$	transformed format of A(t) through Laplace transfer
ΔA_n (n=1, 2, 3, …)	incremental area of the steam zone formed during time interval t_{i-1} to t_i, m^2
c_w	specific heat of water, kJ/kg·°C
erf	error function
erfc	complementary error function
f_{st}	steam quality, mass %
f(t)	the function giving the heat loss per unit time per unit area, $kJ/s \cdot m^2$
$\bar{f}(s)$	transformed format of f(s) through Laplace transfer
$\bar{g}(s)$	transformed format of g(s) through Laplace transfer
h	formation thickness, m
$H_{L,ML}$ (t)	cumulative heat loss at time t of the steam injection oil recovery process, calculated based on the Marx-Langenheim equation, kJ
$H_{L,s}$ (t)	cumulative heat loss at time t of the steam injection oil recovery process, calculated based on the simulation result, kJ
$H_{L,1\text{-}sd}$ (t)	cumulative heat loss at time t of the steam injection oil recovery process, calculated based on the one-sided heat loss equation derived in this study, kJ

h_w	enthalpy of saturated water, kJ/kg
i_{st}	steam injection rate, kg/s
i'_{st}	steam injection rate supplying latent heat to offset the heat loss from only the formation top (or bottom), kg/s
i^*_{st}	steam injection rate supplying latent heat to offset the heat loss from only the formation top (or bottom) used in simulation considering the formation heterogeneity, kg/s
$\bar{i}_{st}$ (n=1, 2, 3, …)	average steam injection rate during time interval t_{n-1} to t_n, kg/s
k_{hob}	thermal conductivity of the overburden and underburden rocks, $kW/m^3 \cdot °C$
L_v	latent heat of steam, kJ/kg
M_{ob}	heat capacity of the overburden and underburden rocks, $kJ/m^3 \cdot °C$
M_s	heat capacity of the reservoir rock, $kJ/m^3 \cdot °C$
$M_{w,st}$	molecular weight of steam, 18 g/mole
M_v	molecular volume of gas
$\Delta N_{p,n}$	oil production from time interval t_{n-1} to t_n, m^3
P_{bh}	producer bottomhole pressure, kPa
p_s	steam saturation pressure, kPa
q	heat loss rate from only the formation top (or bottom), kJ/s
q_{st}	steam production rate, kg/day
q'_{st}	volumetric steam production rate, m^3/day
$\bar{Q}_{i,n}$	average heat injection rate, kJ/s
Q_{loss} (t)	cumulative heat loss as a function of the cumulative heat injected at time t, calculated based on the simulation result, %
$Q_{loss, ML}$ (t)	cumulative heat loss as a function of the cumulative heat injected at time t, calculated based on Marx-Langenheim equation, %
$Q_{loss, 1\text{-}sd}$ (t)	cumulative heat loss as a function of the cumulative heat injected at time t, calculated based on the one-sided heat loss equation derived in this study, %

s	Laplacian operator
S_{oi}	Initial oil saturation, vol.%
$S_{orst,n}$ (n=1, 2, 3, …)	residual oil saturation of ΔV_{sn}, vol.%
t_c	critical time, s
t_D	dimensionless time
t_{Dc}	dimensionless critical time
t, or t_n (n=1,2,3,…)	time, s
T(y, t), or T	temperature of a certain point in the overburden y m to the formation top at time t
$\overline{T}(y,s)$, or $\overline{T}$	transformed format of T(y, t), or T through Laplace transfer
T_r	initial reservoir temperature, °C
T_{bh}	producer bottomhole temperature, °C
T_s	steam saturation temperature, °C
u	a time interval of a steam-injection oil recovery process during which the incremental steam zone area ΔA is formed, s
V_g	gas production rate, m^3/day
V_s	steam specific volume, m^3/kg
V_{sn} (n=1, 2, 3, …)	steam zone volume formed at time ti of a steam-injection oil recovery process, m^3
ΔV_{sn} (n=1, 2, 3, …)	incremental steam zone volume, formed during time interval t_{i-1} to t_i, m^3
y	distance from a certain point in the overburden to the formation top, m

Greek Symbols

ϕ	formation porosity, fraction
α	thermal diffusivity of the overburden (or underburden), m^2/s
∞	infinite distance, m
$\mathcal{L}(f(x))$	Laplace transformation of function f(x)

Abbreviation

SOR	steam-oil ratio, m^3/m^3
CSS	cyclic steam stimulation
SAGD	Steam assisted gravity drainage
VWCSS	vertical well cyclic steam stimulation
HWCSS	horizontal well cyclic steam stimulation
VWinj-HWprod	vertical well injector-horizontal well producer steamflood

Unit

cP	centiPoise
kJ	kiloJoules
D	Darcy
mD	milliDarcy
kPa	kiloPascal

Chapter 1: INTRODUCTION

As of April 2015, production from the oil sands of Alberta (1,670 billion barrels in place) was 1.4 million barrels/day by in situ recovery methods, over 1.2 million barrels/day by mining, and increasing. Another large bitumen resource (over 400 billion barrels) is locked in the Grosmont carbonate. During the past 40 years, several small field pilots have been carried out, but there is still no commercial project. At least one pilot is currently in operation, and more are planned.

Bitumen recovery from the Grosmont carbonate is more complex than from the oil sands, because of the extremely heterogeneous nature of the karstified dolomite, consisting of fractures, vugs, caverns, and sinkholes, and also because the bitumen viscosity is much higher (1 to 10 million cP) than in the oil sands. High water saturation zones may occur at the base, top, and the middle of the formation.

Given that viscosity reduction is the key to bitumen recovery, and steam is the best heating agent, important questions are: how to deliver the heat more evenly under the context of the high formation heterogeneity and a complex fracture system, with minimal migration into water sands, and how to capture the mobilized bitumen. The present study is a step in that direction.

A geological model of Buffalo Creek region is utilized in this work to investigate injection-production schemes for cyclic steam stimulation, SAGD, and steamfloods. The model can be looked upon as a microcosm of Grosmont, as it contains all the dominant geological features of

this reservoir. Specifically, steam injection schemes are examined for several steamflood patterns, after which a combination of vertical injectors and a horizontal producer is proposed. Within this framework, strategies for performance optimization were developed, primarily to increase the bitumen recovery factor and reduce the steam-oil ratio.

Combinations of vertical injector(s) and a horizontal producer offer the greatest flexibility in a complex geology for delivering heat and capturing the bitumen. Performance improvements are possible via well placement, steam injection rate changes, and perforated interval control in both the injectors and the producers. A few of these parameters were examined in this study.

Chapter 2: LITERATURE REVIEW

2.1 Geology of the Grosmont Formation

The Upper Devonian Grosmont Carbonate Formation covers a 500 km long×150 km wide region within the "carbonate triangle" of northern Alberta. As shown in Figs. 2.1.1 and 2.1.2, the Grosmont Formation is situated east of the Peace River oil sands and unconformably underneath the western part of the Athabasca oil sand deposit (Buschkuehle et al. 2007). The shallow marine carbonate strata dip westwards from a depth of less than 200 m under the sub-Cretaceous unconformity in the east to about 1,000 m in the west (Jiang et al. 2010; Buschkuehle et al. 2007). The four members named in the order of decreasing stratigraphic age, Grosmont A, B, C, and D, as shown in Fig. 2.1.2, are separated from each other by marl layers, typically a few metres thick (Edmunds et al. 2009; Jiang et al. 2010). Fractures in the formation are mainly vertical to subvertical (Edmunds et al. 2009, Yuan et al. 2010). Grosmont C and D members contain 80% of the total bitumen in place (Ezeuko et al. 2013) and are mostly dolomitized. Eroded at different locations by caverns and karst zones, the marl layer between Grosmont C and D members has discontinuity at certain locations (Ezeuko et al. 2012; Russel-Houston et al. 2014; Machel et al. 2012). The digenetic history of Grosmont Formation includes recrystallization, fracturing, karstification and biodegradation (Machel et al. 2012). Paleocaves and sinkholes have been found in the Grosmont formation (Russel-Houston et al. 2014).

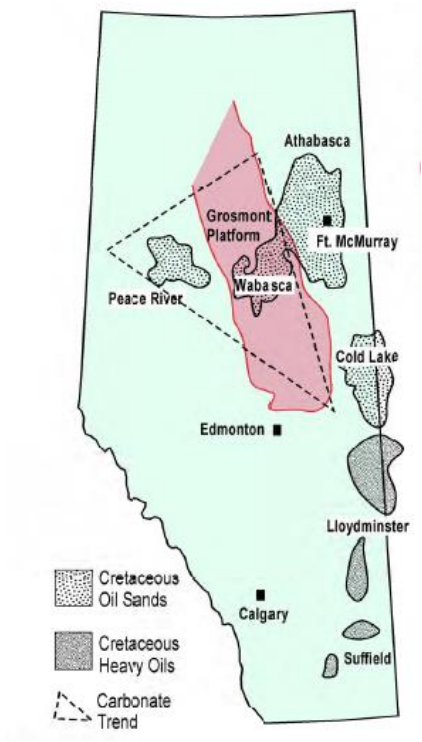

Figure 2.1.1 General map location of Grosmont carbonate bitumen deposit (in white in the diagram), north Alberta, Canada (Alberta Energy & Utilities Board).

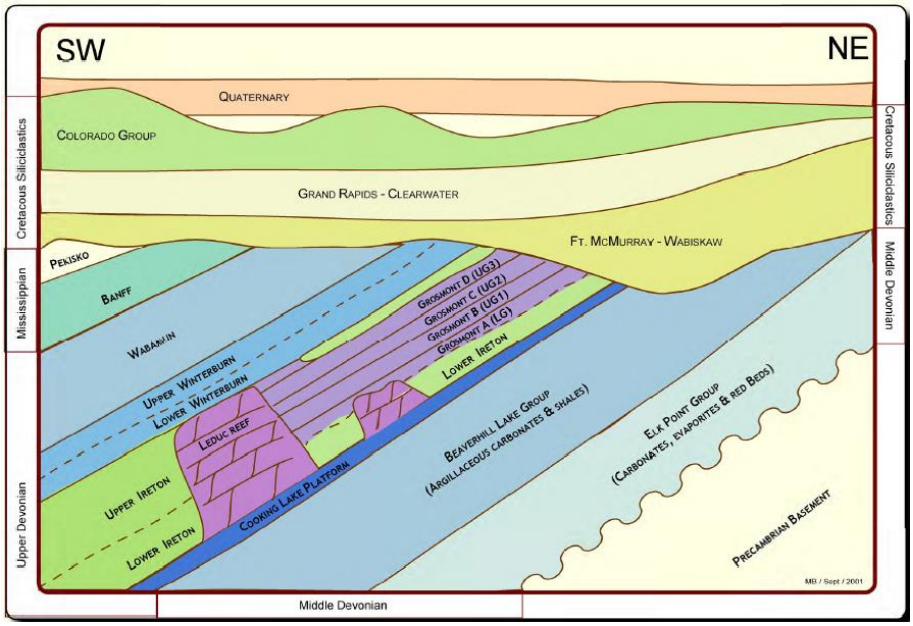

Figure 2.1.2. Stratigraphic nomenclature of Devonian and Cretaceous successions in northern Alberta (Alberta Energy & Utilities Board).

2.2 Petrophysical Properties

Typical values of petrophysical properties of the main bitumen-bearing Grosmont C and D members are listed in the table below.

Table 2.2.1 Typical values of petrophysical properties of the Grosmont C and D members.

	Grosmont C	Grosmont D
Porosity	20%	25%
Initial Oil Saturation	85-95%	
Bitumen Viscosity (cP)	$1\text{-}10\times10^6$	
Wettability	Oil-wet	
Thickness (m)	20	30
Lithology	Both heavily karstified and dolomitized	
Pore Types	Vug Fracture Matrix	Breccia Fracture Matrix

(After Qi et al. 2013, Edmunds et al. 2009, Jiang et al. 2010, Husky 2013, Ezeuko et al. 2013, Yuan et al. 2012, and Qin et al. 2014.)

2.3 Past Oil Recovery Pilots in Grosmont

The first thermal pilot (a single CSS cycle) was conducted in 1975 at Chipewyan River in two wells. At first air was injected, following which steam was injected. Steam injectivity was not a problem, and injection pressures were in the 6-7 MPa range. The steam-oil ratios were very high, and the total water production was much higher than that injected (Yuan et al. 2010; Ezeuko et al. 2012).

In 1977, a CSS thermal pilot was carried out at Buffalo Creek (Phase 1). Considerable volumes of bitumen were produced. It was also determined that steamflooding using vertical well patterns was not a suitable process for this area (Yuan et al. 2010).

Buffalo Creek (Phase 2) was a larger pilot that ran from 1980 to 1986. Twelve cycles were carried out in one well. The fluid injected in the first three cycles was hot water. The performance of these was not acceptable, as the SOR's were high. The steam slug was between 3,500 and 14,000 m^3 (Alvarez 2014). In the remaining cycles, except for one cycle, the SOR's were in the 5.8 to 14 range.

In 1982, encouraged by the response of the Buffalo Creek pilot, the Mclean steamflood pilot was initiated, consisting of a 2.5-acre inverted five-spot pattern. In 1984, two additional wells were drilled to expand the pilot to a 5-acre area. The steam injection well was found to lose steam to the upper zone; therefore, the corner wells were completed to CSS. The steam slug size was 400 to 10,000 m^3. Foam was used in Cycle 9. The pilot was terminated in 1987. The performance was below expectations, with SOR ranging from 5 to 100, confirming the previous conclusion that steamflooding using vertical well patterns was not a suitable process for this reservoir (Hosseininejad et al. 2014, Ezeuko et al. 2012, Alvarez 2014).

In 2010, a horizontal well SAGD and solvent pilot was initiated by Laricina and Osum at Saleski. In view of the observed performance, it was decided to convert the process to cyclic-to-continuous SAGD. In the initial phase, in spite of bullheading, the target temperature of 90℃ between the horizontal injector and producer could not be achieved. The pilot was converted into a combination process, called cyclic-to-continuous SAGD. In this process, the wells were initially steam stimulated, and as the reservoir depletion advanced, well pairs were converted to continuous injection and production (Hosseininejad et al. 2014). The dominant recovery mechanism was said

to be gravity drainage, with thermal expansion and spontaneous imbibition also important (Yang et al. 2014).

Since 2008, Shell has tested a variety of processes in Grosmont, leading to IUP (In Situ Upgrading Process), Hot Wire Test, Heat Injection Test, and Long Heater Test (Clark and Jimenez, 2014).

2.4 Past Modelling and Simulation Work for Grosmont

Novak et al. (2007) constructed a single porosity simulation model for the Buffalo Creek pilot site. Porosity distribution was modeled based on the well log porosity data. Thermal conductivity and heat capacity values were determined according to the reservoir grain density. Constraining the steam injection rate, production liquid rate, initial model injection rate and the steam quality, the model was built to history match the oil production rate and bottomhole temperature of the first five cycles of the pilot. Results showed that the model with one bulk permeability value of 5 Darcies provided similar trend of the oil production rate but not the bottomhole temperature. Heterogeneous permeability distribution had to be introduced to history match the field data.

Cimolai et al. (2010) designed a heavy oil recovery strategy named passive heating assisted recovery method (PHARM) for the layered reservoir. The idea of PHARM is while exploiting one oil-saturated stratum using thermal recovery methods, such as SAGD or in-situ combustion, the adjacent oil-saturated strata separated by a flow barrier can be passively preheated. Oil from the passively heated strata can be recovered either by primary recovery or solvent-assisted processes. This recovery method was simulated in a single porosity, heterogeneous layer cake

Grosmont model. But technical details such as the effect of fractures, property heterogeneity and discontinuity of the marl-layer between Grosmont C and D were not considered.

As reported by Yuan et al. (2010), a facies-based geological model including Grosmont C and D members was built for the Buffalo Creek pilot site. The 11 facies involved in the model were determined based on an analysis of core intervals from 88 wells. According to the lithofacies log, an effective porosity curve, a water saturation curve, the porosity-permeability transform of each facies, and the predictable vertical succession of facies in the carbonate platform, the geological model was built in Petrel^{TM}. From the microresistivity image log data, fractures were identified and recorded using a semi-quantitative method. Five grades of fracture intensity, corresponding to five levels of relative values of fracture porosity and permeability, were defined and assigned to each lithofacies. In the dual porosity/dual permeability dynamic simulation model, fracture porosity and permeability were finally determined through history matching. The model was used to history match the first cycle of the Buffalo Creek pilot. A 2D slice was taken to simulate and test the performance of SAGD.

Another facies-based geological model was built for the Grosmont C member to history match a cyclic steam injection pilot conducted in 2012 by Laricina Energy Ltd. (Qi et al. 2013). Using the routine core analysis, matrix properties were measured incorporating the small-scale vugs, core-scale fractures. The large-scale fractures and vugs that could not be measured by routine coring exercises were assigned as the fracture system. The geological model built in Petrel^{TM} was imported into the CMG STARS dual porosity/dual permeability module to represent the matrix system. Relative values of fracture properties were assigned to each facies and the final values

were determined by history match. Restricted by the long simulation time, a portion of the original 3D was used and the downsized injection rate and boundary wells offsetting the pressure built up were defined proportionally. To match the steam zone growth trend, the fracture parameters needed to be tuned locally.

Based on the cores, well logs, seismic, drilling and geologic data, five pore types were defined for the Grosmont formation: cavern, breccia, vug, fracture and matrix. In the multi-object model built for Grosmont formation, each pore type is treated as an object and is spatially distributed into the 3D geological model using stochastic methods (Ezeuko et al. 2013; Ezeuko and Gates 2013). Available data were used as control limits to reduce the degree of the freedom. In the dynamic simulation model, single porosity modelling is used for the regions where fractures are nonexistent and dual porosity/dual permeability modelling is used for fractured regions. The discontinuity of the marl layer between the Grosmont C and D members is represented with transmissibility. A 2D slice out of the 3D model was used to test and compare the recovery performance of SAGD and CSS.

Chapter 3: STATEMENT OF THE PROBLEM

This study is based on numerical simulations and mathematical analysis of the results obtained for an element of the Grosmont formation. The model includes all of the major features of this reservoir, such as fractures, water zones, highly variable petrophysical properties, high bitumen viscosity, and tight streaks. The principal objectives of this study are as follows:

1. To determine the role of fractures in a general sense — advantages and disadvantages in promoting steam injectivity and oil drainage. Also, to observe the effect of removing the fractures in selected cases.

2. To assess the effect of top water in particular, in the above injection schemes, and suggest ways of reducing steam migration into the water zone.

3. To examine the cyclic steam stimulation process using vertical and horizontal wells, respectively, using a fixed steam slug and cycle length, and to determine the principal production mechanisms.

4. To examine the applicability of steam-assisted gravity drainage (SAGD) in the Grosmont model under study in terms of steam chamber integrity, in addition to oil recovery and the steam-oil ratio.

5. To carry out pattern steamfloods, consisting of five-spot, seven-spot, and nine-spot patterns, to compare them, and to determine the main recovery mechanisms operating in each case.

6. To determine ways of optimizing steamflood performance in selected cases so that steam consumption is reduced, and additional oil is captured.

7. To develop analytical models needed for defining the nature of heat loss, oil saturations ahead of the steam front, steam over-injection, and steam production, with an aim to improve performance.

8. Based on the insight into fluid flow and the drive mechanism gained from the process behaviour of all the steam injection oil recovery processes simulated and analyzed, to propose a steam injection scheme for this formation (which turns out to be steamflooding using vertical steam injectors and a horizontal producer). To assess to what extent this proposed scheme alleviates the problems occurring in the previously simulated steam injection processes.

Chapter 4: GROSMONT ELEMENT MODEL

4.1 Location of the Elemental Model

The numerical simulation model used in this study was donated by Osum Oil Sands Corporation. The model was built to represent the Buffalo Creek pilot site. From 1980 to 1986, a single vertical well cyclic steam stimulation was conducted for the Buffalo Creek pilot (Section 5, Township 88, Range 19, W4M) by UNOCAL (Fig. 4.1.1). The vertical cyclic well was 10A-5 and was completed on Grosmont C member at a depth of 286m (Yuan et al. 2010; Ezeuko et al. 2012). The other four wells are observation wells. Among the ten cycles conducted, cyclic SOR for all cycles was less than 7 m^3/m^3 except Cycles 1 and 6 during which low quality steam or hot water was injected (Yuan et al. 2010; Ezeuko et al. 2012).

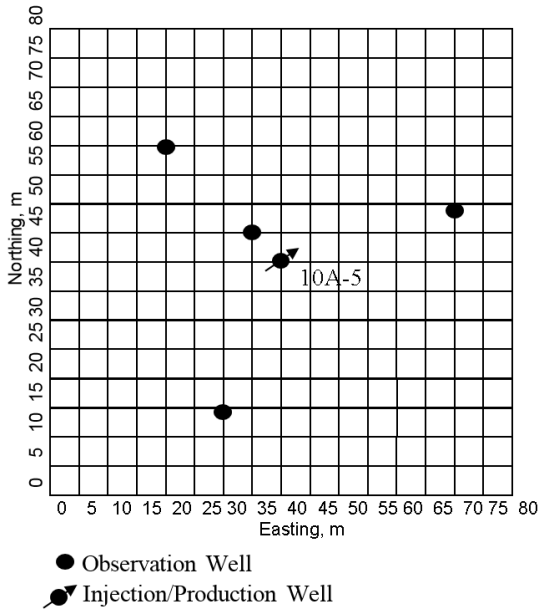

Figure 4.1.1 Buffalo Creek pilot well configuration.

(After Yuan et al. 2010; Novak et al. 2007, and Ezeuko et al. 2012)

4.2 Geological Model

As Yuan et al. (2010) reported, 11 facies were included in the model based on the analysis of core intervals from a total of 88 wells in the study area. Log signatures were also used to define facies contacts for the locations where cores were not available. A facies-based geostatistical model was built in Petrel^{TM} according to the lithofacies log, effective porosity curve, water saturation curve, the porosity-permeability transform of each facies, as well as the predictable vertical succession of facies in the carbonate platform. Five grades of fracture intensity were defined based on the microresistivity image logs and were assigned to each lithofacies. In the dynamic simulation model, values of fracture properties of each grid block were further determined by a history match of the Buffalo Creek pilot field data.

4.3 Numerical Simulation Model

The dynamic simulation model is built on the dual porosity/dual permeability modelling available in CMG STARS. The simulation model contains 29×29×62 (I, J, K) grid blocks. Thus the model covers a 5-acre area. As Yuan et al. (2010) reported, the corner point grid in the geological model was transformed to a Cartesian grid in the simulation model by evenly dividing every column, i.e., the group of grid blocks in the same location of the I and J directions, into 62 grid blocks. Vertical permeability was recalculated using harmonic averaging and other properties were done by arithmetic averaging. Therefore, grid block thickness is the same within one column but varies in other columns, as shown in Fig. 4.3.1a, IK cross-sections of the simulation model. The average grid block thickness is 0.86m. In the IJ cross-section, every layer has 29×29 grid blocks (Fig. 4.3.1 b) and the size is 5m × 5m in the I and J directions. Average formation properties of this model are listed in Table 4.3.1 and rock, fluid and thermal properties in Table 4.3.2. Comparing Table

4.3.1 and Table 2.2.1, this is a representative elemental model of Grosmont carbonate formation. Notice that the average porosity value in Table 4.3.1a appears to be lower than the typical porosity values in Table 2.2.1 as it is the average value for the whole model including the marl layer between Grosmont C and D which was assigned a porosity of 0.01. Figures 4.3.2a and b show the fracture vertical permeability and matrix vertical permeability distributions of the simulation model.

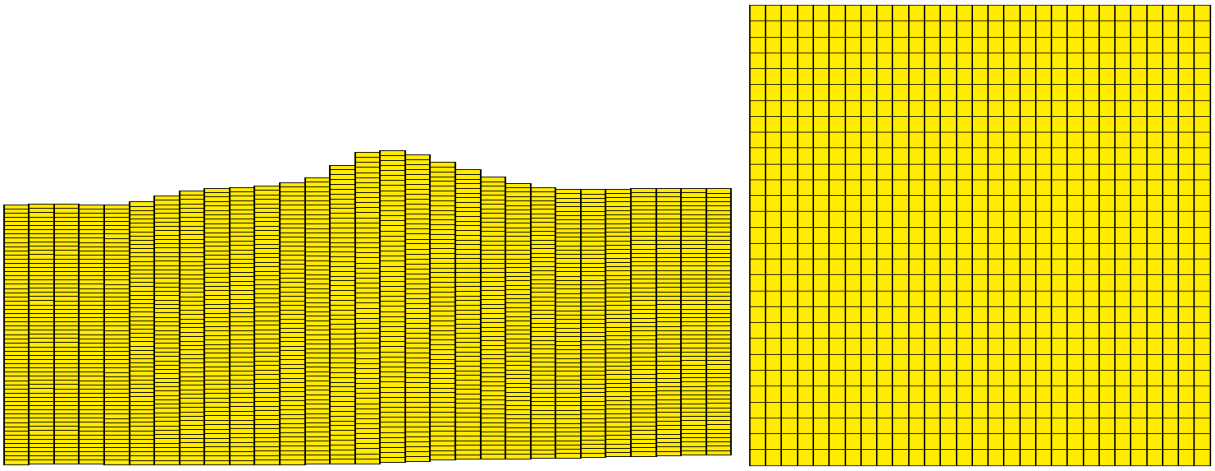

a b

Figure 4.3.1(a) IK cross-section of the simulation model; (b) IJ cross-section of the simulation model.

Table 4.3.1a Average values of formation properties.

Average Thickness (including Grosmont C and D members)	53 m
Average Porosity (%)	18.3
Initial Oil in Place (m^3)	1.4×10^5
Initial Pressure (kPa)	1,500
Initial Oil Viscosity (cP)	3×10^6 @15°C

Table 4.3.1b Range of the matrix and fracture permeabilities.

	I	J	K
Matrix Permeability (mD)	0.0009 ~ 13,029	0.0009 ~ 7,296	0.0009 ~ 629
Fracture Permeability (mD)	0.0009 ~ 37,827	0.0009 ~ 21,385	0.0009 ~ 23,126

Table 4.3.2 Rock, fluid and thermal properties.

Rock Heat Capacity, Ms (kJ/m^3·°C)	2,347
Overburden/underburden heat capacity (kJ/m^3 ·°C)	2,350
Overburden/underburden heat conductivity (kJ/m·day ·°C)	146
Bitumen thermal conductivity (kJ/m·day ·°C)	11.5

The simulation model consists of Grosmont C and D members with the marl layer in between. As can be seen in a 3D view, the marl-layer between Grosmont C and D is represented by a low permeability and high water saturation tight streak in the middle (Fig. 4.3.2a, b, and c). Discontinuity of this middle tight streak can be seen in some of the vertical cross-sections. In the eastern top corner of Grosmont D member, there is a top water zone which is continuous through all the IK planes. At the bottom of Grosmont C member of this model, there is a bottom water zone (Fig. 4.3.3).

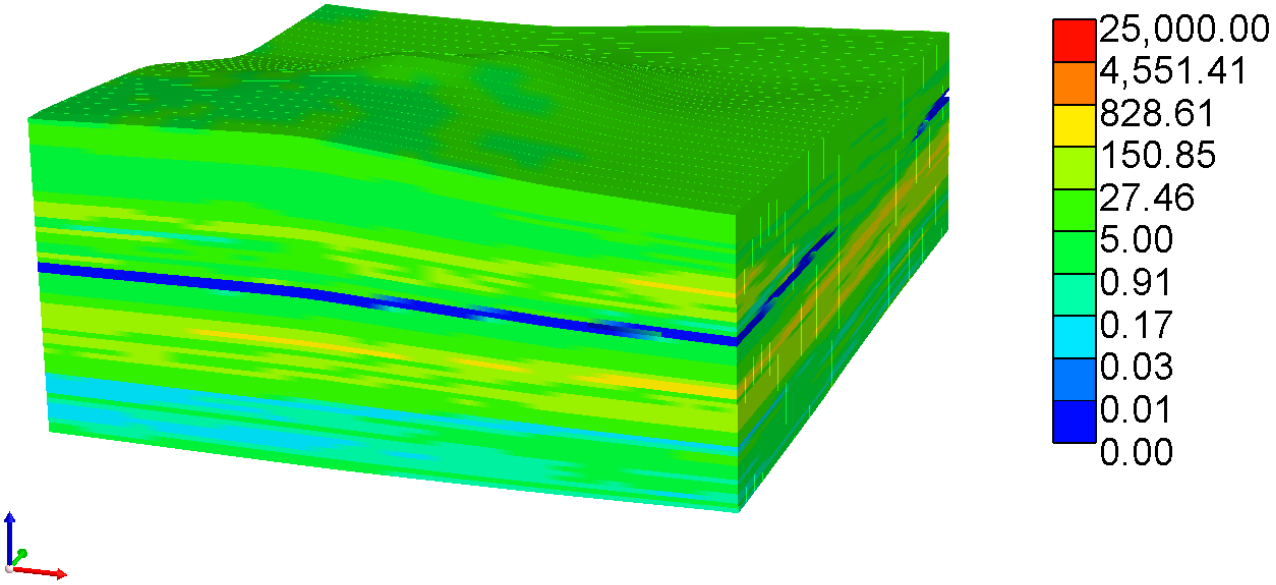

Figure 4.3.2a Matrix vertical permeability of the simulation model (mD).

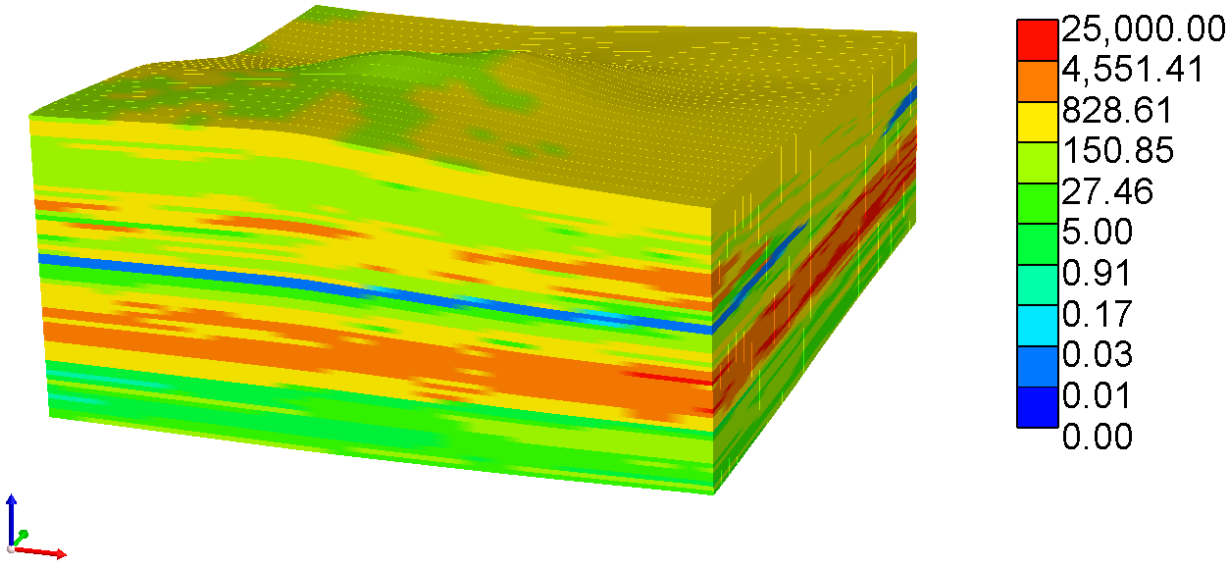

Figure 4.3.2b Fracture vertical permeability of the simulation model (mD).

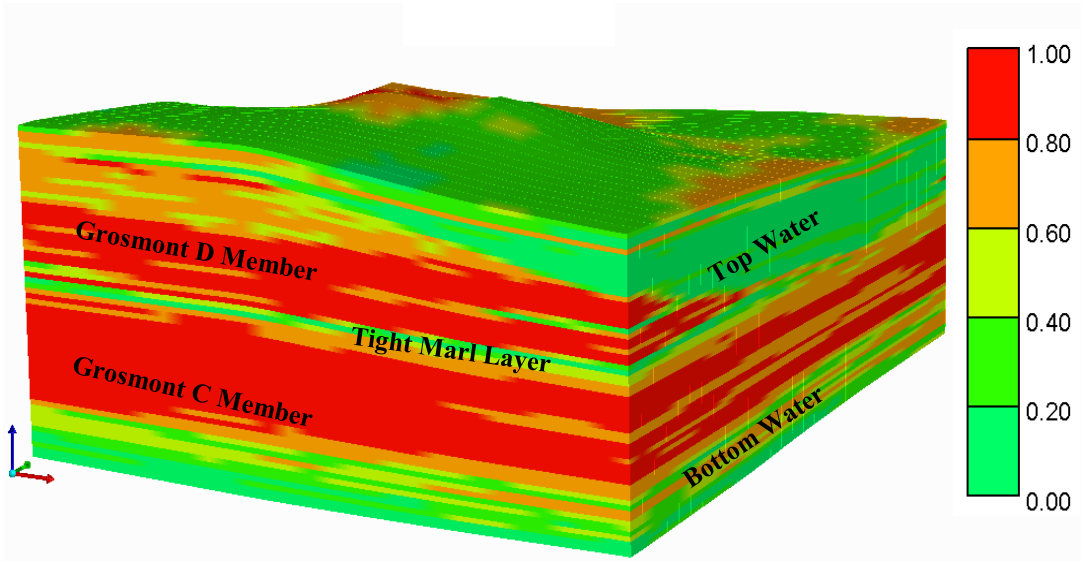

Figure 4.3.2c Oil saturation of the simulation model.

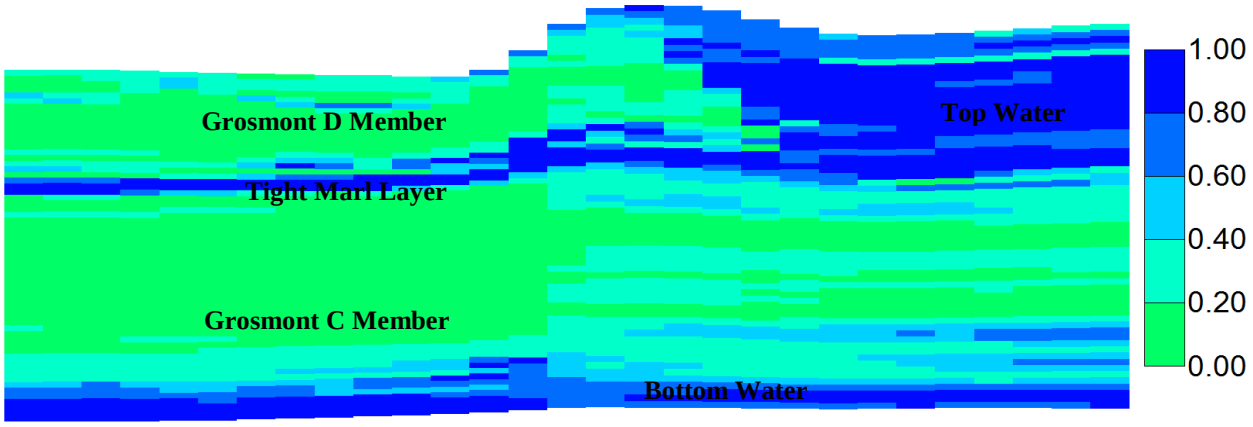

Figure 4.3.3 IK cross-section of the simulation model (J=12).

4.4 Fluid Properties

The thermal compositional model consists of three components, water, oil and methane. The oil-water relative permeability curve demonstrates oil-wet characteristics. Temperature dependence is introduced in the relative permeability curves by providing end points at three different temperatures. The oil viscosity is initially 3×10^6 cP at 15 °C and declines with a temperature increase to less than 10 cP (Fig. 4.4.1).

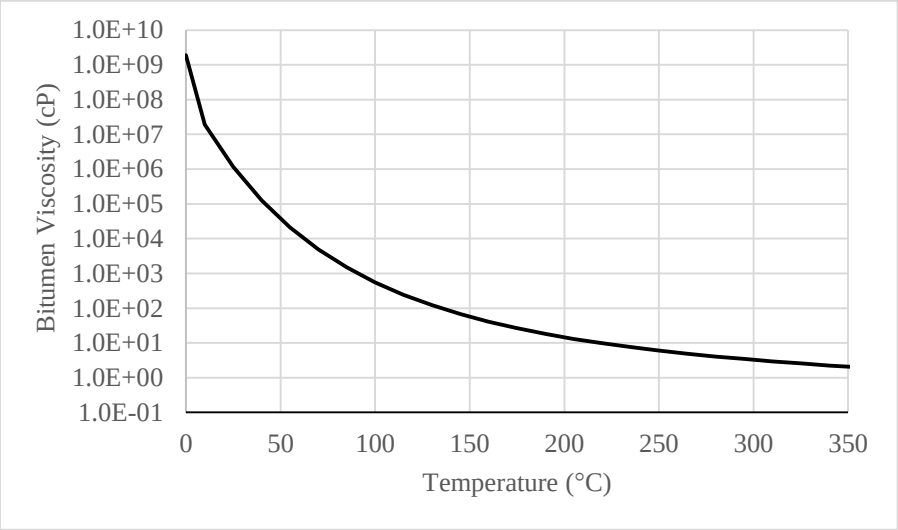

Figure 4.4.1 Bitumen viscosity as a function of temperature.

4.5 Dilation-Recompaction Model

The dilation-recompaction model available in CMG STARS is used to represent the elastic rock behaviour during the injection and fluid production (Fig. 4.5.1). Table 4.5.1 shows the values of critical parameters involved.

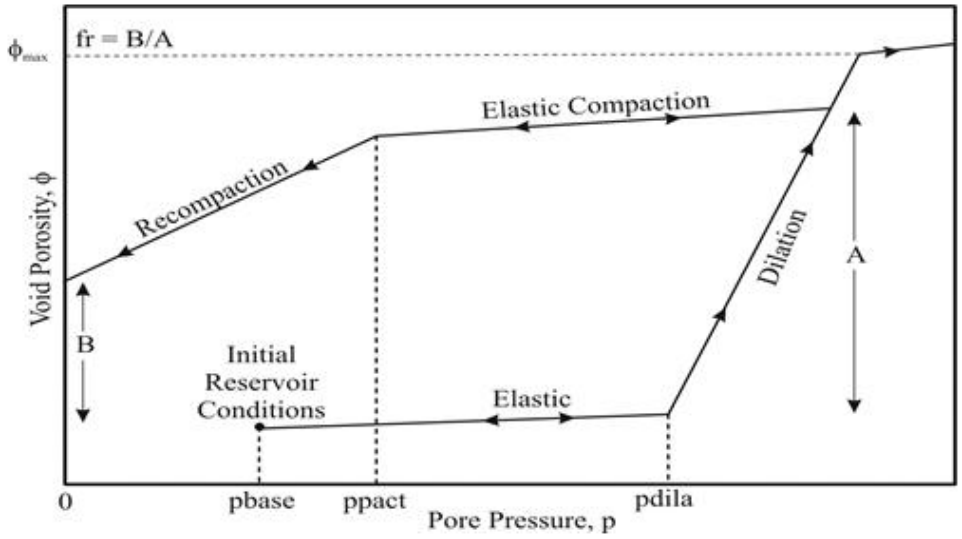

Figure 4.5.1 The dilation-compaction model used in this work

Table 4.5.1 Dilation-recompaction parameters used in this model.

Reference Pressure (kPa)	100
Dilation Rock Compressibility (1/kPa)	1.9×10^{-4}
Residual Dilation Fraction	0.1
Start Dilation (kPa)	3,300
Start Recompaction (kPa)	1,550
Maximum Allowed Proportional Increase in Porosity	1.3
Elastic Compaction Compressibility (1/kPa)	2.02×10^{-6}

Chapter 5: DISCUSSION OF THE SIMULATION RESULTS

5.1 Summary of the Recovery Processes Examined

Seven types of steam injection processes were simulated with 40 simulation cases. The steam injection processes simulated are listed below:

(1) Single vertical well cyclic steam stimulation,

(2) Single horizontal well cyclic steam stimulation,

(3) Steam assisted gravity drainage,

(4) Five-spot pattern steamfood using this 5-acre square model as a repeated pattern,

(5) Seven-spot pattern steamflood using a 4-acre pattern fitted into this model as a repeated pattern,

(6) Nine-spot pattern steamflood using this 5-acre square model as a repeated pattern,

(7) Vertical well injector-horizontal well producer steamflood.

Cyclic steam stimulation is a steam injection method consisting of several operation cycles. Each cycle consists of three stages: injection, soak and production. Steam is injected into the well for several weeks; after injection, the well is shut in for a period, called "soak"; then the same well is switched to production. This process is repeated several times (cycles). Steam assisted gravity drainage (i.e., SAGD) is operated with a pair of horizontal wells, with the injector above and the producer below, usually near the base of a reservoir. Steam is injected into both the injector and producer during the initial preheating phase of the SAGD process. When the formation between the injector and the producer has reached a certain temperature, the producer is switched to

production while the injector continues injecting steam into the formation. Therefore, SAGD is a continuous injection-production process. In the steamflooding process, steam is injected continuously into one or more wells and oil is driven to separate production wells. In this study, the steamfloods of three types of regular patterns are simulated, five-spot, seven-spot and nine-spot. In the vertical well injector-horizontal well producer (VWinj-HWprod) steamflood, vertical wells are used as injectors and horizontal wells are used as producers. Vertical injectors can be offset from the horizontal producer. The production wells in all the steamflooding processes are steam-stimulated during the first few weeks given the extremely high initial oil viscosity (3×10^6cP at 15 °C).

Table 5.1 gives results of the all the simulation cases described in the thesis. All the simulated recovery processes start from 1980-4-7. Conventional pattern steamfloods show a large areal and vertical sweep and a high recovery factor. Considering that vertical well injector-horizontal well producer steamflood cases only target the Grosmont C member while wells in the conventional pattern steamfloods are perforated in both Grosmont C and D members, recovery factors for the vertical well injector-horizontal well producer steamfloods are still comparable. A high SOR is observed for all processes simulated. The lowest SOR is achieved in the horizontal well CSS case. The vertical well injector-horizontal well producer steamflood Case Moon4-3C-1 has an SOR of 8 m^3/m^3 after five years' production, but compared on the basis of the same cumulative steam injection volume, it achieves the same SOR and recovery factor 21 months earlier than the horizontal well CSS Case Q5-2 (see Section 5.5.6).

The extremely large CPU times were a limiting factor, and the simulation cases were terminated at various stages. For example, although optimization methods were applied to all the conventional pattern steamfloods from certain time between the 2nd to 3rd year of production to lower the SOR, the nine-spot pattern steamflood Case Y15-2A-1B-1D-1B had experienced long enough simulated production time after optimization for the SOR to decline to a stable value while the SOR of the five-spot pattern steamflood Case Y8-3F-2C-1G-1J and the seven-spot pattern steamflood Case Y16-2I were still declining by a large gradient by the time the cases were terminated. Therefore, it is not reasonable to evaluate the processes simply according to the numbers in Table 5.1. It is necessary to compare the process performance in the light of dynamic fluid flow, thermal efficiency and drive mechanism using both the simulation output and analytical methods as described in the following sections.

Table 5.1. Summary of Simulation Results.

Process Type	Schematic	Case Number	SOR (m^3/m^3)	Recovery Factor (%)	$\frac{\text{Cumulative Steam Injection Volume}}{\text{Initial Pore Volume}}$	Simulated Time (Years)
Single Vertical Well CSS		Q6-2	11	1.9	0.2	2.5
Single Vertical Well CSS	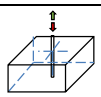	Q6-3	13.8	1.5	0.2	2.5
Single Vertical Well CSS	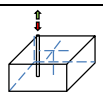	Q6	7.0	3.0	0.1	2.5
Single Horizontal Well CSS		Q5-2	7.0	18.3	0.9	4.5
Single Horizontal Well CSS		Q5	12.7	7.9	0.7	4.5
SAGD		SAGD	6.9	8.9	0.4	5
SAGD		SAGD-1	7.3	17	1.4	5
SAGD		SAGD-2	9.3	6.8	0.8	5
SAGD		SAGD-5	8.8	7.2	0.7	5
5-acre Five-spot Steamflood		Y8-3F-2C-1G-1J	9.1	32.7	2.1	3
5-acre Five-spot Steamflood	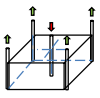	Y8-3F-2C-1G-1H-1C	12.3	16.3	1.5	2
20-acre Five-spot Steamflood		Y9B-2E	127	1.0	0.9	5
4-acre Seven-spot Steamflood	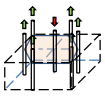	Y16-2I	10.6	45.7	3.4	3
4-acre Seven-spot Steamflood	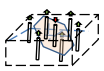	Y17D	19.3	25.6	3.4	3

5-acre Nine-spot Steamflood	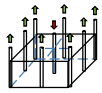	Y15-2A-1B-1D-1B	8.0	41.0	2.3	5
VWinj-HWprod Steamflood		Moon 2A	11	13.6	1.1	5
VWinj-HWprod Steamflood		Moon 4B	9.7	16.6	1.1	5
VWinj-HWprod Steamflood		Y14	8.3	11	0.64	3
VWinj-HWprod Steamflood		Y14-1	9.4	15.6	1.0	5
VWinj-HWprod Steamflood		Moon 3	13.8	10	1.0	5
VWinj-HWprod Steamflood		QY3	12.1	10.9	1.0	5
VWinj-HWprod Steamflood		Moon 4-2D	9.5	16.9	1.1	5
VWinj-HWprod Steamflood	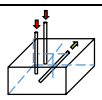	Moon4-3c-1	8.6	22.0	1.3	5
Single Horizontal Well CSS (Without the Fracture System)		Q5-2-1	5,127	0.002	0.07	4.5
SAGD (Without the Fracture System)		SAGD-3	25.0	2.0	0.34	8.5

5.2 Cyclic Steam Stimulation using Vertical and Horizontal Wells

5.2.1 Vertical Well Cyclic Steam Stimulation

5.2.1.1 Geological model

The elemental geological model of the Grosmont carbonate reservoir used for the simulations contains Grosmont C and D members, with the marl layer in between. As can be seen in permeability distribution of the simulation model, the marl-layer between Grosmont C and D is represented by a low permeability (vertical permeability less than 0.1 Darcy), high water saturation tight streak in the middle (Fig. 4.3.2). Discontinuity of this middle tight streak can be seen in vertical cross-sections, (Fig. 4.3.2) in accordance with the fact that the marl layer separating the Grosmont C and D members is not laterally continuous (Russel-Houston et al. 2014, Ezeuko et al. 2013). Examining permeability of all the IK planes from J=1 to J=29, the middle tight streak is not continuous in 12 of the total 29 planes. Except for some of the IK planes in the west, i.e., J=5 to 9, discontinuity of the middle tight streak occurs mostly in the eastern portion, above which there is a top water zone (Fig. 4.3.2c). This zone is in the western top corner of the Grosmont D member and is continuous through all the IK plane (Figs. 4.3.2c and 4.3.3). At the bottom of Grosmont C member of this model, there is a continuous bottom water zone (Figs. 4.3.2c and 4.3.3).

5.2.1.2 Well placement and operation

Given the geological properties of this model as described above, three cases were carried out for the vertical well cyclic steam stimulation (VWCSS). In Case Q6-2, a vertical well is placed in the middle of the reservoir (I=15, J=15) and perforated in the high oil saturation layers of Grosmont D member (Fig. 5.2.1.1a), while, for Case Q6-3, the vertical well is drilled at the same location

but perforated in the high saturation layers of both Grosmont C and D members (Fig. 5.2.1.1b). In the last case, Case Q6, the vertical well is placed in the same IJ plane as Q6-2 and Q6-3, but is shifted westwards to increase the distance from the top water (Fig. 5.2.1.1c).

All three cases of vertical CSS are conducted from 1980-4-7 to 1982-10-10 for 5 cycles. Each cycle consists of 30 days' injection with a fixed injection rate of 200 m^3/day, 10 days' soak and 142 days' production. In addition, there is 1 day of no operation between the end of production and the start of injection.

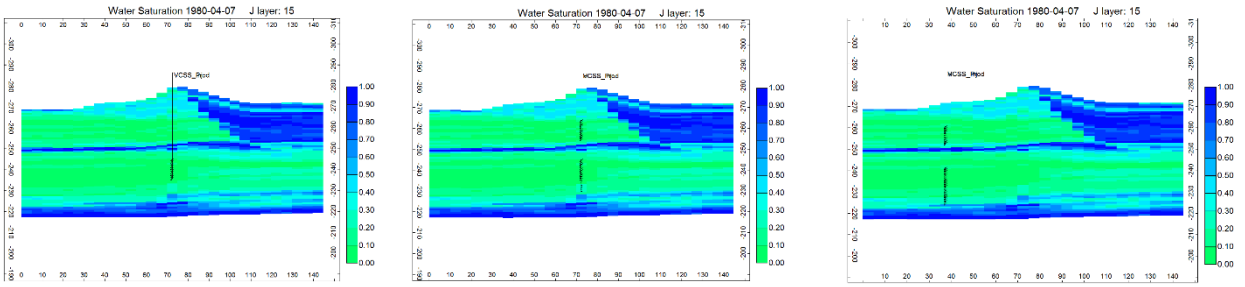

(a) Case Q6-2 (b) Case Q6-3 (c) Q6

Figure 5.2.1.1. Well placement and the perforation interval of vertical well CSS Cases Q6-2, Q6-3, and Q6.

5.2.1.3 Oil production, steam-oil ratio, and oil recovery

Table 5.2.1.1 shows the steam-oil ratio (SOR) and oil recovery factor at the end of production for all the three cases. Judging by the cumulative SOR and oil recovery, although perforating into both Grosmont C and D members, Case Q6-3 yields lower recovery than Case Q6-2. The reason is that the perforations in Grosmont D in Case Q6 are very close to the top water so that a large amount of steam channels into the top water instead of helping to recover oil. In Case Q6, taking

advantage of perforating into both oil intervals and being far away from the top water, the recovery performance is the best.

Table 5.2.1.1. Cumulative steam-oil ratio and oil recovery factor of three VWCSS cases.

Case Name	Cumulative Steam-oil ratio (m^3/m^3)	Oil Recovery Factor (%)
Q6-2	11	1.9
Q6-3	13.84	1.5
Q6	7	3.0

5.2.1.4 Temperature distribution

Looking at the temperature distribution at the end of injection for any cycle of Case Q6-3, it can be seen that the eastern side of the well is heated more than the other side, showing the preference of steam migrating towards the top water in the east (Fig. 5.2.1.2). This can also be seen from the temperature change at the edge of the top water zone. At the end of the fifth cycle, the temperature at the edge of the top water close to the well is about 100°C and 28°C in the middle as it is heated by steam.

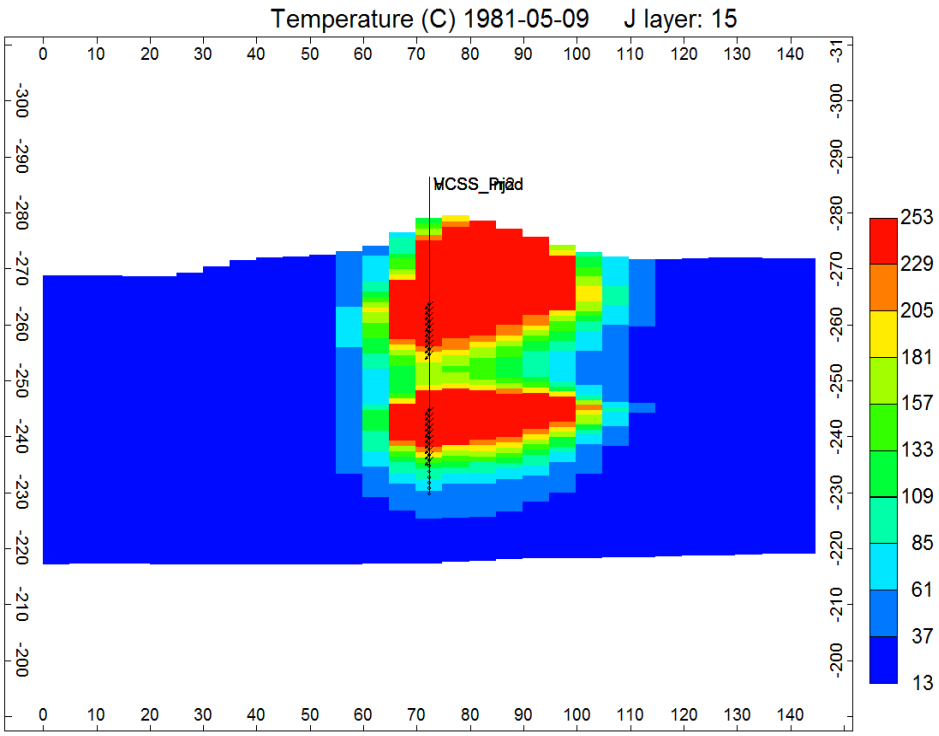

Figure 5.2.1.2. Temperature distribution at the end of the injection of the third cycle in Case Q6-3.

5.2.1.5 Steam zone

A steam zone is formed at the end of injection for each cycle. Theoretically, the steam zone should be the volume bounded by the iso-temperature surface at the steam saturation temperature corresponding to the injection pressure at the end of steam injection. From the bottomhole pressure curve, steam injection pressure, p_s, can be obtained at the end of injection period of each cycle (Fig. 5.2.1.3). Accordingly, the steam zone temperature, T_s, is obtained from steam tables. This method is precise as T_s is found to be the highest temperature for which an iso-temperature surface can be determined. Considering the fact that the steam injection pressure is not constant (Fig. 5.2.1.3) and some pressure gradient should be allowed inside the steam zone, a temperature of (T_s-5) is used to plot the steam zone surface (Table 5.2.1.2). As can be seen from Fig. 5.2.1.4,

there are always two separate steam zones along the vertical well due to the effect of the tight streak in the middle. The steam zone is obviously skewed towards the top water zone from the very first cycle. Although the vertical well is perforated through both oil intervals in the Grosmont C and D members, respectively, the steam zone only forms at the top of each member, as a result of severe steam override. The strong steam override is due to the high vertical fracture permeability.

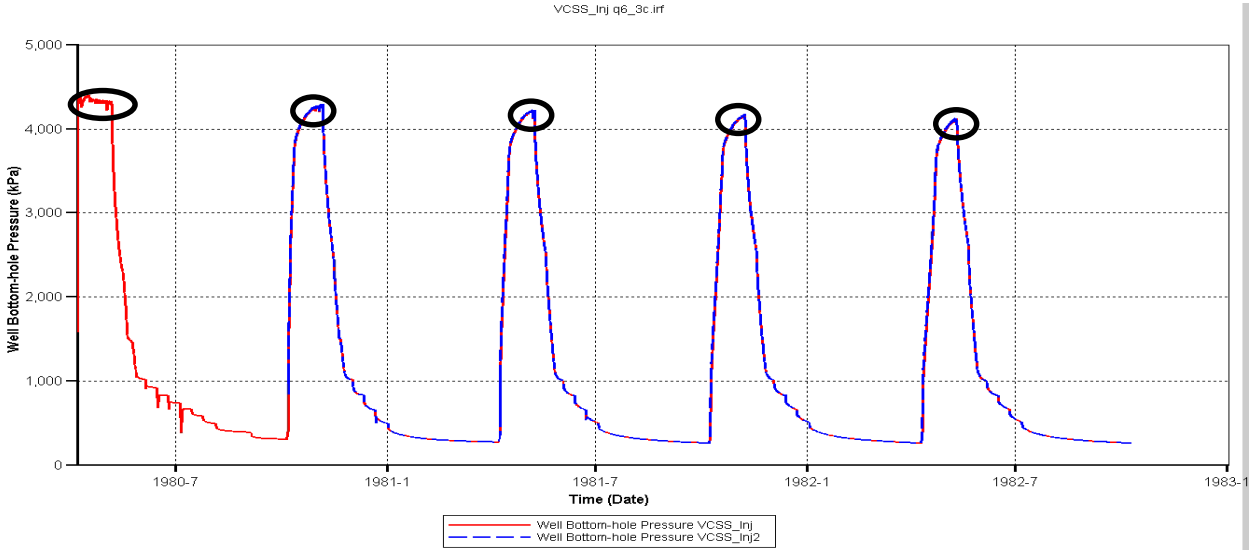

Figure 5.2.1.3. Bottomhole pressure of the vertical well during Case Q6-3. The ellipses mark the pressure at the end of injection for each cycle, p_s, which are used to determine steam zone temperature.

Table 5.2.1.2. Procedure to determine steam zone temperature for Case Q6-3.

	Bottomhole Pressure at the End of Injection, p_s (kPa)	Steam Saturation Temperature at p_s, T_s (°C)	T_s-5 (°C)
Cycle 1	4,332.19	254	249
Cycle 2	4,290.48	254	249
Cycle 3	4,230.38	253	248
Cycle 4	4,170.3	252	247
Cycle 5	4,132.76	251	246

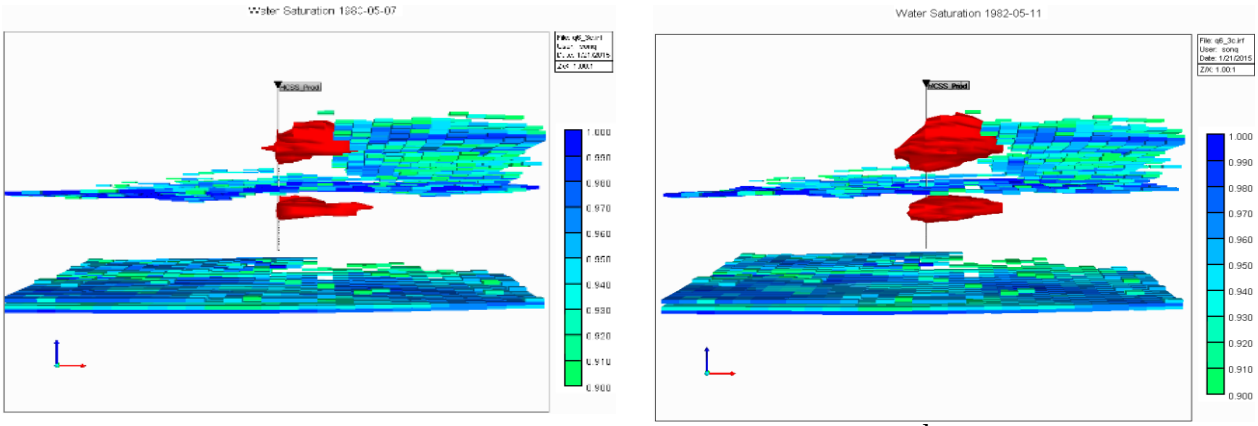

a b

Figure 5.2.1.4. Steam zone (in red) at the end of injection for the first cycle (a), and the fifth cycle (b) of Case Q6-3. Grid blocks with water saturation higher than 90% are used as background so that it is easy to see that steam zone is connected with the top water.

5.2.1.6 Water retention

The temperature distribution, the temperature change of the top water and the steam zone shape show that there is severe steam channelling into top water from the very early stage of Case Q6-3. One consequence of this steam channelling is low oil production. Another consequence is the negative cycle water saturation retention. Cycle water retention is defined as the difference between water injection volume and the water production volume for each cycle. The top water zone serves as a huge source of water to the wellbore through steam channels (Fig. 5.2.1.5). Also, from the temperature increase and water saturation decrease in the bottom water zone, it is believed that the bottom water zone is another source of water production. But as the steam volume shape and temperature distribution are both skewed towards the top water, it is believed to be the more dominant water source.

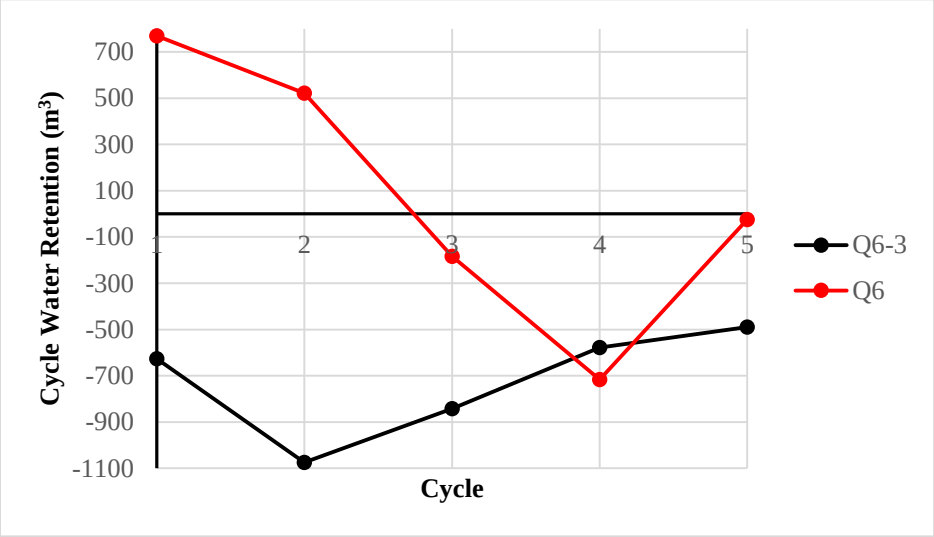

Figure 5.2.1.5. Cycle water saturation retention curve for Cases Q6-3 and Q6

However, for Case Q6, as the well is shifted further away from the top water, it can be seen from the steam zone shape that the well is less connected to the top water (Fig. 5.2.1.6), resulting in higher oil production. But there is still steam channelling as both the temperature distribution and steam zone are skewed towards the top water. The water retention curve is positive for the first two cycles but becomes negative in the following cycles, indicating that steam eventually gets connected with top water. In addition, perforations of the vertical well in Case Q6 are connected with the bottom water in the first cycle (Fig. 5.2.1.6a). When communication with bottom water does develop, the deeper perforations are closed for the following cycles to reduce steam loss (Fig. 5.2.1.6b).

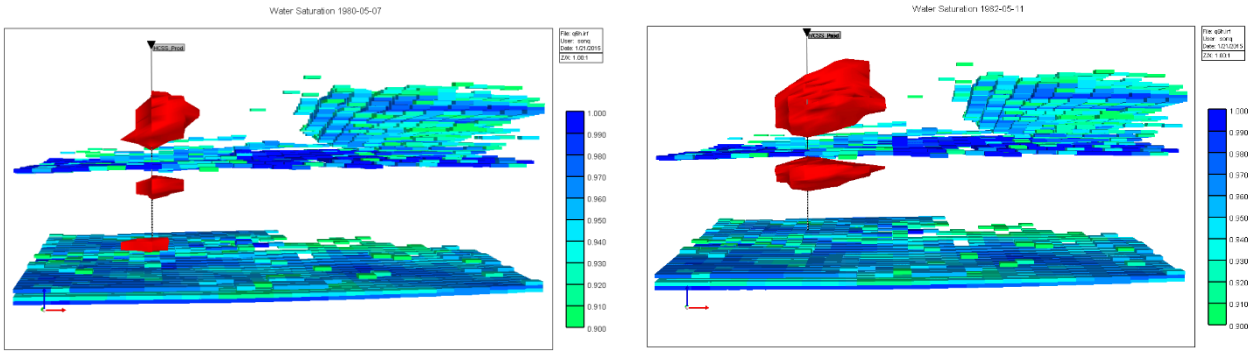

(a) (b)

Figure 5.2.1.6. Steam zone (in red) at the end of injection for the first cycle (a) and the fifth cycle (b) for Case Q6. Grid blocks with water saturation higher than 90% are used as background so that it is easy to see that the steam zone is not connected with the top water.

5.2.1.7 Steam-oil ratio and oil recovery

Comparing the oil production volume, SOR and oil recovery factor from cycle to cycle (Table 5.2.1.3), intermediate cycles have the highest production. Although the volume of steam slug injected in every cycle is the same, a large portion of steam condenses during the first two cycles, leaving a small steam zone and not much oil mobilized enough to flow to the wellbore (Fig. 5.2.1.6a), while in the intermediate cycles, the injected steam in addition to the heat left in the reservoir from previous cycles results in a larger steam zone and more oil mobilized, so that the cycle oil production increases. However, as can be seen from the location of the steam zone and oil saturation change (Figs. 5.2.1.6 and 5.2.1.7), oil production is mostly from only the immediate vicinity of the wellbore. As there is less oil left in the limited drainage area, the oil production rate declines in the last cycles. Given this observation, one way to further optimize the vertical well CSS cases is to restart each case from the cycle of the lowest SOR, increasing production time of

this most productive cycle, and gradually reduce the steam injection slug size and shorten production time in the following cycles.

Table 5.2.1.3. Oil production, steam-oil ratio and oil recovery factor for each cycle of Case Q6

	Cycle 1	Cycle 2	Cycle 3	Cycle 4	Cycle 5
Cycle Oil Production (m^3)	401.325	805.855	1,023.81	1,093.16	927.44
Cycle Steam-Oil Ratio (m^3/m^3)	15	7	6	5	6
Cycle Oil Recovery Factor (%)	0.3	0.5	0.8	0.7	0.7

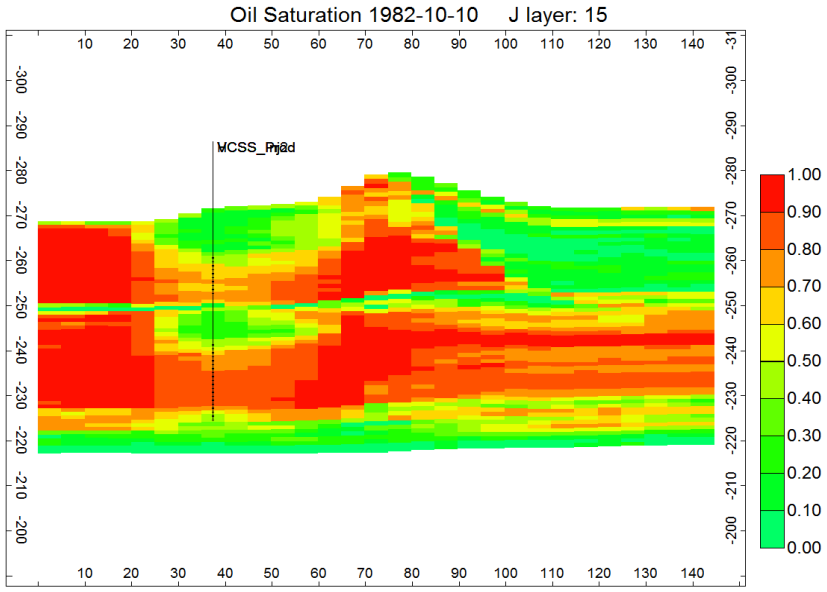

Figure 5.2.1.7. Oil saturation of IK-2D cross-section J=15 at the end of case Q6 showing the effective well vicinity

5.2.2 Horizontal Well Cyclic Steam Stimulation

5.2.2.1 Well placement and operation

Three cases were carried out for horizontal well cyclic steam stimulation: Cases Q5, Q5-2 and Q5-2-1. As some portions of Grosmont D are very thin and a considerable part of it is occupied by the top water (Figs. 4.3.2c and 4.3.3), the horizontal well is placed only in Grosmont C for all the

three cases. Considering that in typical field development, wells are distributed evenly in a given space, the horizontal well is placed in the middle of the areal cross-section along the I-direction, i.e., I=3 to 27, J=15, in the Case Q5 (Fig. 5.2.2.1a). For the same reason, the well is placed in Layer 42 as it is the middle of high oil saturation zones of Grosmont C (Fig. 5.2.2.1b), while in Case Q5-2, based on the observation of the result of Q5, the well is shifted towards the western boundary to I=7 and placed along the J-direction in order to increase the distance from the top water (Fig. 5.2.2.2a). Also, vertically the well is placed downwards in Layer 48 which is the approximate boundary between the highly oil-saturated and permeable layers above and the low permeability layers below in an effort to maximize production by gravity flow (Figs. 5.2.2.2b, c, d).

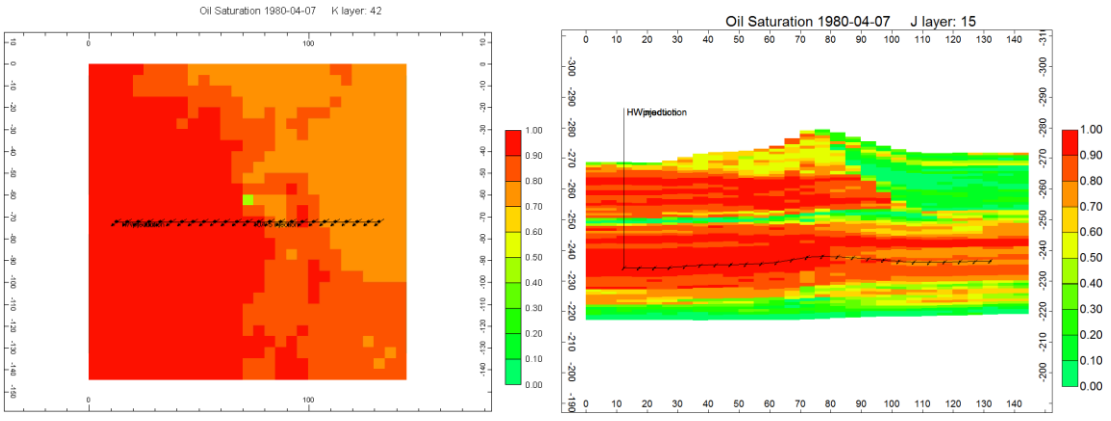

Figure 5.2.2.1. (a) The horizontal well placed along I-axis, in the middle of IJ cross-section, K=42 for Case Q5; (b) Horizontal well of Case Q5 placed in Layer 42, the middle of the oil-bearing interval in Grosmont C member. IK cross-section, J=15.

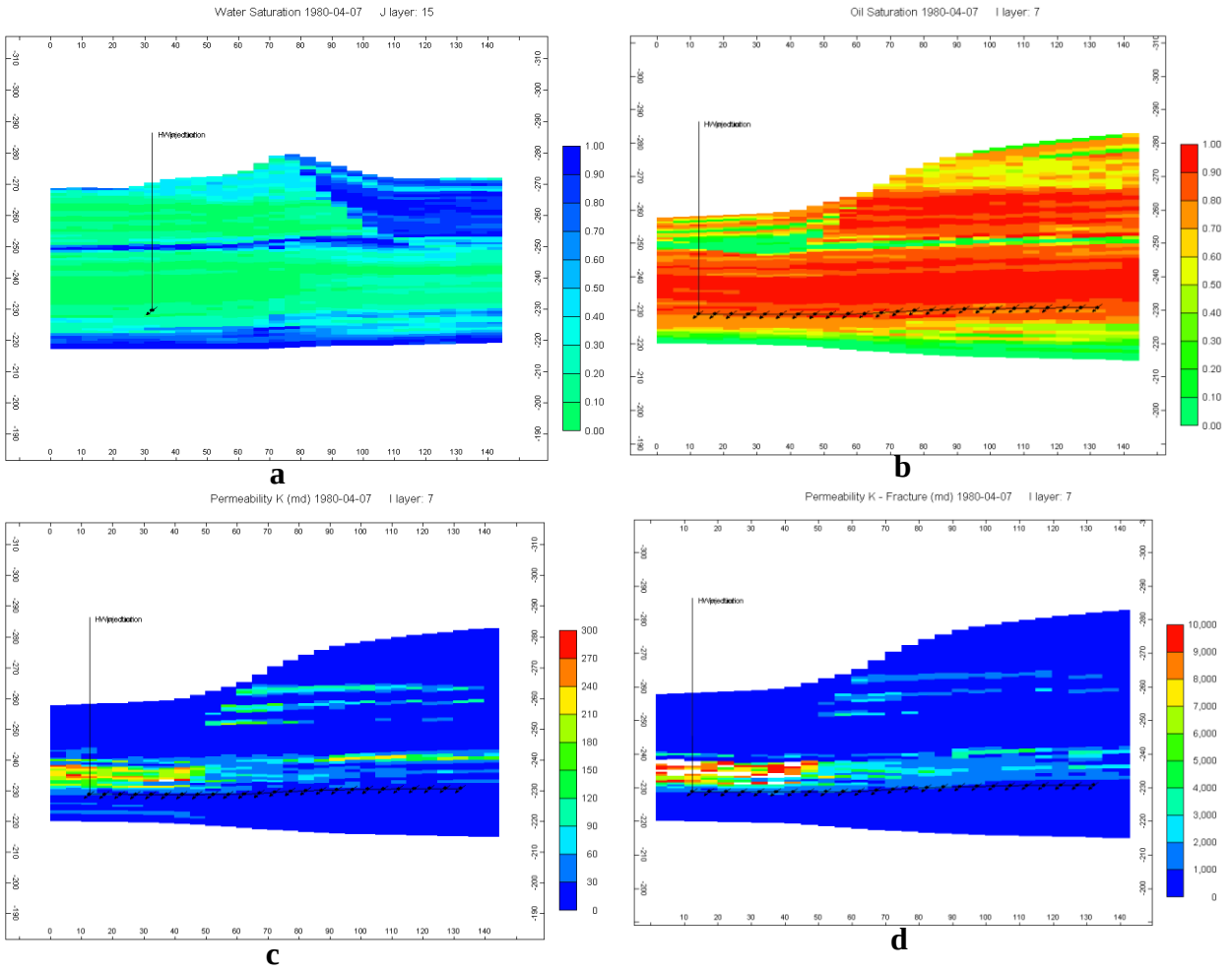

Figure 5.2.2.2. (a) An IK cross-section perpendicular to the horizontal well of Case Q5-2. The horizontal well placed along J axis close to the western border away from the top water. (b) Horizontal well of Case Q5-2 placed close to the bottom of the oil-bearing interval in Grosmont C member. JK cross-section, I=7. (c) Horizontal well placed close to the bottom of the high matrix vertical permeability interval in Grosmont C member. JK cross-section, I=7. (d) Horizontal well of Case Q5-2 placed close to the bottom of the high matrix vertical permeability interval in Grosmont C member. JK cross-section, I=7. Vertical fracture permeability in the white grid blocks is higher than 10,000 mD.

In order to see the effect of fractures on oil production, the fracture system was removed and the horizontal well CSS was simulated in the single porosity model of only the matrix properties in Case Q5-2-1 which has the same well placement as Case Q5-2.

Horizontal well CSS is simulated from 1980-4-7 for 5 cycles for Case Q5 and 6 cycles for Case Q5-2. Each cycle includes a 60 days' injection period with a fixed injection rate of 500 m^3/day, 30 days' soak and 180 days' production.

5.2.2.2 Oil production due to the dominant gravity flow

From the initial oil saturation distribution, matrix vertical permeability and fracture vertical permeability of the cross-section along the well of Case Q5-2, i.e., the JK cross-section, I=7 (Figs. 5.2.2.2b, c, and d), it can be seen that the well is placed at the boundary between the permeable high oil saturation layers and above and the low permeability layers below. By comparing the oil saturation distribution before and after production, we can see that oil production is from the oil column between the well and the middle tight streak. Surprisingly, although the oil viscosity in the layers below the well is low at the end of production, 30-200 cP, more oil accumulates there instead of being produced (Fig. 5.2.2.3a). A similar behaviour is observed for Case Q5 in which the well is placed in the middle of the highly permeable oil-saturated zone of the Grosmont C member (Fig. 5.2.2.1b). At the end of production, there is only oil desaturation in the interval between the well and the middle tight streak and there is oil accumulated below the well (Fig. 5.2.2.4). This phenomenon indicates overwhelmingly dominant gravity flow. In other words, the dominant drive mechanism during horizontal well CSS in this model is gravity, not the pressure drop between the wellbore and the formation.

As can be seen from Table 5.2.2.1, given the same production time, i.e., at the end of the fifth cycle, oil production for Case Q5-2 is about twice as much as that for Case Q5, and SOR is about one-half. This is simply because with the horizontal well placed in the middle of the highly oil-saturated and permeable interval of Grosmont C, the efficient oil drainage area of Case Q5 is one-half of that of Case Q5-2, under the circumstance of the dominant gravity flow. Water saturation increases in the oil desaturation zone (Fig. 5.2.2.3b).

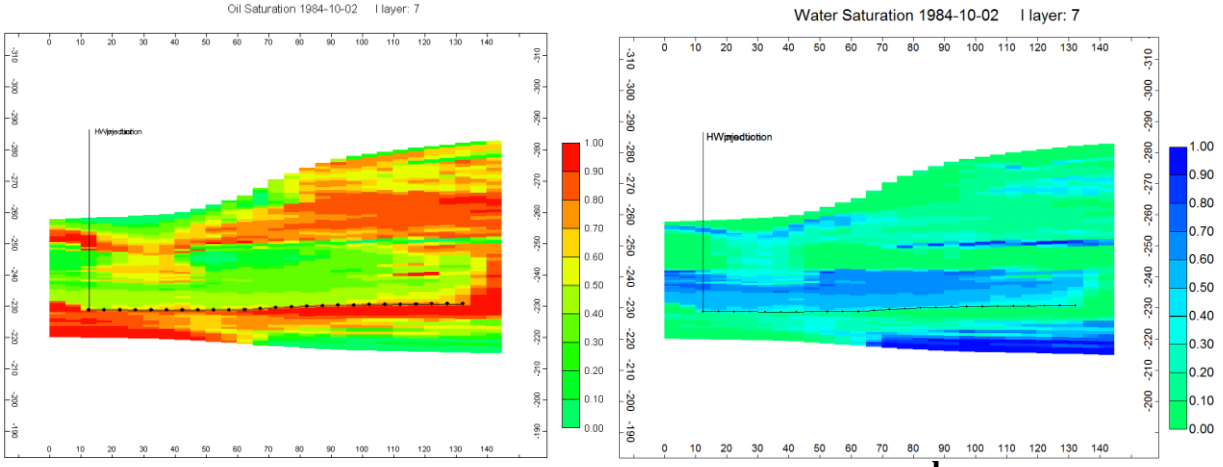

Figure 5.2.2.3. (a) Oil saturation distribution in the cross-section across the horizontal well at the end of Case Q5-2. Oil depleted from above the well and accumulated below the well. (b) Water saturation distribution of the cross-section across the horizontal well at the end of Case Q5-2. Water accumulates in the oil desaturation zone.

Table 5.2.2.1. Cumulative steam-oil ratio and oil production at the end of the 5th cycle of Cases Q5 and Q5-2

Case Name	Cumulative Steam-Oil Ratio (m^3/m^3)	Oil Production (m^3)
Q5	12	11,214
Q5-2	7	22,121

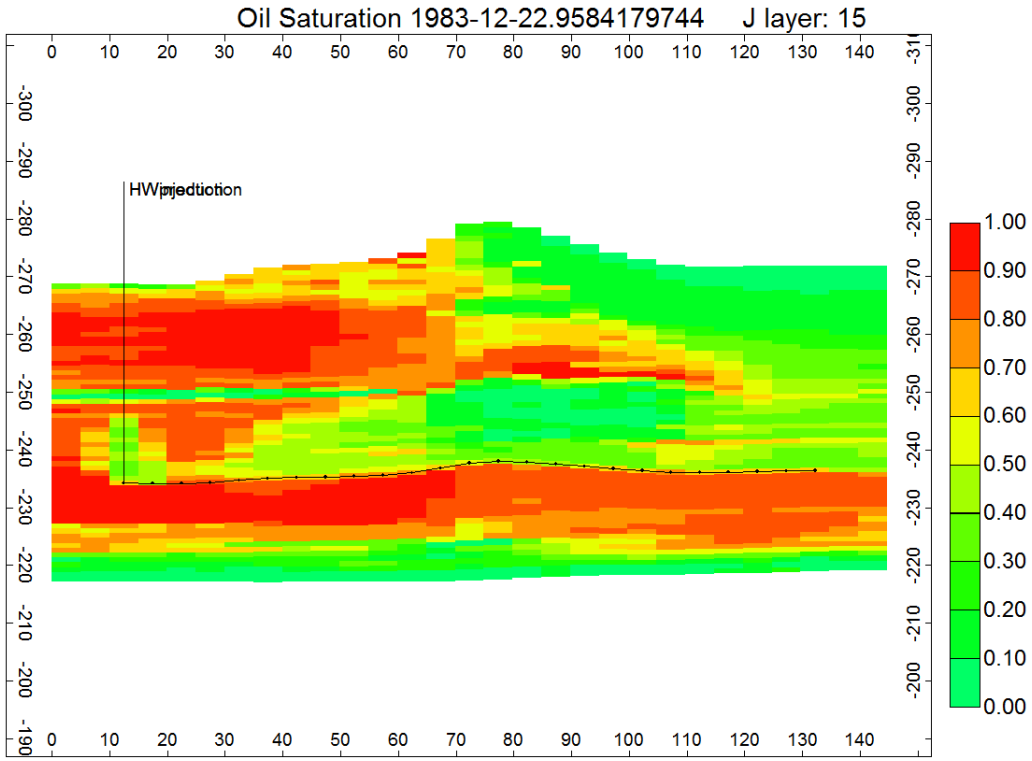

Figure 5.2.2.4. Oil saturation distribution of the cross-section across the horizontal well at the end of Case Q5. Oil depleted from above the well and accumulated below the well.

5.2.2.3 Effect of fractures on injection and production

In Case Q5-2-1 with the fracture system removed, the simulation crashed when the steam injection was fixed at 500 m^3/day, while in the other two cases there was no problem, so in this case there is no steam injection rate constraint, only the injection pressure constraint. The average injection pressure during the injection of each cycle in Case Q5-2 is used as constant injection pressure for the corresponding cycles in Case Q5-2-1, to make comparable simulations. As we can see in Fig. 5.2.2.5, except the peak at the beginning of each injection period, the steam injection rate is very low, indicating the extremely low injectivity of the pure dolomite matrix. Therefore, the high injectivity of this model is attributed to the fracture network.

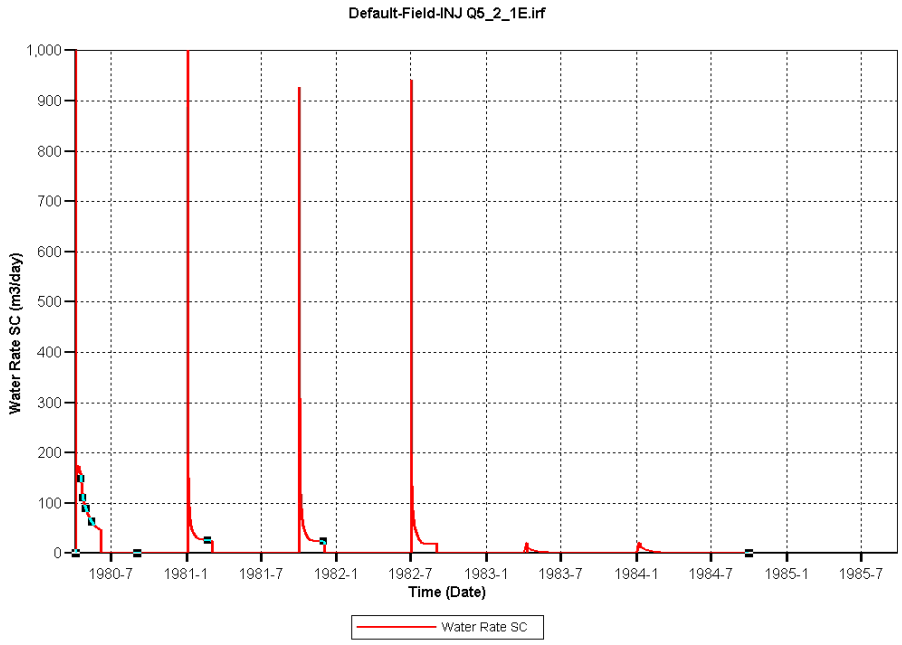

Figure 5.2.2.5. Steam injection rate of the horizontal well CSS Case Q5-2-1 with the fractures removed.

5.2.2.4 Steam override and limited drainage area

Figure 5.2.2.6a shows the temperature distribution at the end of the injection in the third cycle of Case Q5-2. Because of the heterogeneity, the steam injection along the wellbore is non-uniform so the formation is not evenly heated and oil is not evenly drained along the wellbore. For example, in Case Q5-2, due to the heterogeneous permeability along the wellbore, steam penetrates mainly through the high permeability portions of the formation, leaving the less permeable portions less heated (Fig. 5.2.2.6a). Permeability is generally higher above the heel of the well and low above the toe (Fig. 5.2.2.2c and d). As can be seen from the JK cross-section along the horizontal well in Case Q5-2, steam preferentially flows into the formation around the heel where permeability is relatively high. In addition, the steam zone does not change very much from the first cycle to the sixth, which means that the same steam zone is repeatedly formed and drained from cycle to cycle.

As a result, the drainage area is restricted to the high permeability region near the heel (Fig. 5.2.2.6b). Also, as shown in Fig.5.2.2.7, severe steam override occurs in the heated formation as a result of the high vertical permeability. As an extension of this study, two methods could be used to achieve more uniform heating. One way is to perforate only the portion of the horizontal well exposed to permeable zones. The other is by using a discretized well model, e.g., Flexwell in CMG STARS, the flow control device can be used in the simulation to distribute steam flow in a horizontal well more evenly.

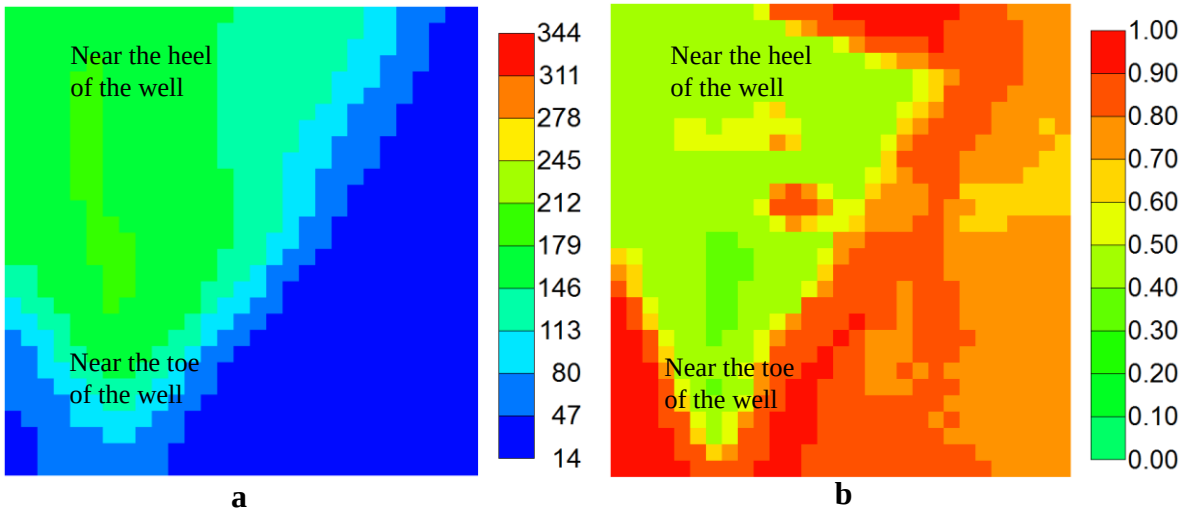

Figure 5.2.2.6. (a) Temperature distribution at the end of production of the IJ cross-section 5 m above the well for the horizontal well CSS Case Q5-2. (b) Oil saturation distribution at the end of production of the IJ cross-section 5 m above the well for the horizontal well CSS Case Q5-2.

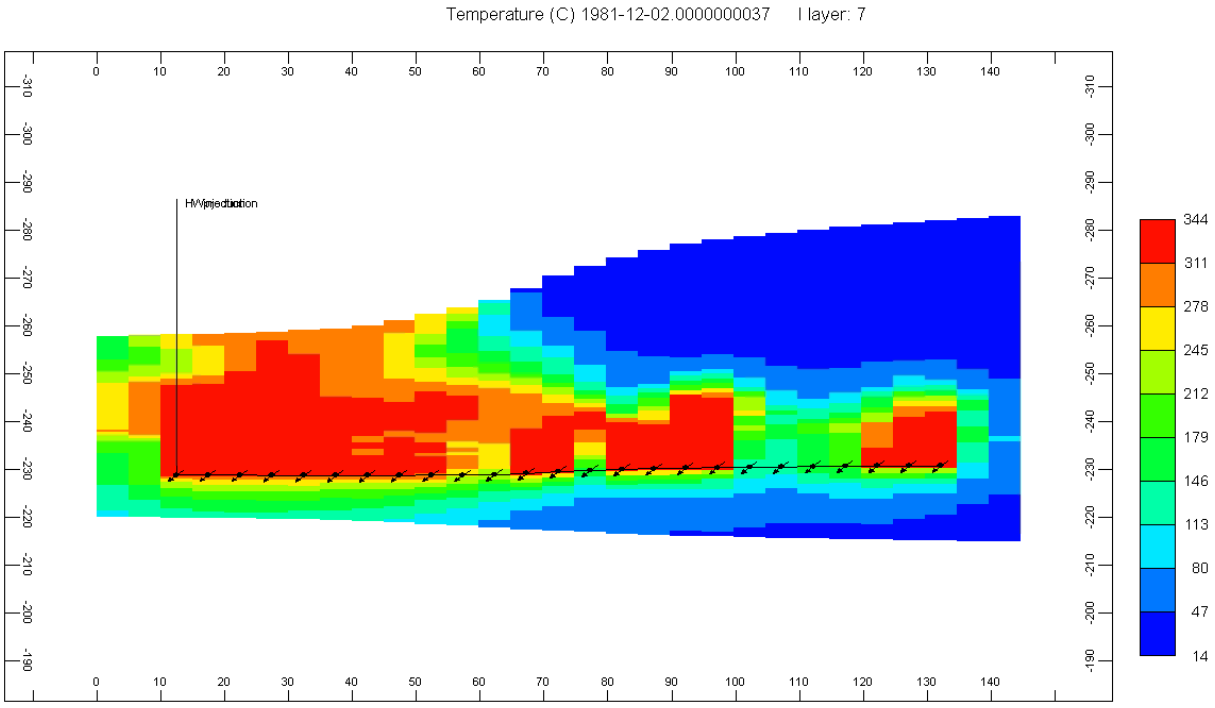

Figure 5.2.2.7. Temperature distribution at the end of the injection of the third cycle of Case Q5-2. Because of the permeability variation along the well, steam is unequally injected, thus the formation is heated unevenly.

5.2.2.5 Water retention, cycle oil production and steam-oil ratio

As noted for vertical well CSS, the water retention for both Cases Q5 and Q5-2 for horizontal well CSS is positive in the first cycle and becomes negative in the following cycles, indicating that the well eventually gets connected with the top water (Fig. 5.2.2.8). The cycle oil production also shows behaviour similar to that of vertical well CSS. The oil production declines after the peak in the second cycle since there is a limited oil volume in the steam-invaded well vicinity (Table 5.2.2.2a and b). To gain insight into recovery behaviour in the short term, the cycle steam injection slug is treated as a fixed parameter. However, the increasing steam-oil ratio in the cycles following the second cycle means that less steam is needed for the dwindling recoverable oil resource.

Another way is to restart Cases Q5 and Q5-2 from the third cycle, increasing the production time, and gradually reducing the steam injection slug and production time, in each cycle after the third cycle.

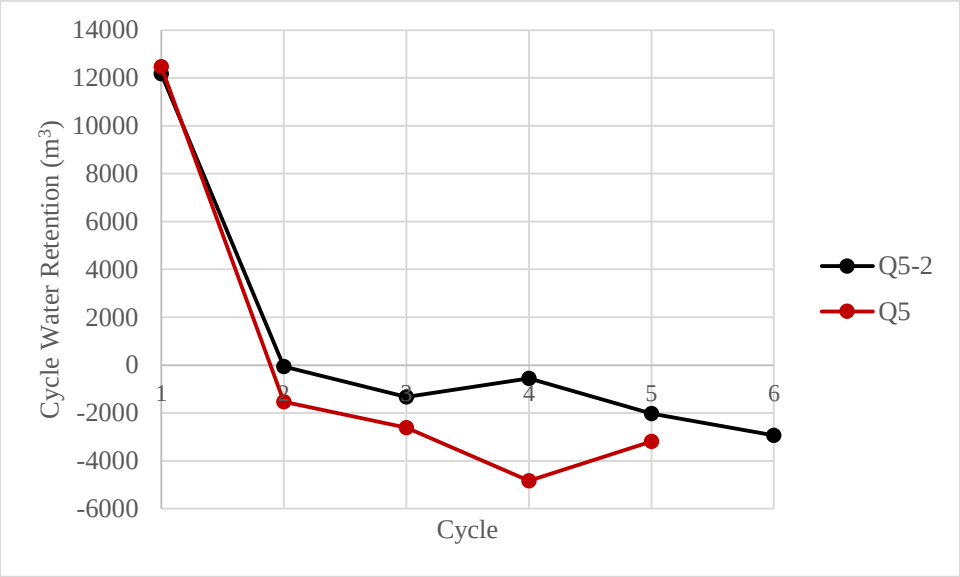

Figure 5.2.2.8. Cycle water saturation retention curve for Case Q5 and Q5-2.

Table 5.2.2.2a. Oil production, steam-oil ratio and oil recovery factor for each cycle of Case Q5.

	Cycle 1	Cycle 2	Cycle 3	Cycle 4	Cycle 5
Cycle Oil Production (m^3)	1,635	3,285	2,454	1,637	2,002
Cycle Steam-oil ratio (m^3/m^3)	18	9	12	13	15

Table 5.2.2.2b. Oil production, steam-oil ratio and oil recovery factor for each cycle of Case Q5-2.

	Cycle 1	Cycle 2	Cycle 3	Cycle 4	Cycle 5	Cycle 6
Cycle Oil Production (m^3)	2,865	5,260	4,875	4,841	3,661	3,662
Cycle Steam-oil ratio (m^3/m^3)	10	6	6	6	8	8

5.2.3 Comparison of VWCSS and HWCSS

The optimal simulation case of each process, Cases Q6 and Q5-2 can be compared in a general sense as typical cases of the vertical well CSS and the horizontal well CSS, respectively. Case Q6 was continued to the end of the 10th cycle (from 1980-4-7 to 1985-4-10) to reach the same cumulative steam injection volume at a certain time of Case Q5-2 to make a fair comparison. The oil production per production day per metre of the perforation length is used as one criterion to compare. As in Case Q6 (HWCSS) the well is only placed in Grosmont C member and in Case Q6 (VWCSS) the well is perforated in both Grosmont C and Grosmont D members, the oil production per production day per metre of the perforation length of Case Q6 is calculated proportionally to the well perforation interval in Grosmont C member. As we can see in Table 5.2.2.3a, the horizontal well CSS is more productive than the vertical well CSS. Also, as shown in Table 5.2.2.3b, based on the cumulative steam injection volume, horizontal well CSS gives a comparable recovery performance much faster than the vertical well CSS. The main reason is that the horizontal well CSS makes better use of gravity flow, which is the main recovery mechanism for this model during thermal recovery processes. Therefore, if the horizontal CSS is used to recover oil from this reservoir, the horizontal well should be placed at the bottom of the permeable, oil-bearing intervals, i.e., Grosmont C and D.

On the other hand, the main drawback of a horizontal well is that the perforation interval is fixed because it is usually a liner completion and the use of packers inside a horizontal well is not effective. As we can see in Fig. 5.2.2.7 of Section 5.2.2.4, only 70% of the well length is heated because of the heterogeneity. If the cold portion of a horizontal well could be efficiently isolated

or a flow control device could be used to evenly distribute the steam, performance of the horizontal well CSS process could be improved.

Table 5.2.2.3a Oil production per production day per metre of perforation length, $m^3/(day \cdot m)$ of the HWCSS Case Q5-2 and VWCSS Case Q6.

	Oil production per production day per metre of perforation length, $m^3/(day \cdot m)$
VWCSS (perforation portion in Grosmont C only)	0.16
HWCSS	0.19

Table 5.2.2.3b SOR and recovery factor of the HWCSS Case Q5-2 and VWCSS Case Q6 given the same cumulative steam injection volume.

	$\frac{\text{Cumulative steam injection volume}}{\text{Initial pore volume}}$	SOR (m^3/m^3)	Recovery factor	Process time (years)
VWCSS	0.3	7	6%	5
HWCSS	0.3	7	5%	1.5

5.3 Steam Assisted Gravity Drainage (SAGD)

5.3.1 Choice of Well Location, Well Length, and Operating Conditions

Based on previous simulation experience, the horizontal well pair placed along the N-S direction, parallel to the top water, is likely to have better recovery performance as its effective drainage area is less connected to the top water (Fig. 4.3.2c and 4.3.3). So in four cases, SAGD, SAGD-1, SAGD-2 and SAGD-3, the well pair was placed in the N-S direction. The base Case SAGD-2 has the well pair placed at the centre of the reservoir (I=15, J=3 to 27) and in cases SAGD, SAGD-1 and SAGD-3 the well pair is shifted closer to the western edge of the reservoir to increase the distance from the top water zone (I=7, J=3 to 27). In one case (SAGD-5), the well pair was placed in the E-W direction (I=3 to 27, J=15) for comparison.

The optimal placement for the production well in a SAGD well pair is the boundary between the high vertical permeability layers above and the low vertical permeability layers below (Fig. 5.3.1) to maximize the oil recovery. As a result, the producer penetrates different layers. Note that the block thicknesses are variable, so for maintaining a vertical well spacing of 5 m the injector also penetrates different layers. In other words, given the grid, the wells cannot be placed in a single layer, for a constant spacing between the wells.

Perforated though eight grid blocks, the length of each well is 125 m for the given geological model. Most of the SAGD wells in Alberta have a length of 1,000 m, so the simulated well pair represents one-eighth of a typical SAGD pair. Accordingly, the scaled steam injection rate is 50 m^3/day in three simulations. In one simulation, Case SAGD-1, the injection rate was doubled to observe the effect of the rate. In another special case, Case SAGD-3, fractures were removed to assess the role of fractures and injection bottomhole pressure was used as the only constraint, instead of a steam injection rate, because of the low steam injectivity.

For all the SAGD cases, preheating is simulated for the first three months to increase the temperature at the mid-point vertically between the two wells to about 100°C, at which oil viscosity is 500 cP. All the cases were conducted for at least 5 years' production time from 1980-4-7 to 1985-6-7. After that, each case was continued for different lengths of time to see the effect of a larger steam injection slug.

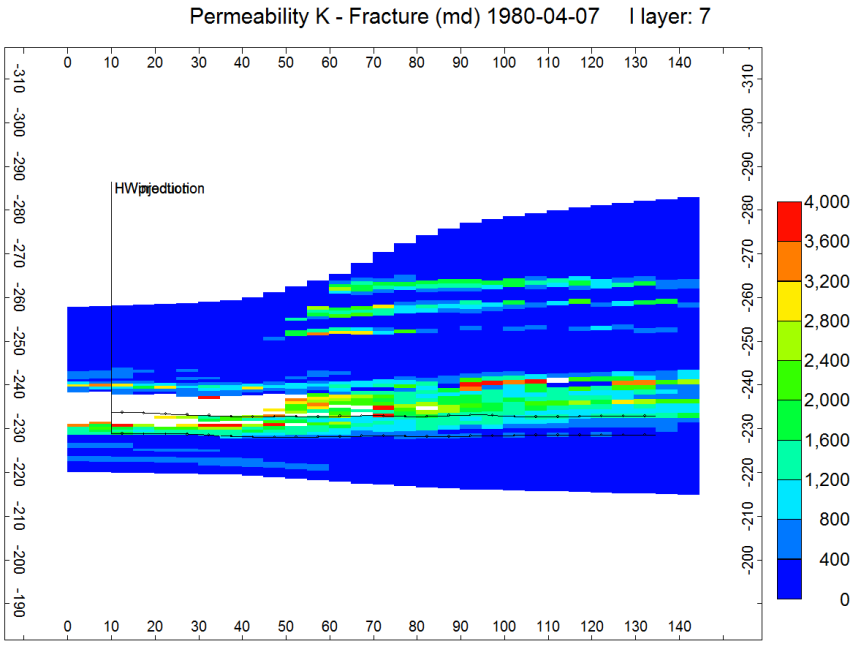

Figure 5.3.1. Vertical fracture permeability distribution of the JK cross-section along the well pair for Case SAGD (I=7). The producer is at the boundary between the high permeability and the low permeability layers. The white portion has a vertical fracture permeability higher than 4,000 mD.

5.3.2 Base Case: SAGD-2 and Improved Case SAGD

After five years' production, the SOR for the base case on the injection of 91,300 m^3 of steam is 9.3 and recovery is 6.96%. In Case SAGD, with a more favourable well location, SOR and recovery are 7.0 and 9.22%, respectively, for the same volume of steam injection.

Figures 5.3.2a and 5.3.3a show the temperature distribution and Figs. 5.3.2b and 5.3.3b show the oil saturation distribution for the two cases at the end of the five years' production. Even though the well pair is off-centre in Case SAGD, it produces more oil than that produced in the base Case SAGD-2. Case SAGD-2 is continued further to 170,902 m^3 of steam injection, however, although the recovery increased to 12.0% and the SOR increased to 10.0.

Fluid flow is by gravity, as also noted for horizontal well CSS cases, and so formation heating above and along the wells and vertical permeability are the key variables. During CSS, the desaturation above the well pair leads to a water saturation increase in the desaturated zone; in the continuous injection–production process, SAGD, there is a water saturation increase at the bottom of the oil-desaturated zone and gas, viz. steam, saturation increases above it (Figs. 5.3.3c and d).

In Case SAGD-5, the well pair is positioned at the centre of the reservoir, in the same layers as in the other cases. The SOR in this case is quite similar to that observed for Case SAGD-2 (9.1 vs. 9.3 for SAGD-2), as is the oil recovery (7.3% vs. 6.8% for SAGD-2).

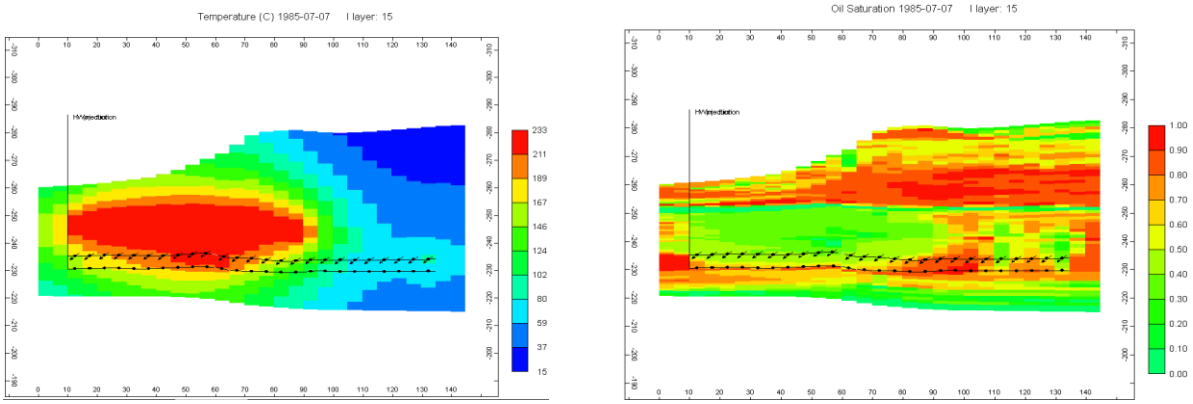

a **b**

Figure 5.3.2. (a) Temperature distribution of Case SAGD-2 at the end of five years' production. (b) Oil saturation distribution of Case SAGD at the end of five years' production.

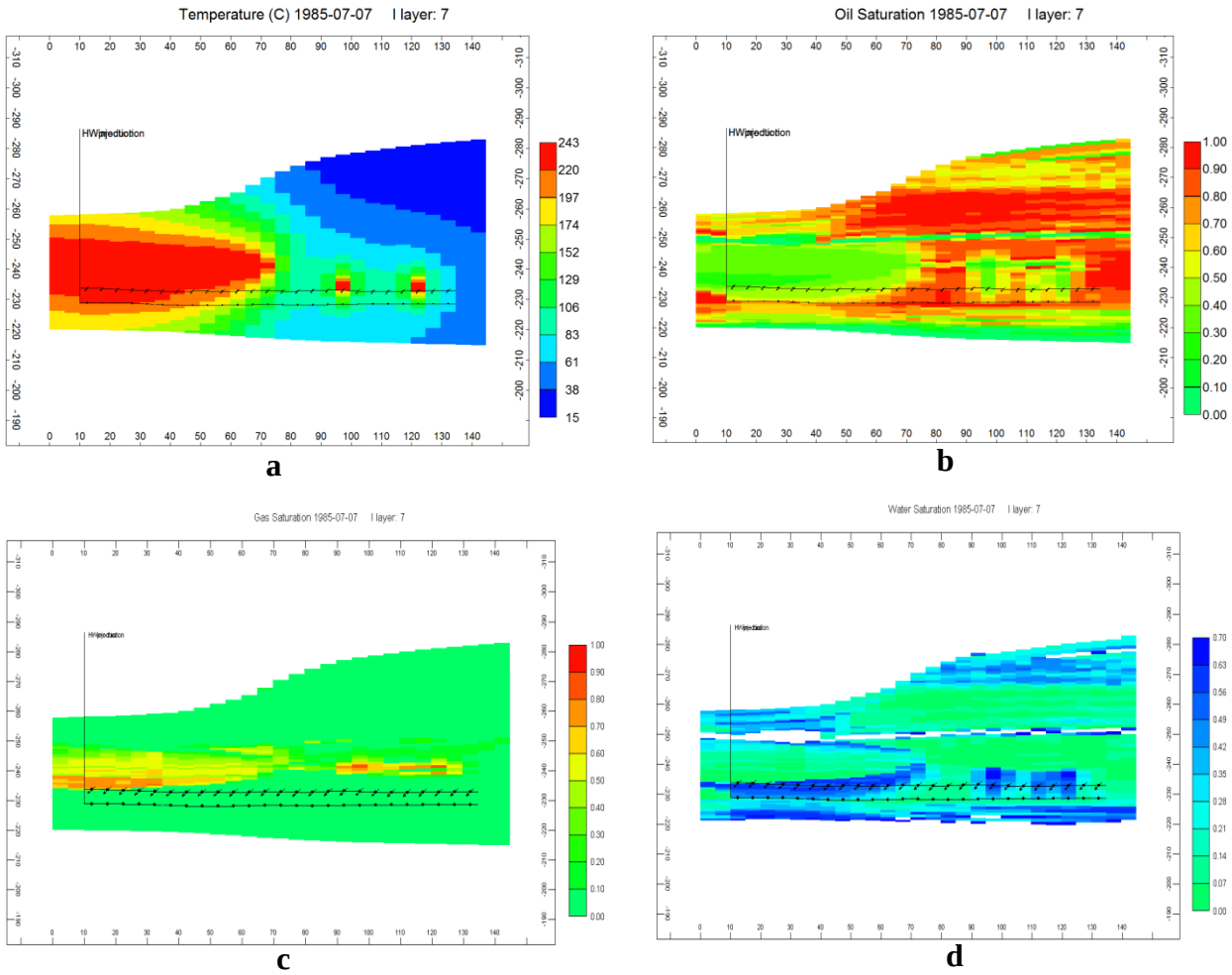

Figure 5.3.3. (a) Temperature distribution for Case SAGD at the end of five years' production. (b) Oil saturation distribution of Case SAGD at the end of five years' production. (c) Gas (i.e. steam) accumulated at the top of the oil desaturation zone. (d) Water accumulated at the top of the oil desaturation zone.

5.3.3 Effect of Steam Injection Rate

In Case SAGD-1, the steam injection rate was increased to 100 m^3/day from 50 m^3/day in other cases. After five years' production, the SOR is 7.3, almost the same as that for Case SAGD (recovery 9.2%), and recovery increased to 17% on the injection of 182,549 m^3 of steam. The SOR and recovery were 9.3 and 22%, respectively, for 293,179 m^3 of steam injection. The oil saturation distribution and temperature distribution after five years' production for the higher rate Case SAGD-1 are shown in Figs. 5.3.4a and b. It is clear that the higher rate is more desirable. Like all steam processes, heat loss decreases with decreased steaming time, leading to higher recovery. Note that the steam injection rate of Case SAGD-1, scaled to a typical SAGD pair would be 800 m^3/day, which is considered to be very high.

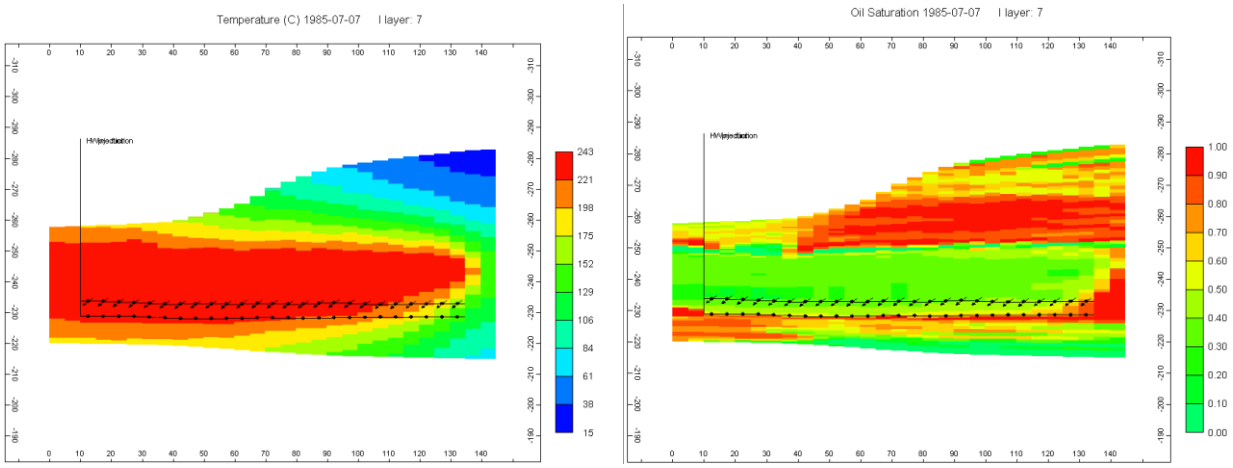

a **b**

Figure 5.3.4. (a) Temperature distribution of Case SAGD-1 at the end of five years' production. (b) Oil distribution of Case SAGD-1 at the end of five years' production.

5.3.4 Effect of Fractures

In Case SAGD-3, fractures are removed to assess the role of fractures. Otherwise, this case is similar to Case SAGD. The SOR was 27 and recovery was 0.86% on the steam injection of 29,708 m^3 for five years' production, and 24.9 and 1.9%, respectively on the steam injection of 62,512 m^3. The oil saturation and temperature distributions at the end are shown in Figs. 5.3.5a and b, and can be compared with Figs. 5.3.3a and b, for Case SAGD. It is seen that the oil saturation of Case SAGD-3 does not change much before and after production. Unlike other simulations, in the no-fracture case, the SOR slightly decreases with time, as the steam injection is low and the heating process takes longer to mobilize the oil in this case. The role of fractures is clearly important, as they provide flow paths into the producer, and also into the formation. The matrix does not have a high enough permeability to accomplish that. The temperature profiles show that the fractures are also effective in improving heating of the formation. This is somewhat unexpected because normally fractures are considered to have an adverse effect on SAGD performance.

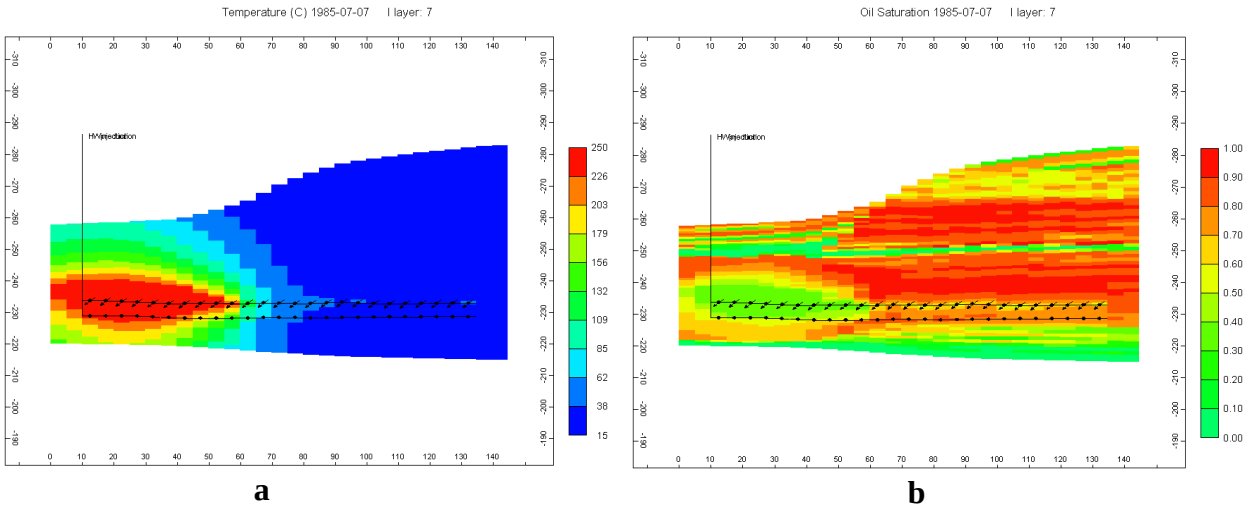

Figure 5.3.5. (a) Temperature distribution of Case SAGD-3 at the end of five years' production. (b) Oil distribution of Case SAGD-3 at the end of five years' production.

It should be noted that in one of the horizontal well CSS cases (Section 5.2.2.3), fractures were removed for comparison; it was found that the injection rate declined to extremely low rates of the order of 20 m^3/day, and the resulting oil recovery was nearly zero. The injection rates for the six cycles are shown in Fig. 5.2.2.5 for HWCSS.

5.3.5 Overall SAGD Evaluation

Tables 5.3.1a and 5.3.1b compare the typical HWCSS Case Q5-2 with the typical SAGD Case SAGD based on the oil production per production day per metre of perforation length and the same cumulative steam injection volume, respectively. As we can see HWCSS is more productive than SAGD. As demonstrated in Sections 5.2.2.3 and 5.3.4, fractures provide the main fluid flow paths in this heavily dolomitized reservoir. Because the fractures are mostly vertical to subvertical, gravity drainage is observed to be the main drive mechanism during every steam injection process

applied to this reservoir. However, the oil gravity flow in the vertical/subvertical fractures of Grosmont reservoir is different from the oil gravity flow in oil sands. During the SAGD process applied to oil sands, steam propagates to oil sands as a steam chamber and the oil flows to the producer by gravity flow along the edge of the steam chamber. For the Grosmont carbonate reservoir, because of the great contrast between the primary porosity system (mostly dolomite), and the secondary porosity system (fractures and vugs), oil flows to the producer mainly through the vertical/subvertical fractures during any steam injection process. For this reason, a steam chamber hardly forms during SAGD for the Grosmont reservoir. In addition, during the continuous injection-production though two parallel horizontal wells of the SAGD process, the overriding steam flow counters the downward oil flow in the same path. While during the HWCSS, production is conducted after injection. This is why SAGD is less productive than HWCSS for Grosmont carbonate reservoir.

Table 5.3.1a Oil production per production day per metre of perforation length, $m^3/(day \cdot m)$ of the HWCSS Case Q5-2 and SAGD Case SAGD.

	Oil production per production day per metre of perforation length, $m^3/(day \cdot m)$
SAGD	0.04
HWCSS	0.19

Table 5.3.1b SOR and recovery factor of the HWCSS Case Q5-2 and SAGD Case SAGD given the same cumulative steam injection volume.

	$\frac{\text{Cumulative steam injection volume}}{\text{Initial pore volume}}$	SOR (m^3/m^3)	Recovery Factor	Process Time (Years)
SAGD	0.9	10	13%	10
HWCSS	0.9	7	18%	4.5

5.4 Pattern Steamfloods

5.4.1 Five-spot Pattern Steamflood

5.4.1.1 Pattern selection and perforations

This simulation model has $29 \times 29 \times 62$ (I, J, K) grid blocks, and the grid block size is 5m in the I and J directions. So the lateral area of this model is $(29 \times 5)^2 = 21{,}025\ m^2 = 5.2\ acres$. Two pattern sizes of five-spot steamflood are simulated. In one case, Case Y9B-2E, this simulation model is used as one-quarter of a 20-acre repeated five-spot pattern. Steam is injected from the southwest corner and produced from the northeast corner during the first three years, and then switched to injection from the southeast corner and production from the northwest corner. Both the injector and the producer are quarter wells (Fig. 5.4.1.1). In Case Y8-3F-2C-1G-1J and its improved version Y8-3F-2C-1G-1H-1C, one injector is placed at the centre of the reservoir and one producer (quarter well) at each of the four corners to simulate a 5-acre five-spot steamflood (Fig. 5.4.1.2).

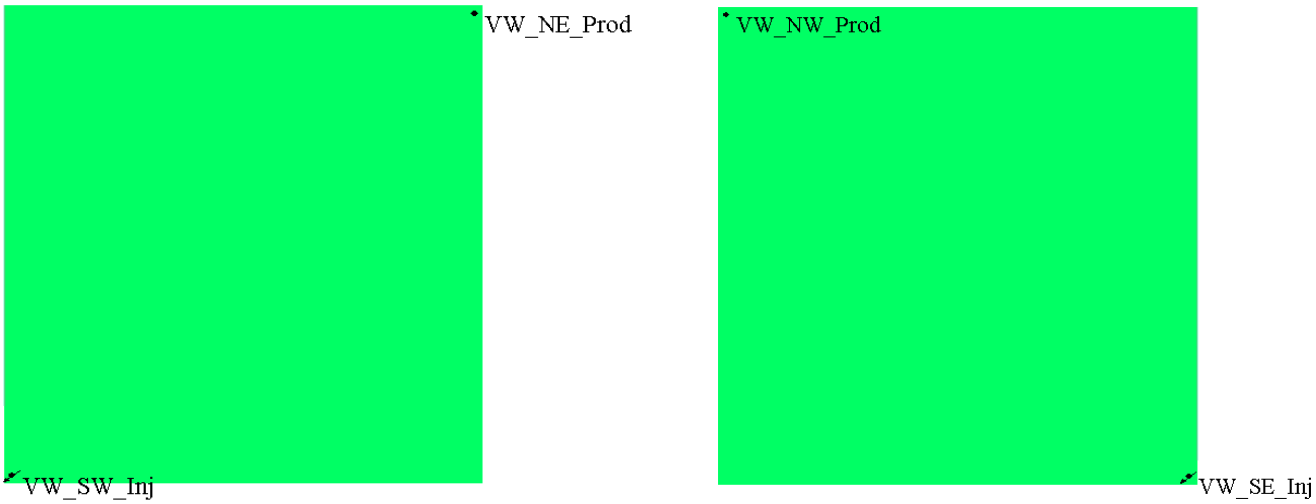

Figure 5.4.1.1 Well configurations of the 20-acre five-spot steamflood case, Case Y9B-2E. A repeated 20-arce five-spot pattern. Note the quarter wells at each corner.

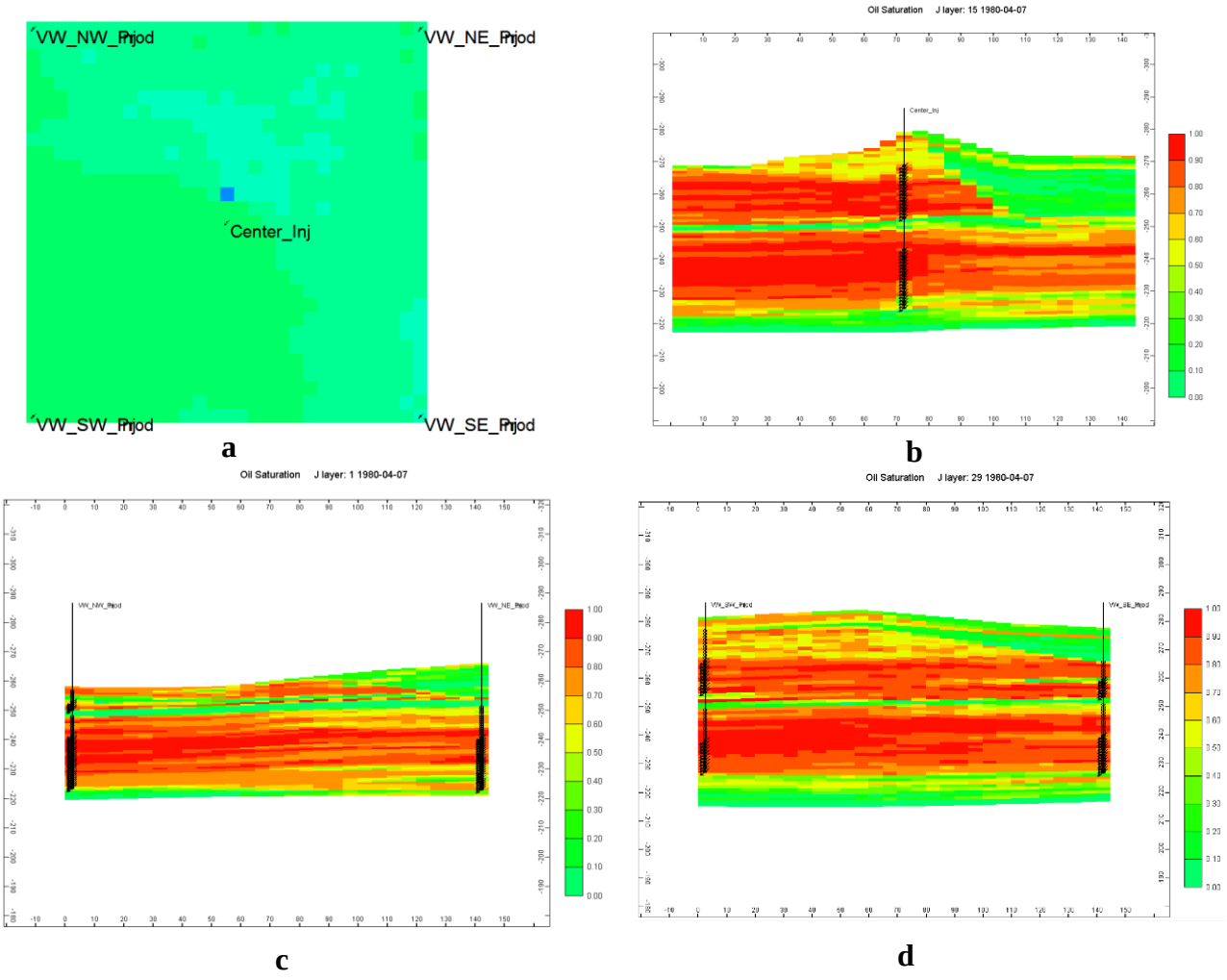

Figure 5.4.1.2. (a) Well configurations of the 5-acre five-spot steamflood case, Case Y8-3F-2C-1G-1J. A repeated 5-arce five-spot pattern. Note the quarter wells at each corner. (b) Initial perforation interval of the centre injector of the five-spot steamflood case, Y8-3F-2C-1G-1J. (c) Initial perforation interval of the producers of the five-spot steamflood case, Case Y8-3F-2C-1G-1J. The injection perforations are only for the steam stimulation in the first 61 days of the process. (d) Initial perforation interval of the producers of the five-spot steamflood case, Case Y8-3F-2C-1G-1J. The injection perforations are only for the steam stimulation in the first 61 days of the process.

In all five-spot steamflood simulation cases, injectors and producers are perforated into both above (Grosmont D member) and below (Grosmont C member) the middle tight streak, in order to contact the largest possible volume of oil. Considering steam override, while producers are perforated into the entire oil-bearing zones, the injector is perforated near the base of the oil-bearing zones.

The simulation starts on 1980-4-7. Because of the high oil viscosity and model heterogeneity, producers have to be initially steam-stimulated. During the first 61 days of Case Y8-3F-2C-1G-1J, a steam injection rate of 500 m^3/day and bottomhole pressure of 4,500 kPa are used to stimulate the producers, after which the producers are switched to production. Steam is continuously injected into the centre injector, with a bottomhole pressure of 5,000 kPa and a steam injection rate of 500 m^3/day. In the 20-acre repeated five-spot pattern, Case Y9, steam is injected into both the injector and the producer at 400 m^3/day during the first 30 days. The producer is then switched to production and the injector is kept on. It continued injecting steam from the southwest corner and producing from the northeast during the first three years and then switched to the "southeast injection, northwest production" mode.

5.4.1.2 Simulation cases

For the 5-acre five-spot pattern steamflood simulation cases, severe steam override, early steam breakthrough, and dominant gravity drainage are observed. Due to these fluid flow characteristics during this process, two methods, (i) closing upper perforations and (ii) reducing the steam injection rate with time, are used to optimize the recovery performance.

The steam injection, oil and water production rate curves for the 5-acre five-spot steamflood Case Y8-3F-2C-1G-1J are shown in Fig. 5.4.1.3a, and the injection rate of each producer during the first 61 days' steam stimulation is shown in Fig. 5.4.1.3b. As seen in Fig.5.4.1.3b, the injection rate varies from one well to another due to the injectivity difference. The field oil production rate curve in Fig. 5.4.1.3a shows that after the simulation period, there are oil rate peaks as a result of cyclic steaming. However, the oil rate declines rapidly to almost zero for 2 months, after which, as a continuous connection forms between the injector and the producer, it increases and stays at a low level of 50 m^3/day until 1982-3-22, i.e., two years' production.

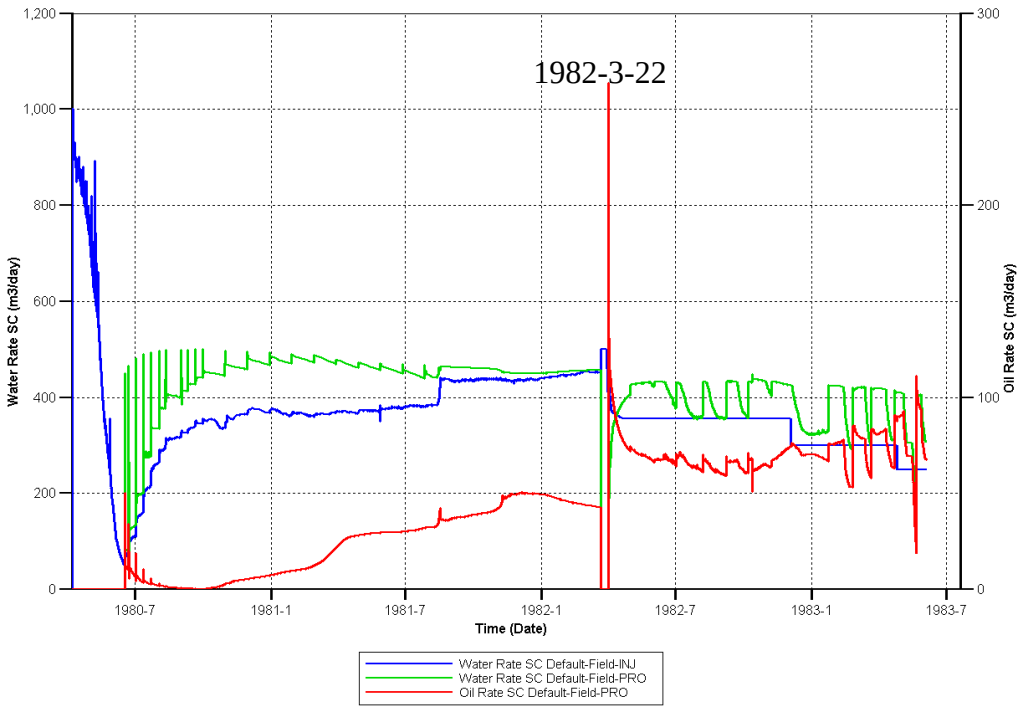

Figure 5.4.1.3a. The steam injection, oil and water production rate curves of the 5-acre five-spot steamflood Case Y8-3F-2C-1G-1J.

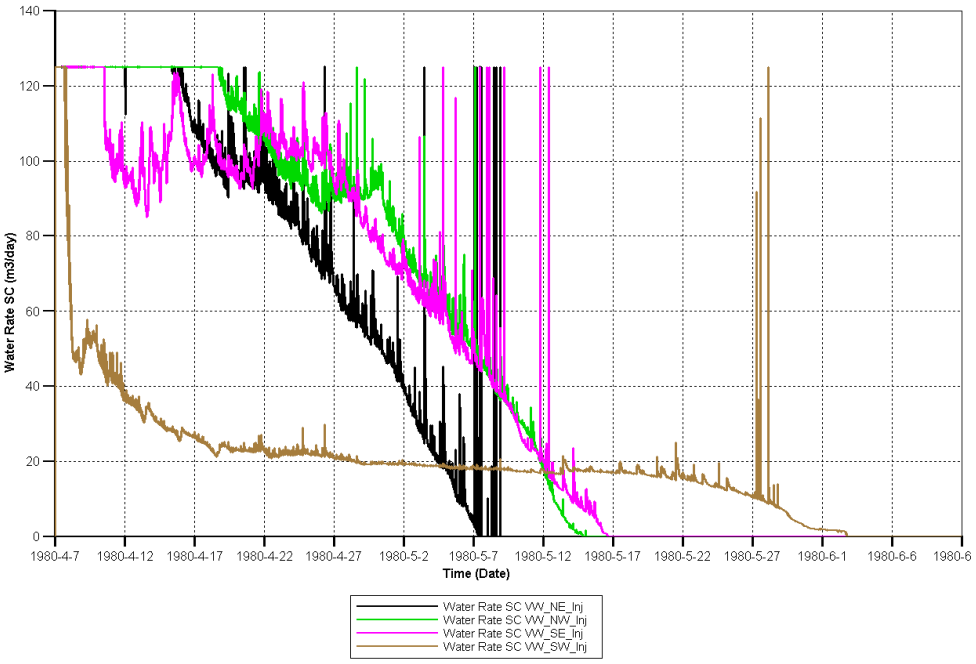

Figure 5.4.1.3b. The injection rate of each producer during the first 61 days' steam stimulation.

Two changes were made to improve recovery after 1982-3-22. One was to close the upper perforations in the injector and producers. As can be seen from the gas saturation, the mole fraction of water in gas saturation, temperature and oil saturation profiles on 1982-3-22, there is severe steam override in the oil intervals above (Grosmont D member) and below (Grosmont C member) the middle tight streak. Grosmont D member gets sufficiently heated and mostly depleted (Fig. 5.4.1.4). However, in the Grosmont C member, steam only flows towards the top layers and keeps rising up towards the top water in Grosmont D. As shown in Fig. 5.4.1.4a, b, and c, although temperature at the top can rise to 264℃, a considerate portion of the lower layers is still cold. Therefore, in both formation members, oil has only been depleted from a limited region at the top. To force steam to go through the cold layers of Grosmont C member, from 1982-3-22, injector perforations in Grosmont D and upper layers of Grosmont C are closed, leaving only 40% of the

perforated intervals open. Also, producer perforations in the oil-depleted layers are closed to help enhance the steamflood in the depleted zones (Fig. 5.4.1.5 a, b, and c).

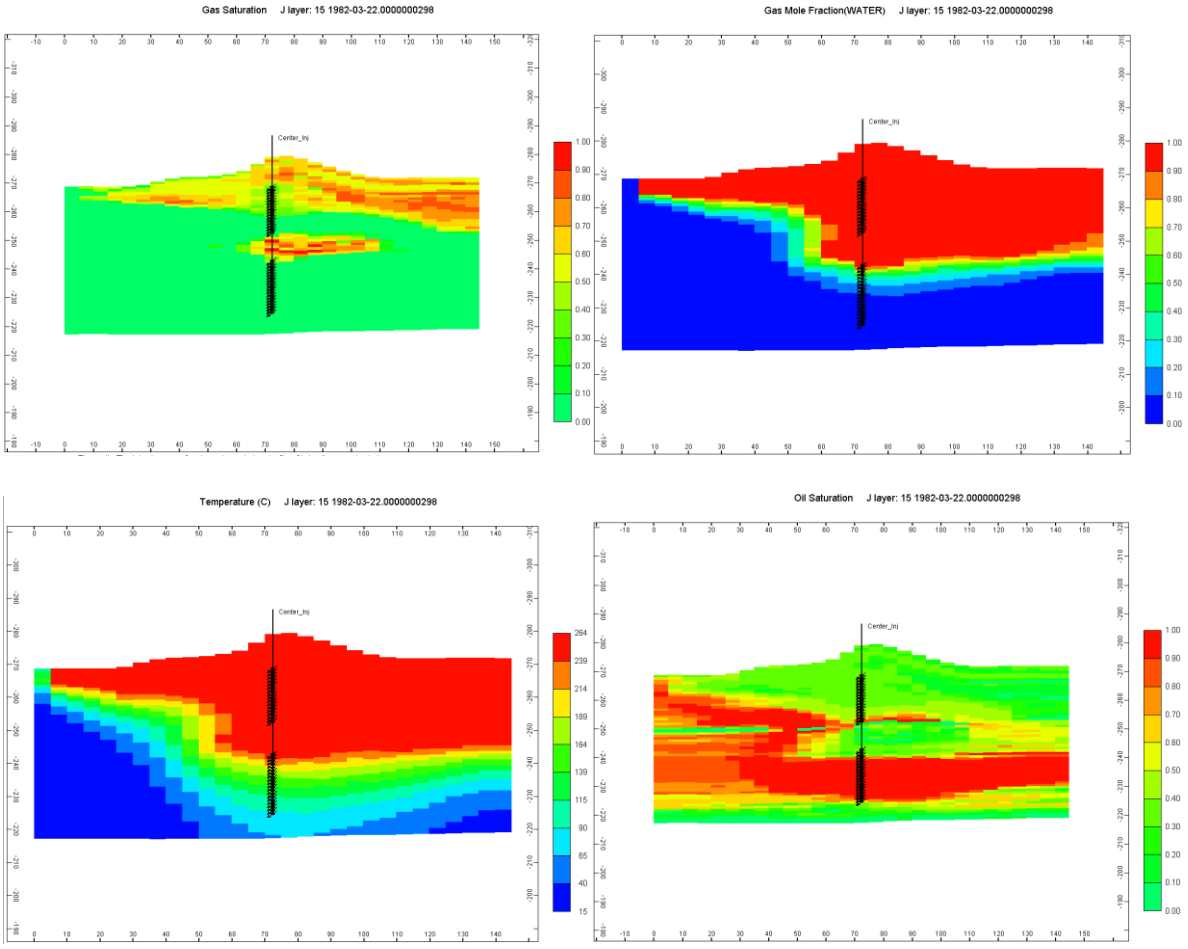

Figure 5.4.1.4a. The gas saturation, mole fraction of water in gas saturation, temperature and oil saturation profile of the cross-section across the centre injector of Case Y8-3F-2C-1G-1J on 1982-3-22.

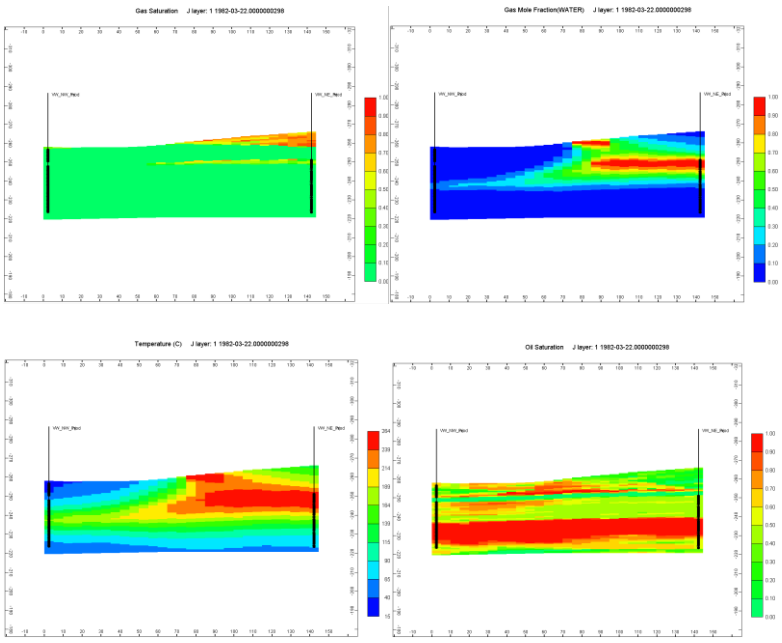

Figure 5.4.1.4b. The gas saturation, mole fraction of water in gas saturation, temperature and oil saturation profile of the cross-section across the producers in the north of Case Y8-3F-2C-1G-1J on 1982-3-22.

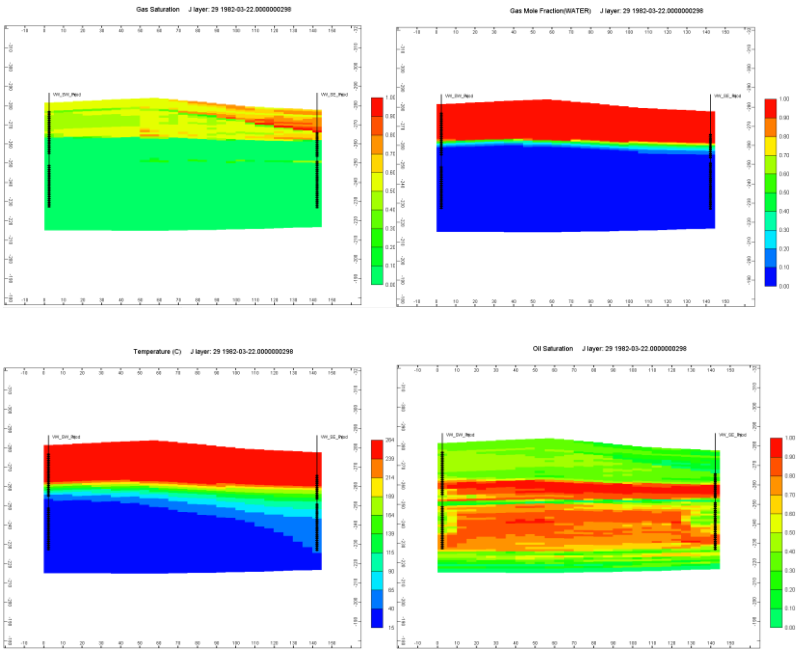

Figure 5.4.1.4c. The gas saturation, mole fraction of water in gas saturation, temperature and oil saturation profile of the cross-section across the producers in the south of Case Y8-3F-2C-1G-1J on 1982-3-22.

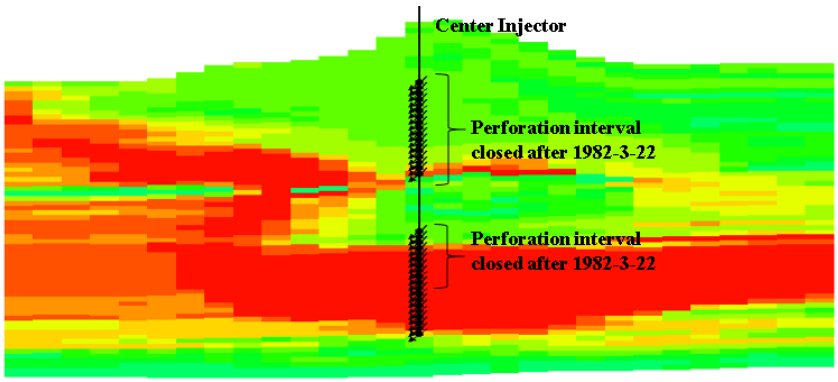

Figure 5.4.1.5a. The portion of the injector perforation closed on 1982-3-22, after two years' production of the 5-acre five-spot pattern steamflood Case Y8-3F-2C-1G-1J.

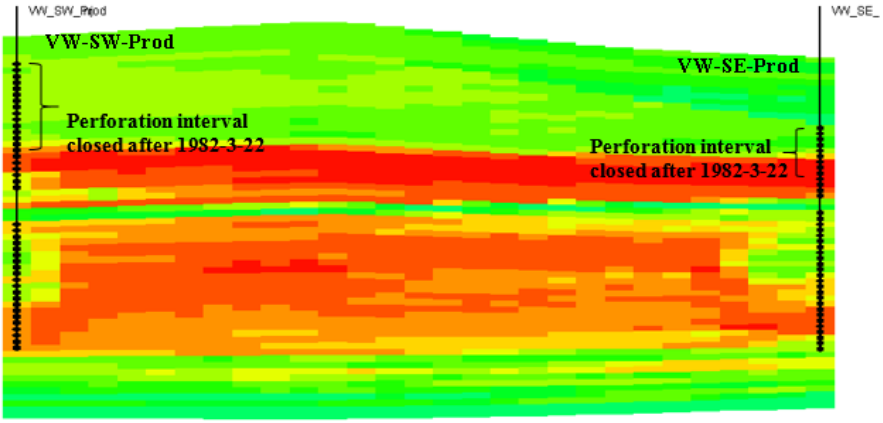

Figure 5.4.1.5b. The portion of the producer perforation closed on 1982-3-22, after two years' production of the 5-acre five-spot pattern steamflood Case Y8-3F-2C-1G-1J.

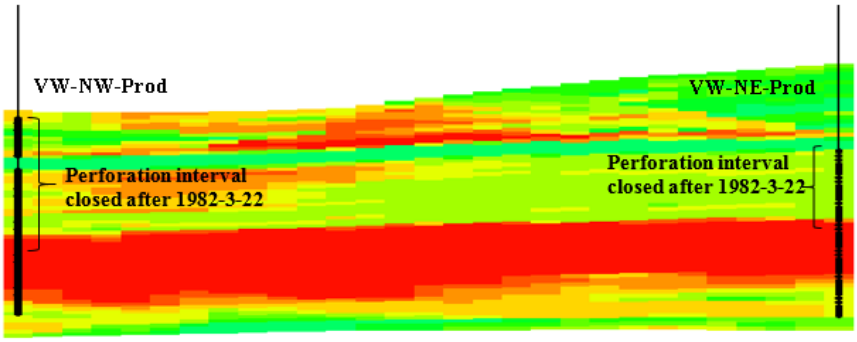

Figure 5.4.1.5c. The portion of the producer perforation closed on 1982-3-22, after two years' production of the 5-acre five-spot pattern steamflood Case Y8-3F-2C-1G-1J.

The other change is to reduce the steam injection rate. As we can see from the steam injection and oil production rate curves (Fig. 5.4.1.3a), after 1982-3-22, the steam injection rate is reduced from 500 m^3/day to 355 m^3/day on 1982-4-23, to 300 m^3/day on 1982-12-4, and to 250 m^3/day on 1982-4-25. The reason for this is that having injected a cumulative steam volume of 40,000 m^3, twice the initial pore volume, the reservoir should have already been heated as well as it could be. On the other hand, as the early steam breakthrough makes the bottomhole pressure of the injector and producers so close (Fig. 5.4.1.6), gravity flow is dominant in this process. For this reason, reducing the steam injection rate does not slow down oil recovery but helps to improve the recovery performance as the upward moving steam stream countered by the downward oil gravity flow is slowed down.

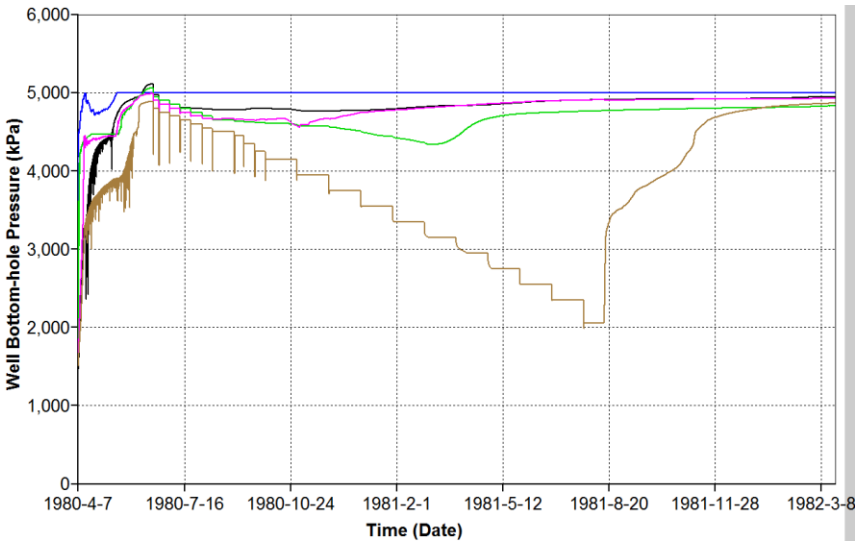

Figure 5.4.1.6. Bottomhole pressure curves of the injector and producers of the 5-acre five-spot steamflood Case Y8-3F-2C-1G-1J. Bottomhole pressure of the centre injector is plotted in blue, the northeast producer in black, the northwest producer in green, the southeast producer in purple, the southwest producer in brown.

The above two changes proved to have a positive effect on the oil rate. As shown in Fig. 5.4.1.3a; after closing upper perforations and reducing the steam injection rate by stages, the oil rate is lifted to a higher level and stays relatively steady.

As reducing the steam injection rate is efficient, another restart case of the 5-acre five-spot steamflood, Case Y8-3F-2C-1G-1H-1C, was conducted using the steam injection rate reduction calculation to further improve the performance (see Section 5.4.4.2).

Looking at the oil production rate curves of each producer (Fig. 5.4.1.7), the production well at the southwest corner has the lowest oil rate, because permeability is also lower in this corner and steam preferentially channels to the east leaving the southwest insufficiently heated.

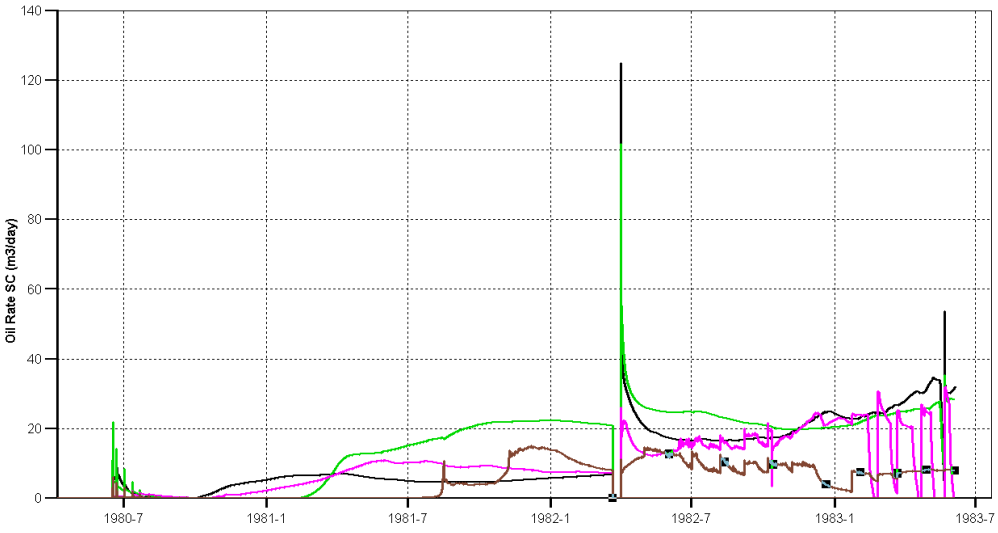

Figure 5.4.1.7. Oil production rate curves of producers of the 5-acre five-spot steamflood Case Y8-3F-2C-1G-1J. Oil production rate of the northeast producer is plotted in black, the northwest producer in green, the southeast producer in purple, the southwest producer in brown.

5.4.1.3 Oil recovery and SOR

The 5-acre five-spot steamflood Case Y8-3F-2C-1G-1J is continued until 1983-6-5, for about 3-year production. Although the recovery factor is relatively high, 33%, SOR is 9 m^3/m^3. The high SOR indicates steam over-injection, which can be appreciated from the fact that the produced enthalpy represents 46.3% of the injected enthalpy. However, the SOR curve is still declining at the end of the case. If there was sufficient CPU time to test other optimization schemes in terms of perforation interval and a steam injection rate with time, a lower SOR could have been obtained.

5.4.1.4 Effect of well spacing

In Case Y9B-2E, the area of the five-spot was increased by a factor of 4, so that now the injector and producer are quarter wells (Fig.5.4.1.1). Initially injection is from the southwest corner and production from the northeast corner. The oil rate increase in the first five months is essentially the result of cyclic steaming as we inject into the producer for one month before production, followed by a rapid oil rate decline (Fig. 5.4.1.8). The long no-production period followed by a slight increase in the oil rate indicates that it takes a long time to form a continuous connection between the producer and the injector. For this reason, it was decided to inject from the southeast corner and produce from the northwest corner to increase oil production. The oil rate rises after the steamflood is switched to the other diagonal but then stays at a low level until the end of five years' production. Heating was insufficient, and steam override led to excessive heat loss early in the operation. The final SOR was 133 and the recovery factor was 1.05%. This simulation case, compared to the previous 5-acre five-spot steamflood cases, shows the critical importance of well spacing in a conventional pattern steamflood.

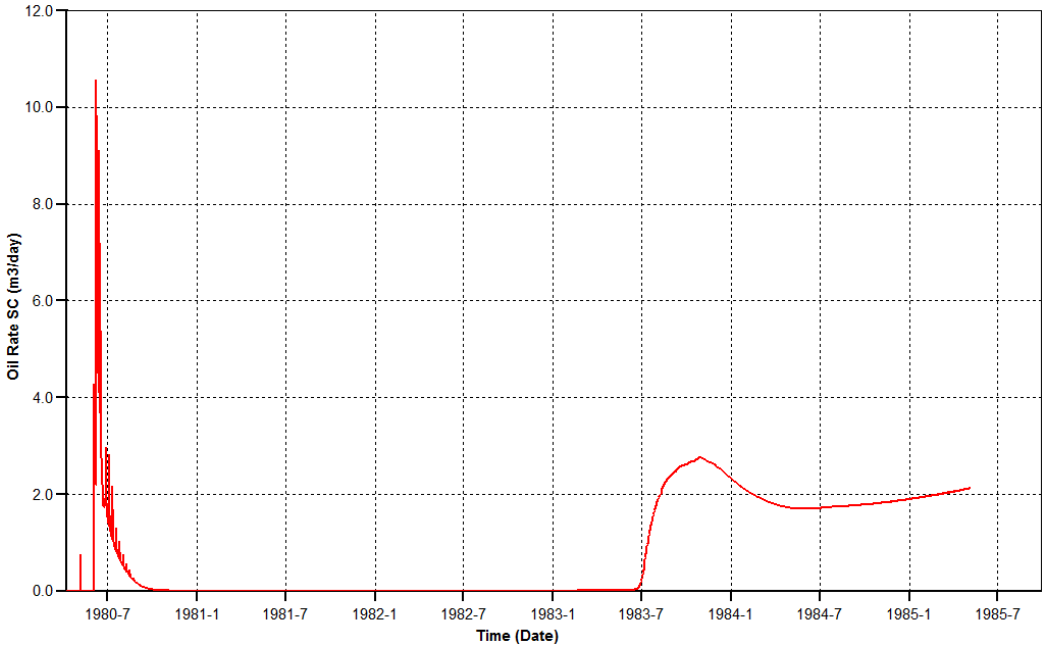

Figure 5.4.1.8 Oil production rate for the 20-acre five-spot pattern steamflood Case Y9-2E.

5.4.2 Nine-spot Pattern Steamflood

5.4.2.1 Pattern selection and perforations

As noted above, in steamflooding, often one producer cannot provide enough voidage to support the steam injection rate, leading to an increase in the steam injection pressure, and a decline in rate. A repeated nine-spot pattern has three producers for one injector, and thus has a much better chance of supporting the design steam injection rate. In practice, all wells may be drilled at the start, if past experience is favourable. In other instances, the wells on the sides of the patterns may be added later.

In the nine-spot steamflood case, Case Y15-2A-1B-1D-1B, this simulation model is used to simulate a 5-acre nine-spot repeated pattern. There is one injector in the centre and eight producers at the side of this square model (Fig. 5.4.2.1a). Each producer at the corner is a quarter-well and

each producer in the middle of a side is a half-well. The injectors and producers are perforated into both above (Grosmont D member) and below (Grosmont C member) the middle tight streak to contact the largest possible volume of oil. Considering steam override, while producers are perforated into the entire oil-bearing zones, the injector is perforated in the lower levels of the oil-bearing members (Fig. 5.4.2.1b). The process starts at 1980-4-7 and ends at 1985-5-7. Steam is continuously injected into the centre injector at the initial rate of 500 m^3/day, and injection pressure of 5,000 kPa. Producers are steam stimulated under the same circumstances as the injector during the first 61 days before being switched to production. The initial flow bottomhole pressure is set 50 kPa lower than the bottomhole pressure at the beginning of production and then gradually reduced with time. As the ratio of the number of producers to injectors is 3:1, liquid production is defined as one-third of the injection rate.

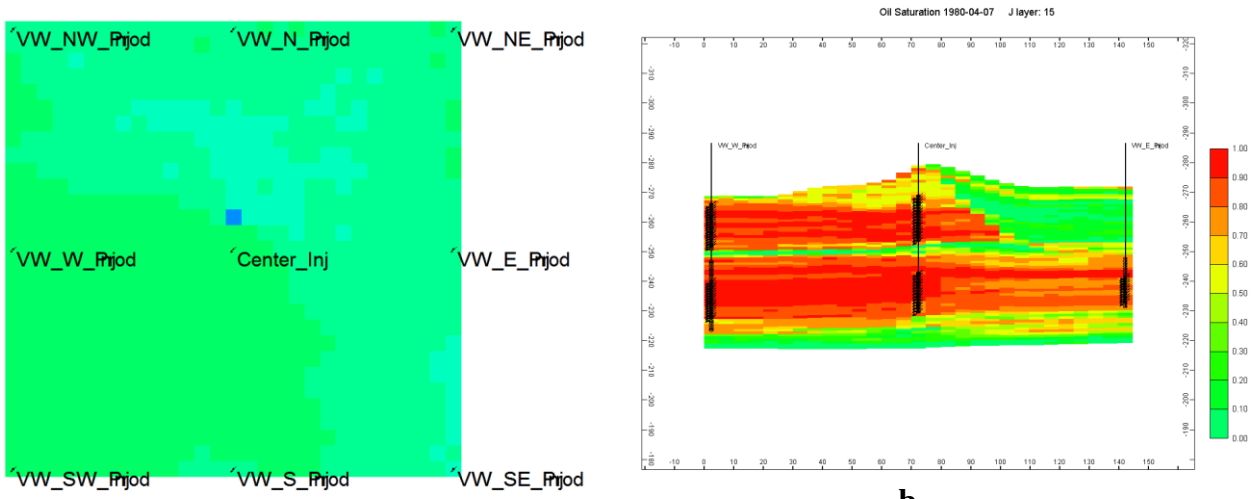

Figure 5.4.2.1. (a) Well configurations of the nine-spot steamflood Case Y15-2A-1B-1D-1B. A repeated 5-arce nine-spot pattern. Note the wells at each corner are quarter-wells; the wells at the middle of each side are half-wells. (b) Initial perforation intervals of the centre injector and two producers in the IK cross-section across the injector of the nine-spot steamflood Case Y15-2A-1B-1D-1B. The injection perforations in producers are only for the steam stimulation in the first 61 days of the process.

5.4.2.2 Simulation cases

As observed for the five-spot pattern steamflood simulation cases, severe steam override, early steam breakthrough, and dominant gravity drainage also occur during the nine-spot pattern steamflood. The process is optimized by closing upper perforations and reducing the steam injection rate with time.

Figure 5.4.2.2a shows the steam injection rate, oil and water production rate for Case Y15-2A-1B-1D-1B and Fig. 5.4.2.2b shows the production rate of all producers. Immediately after steam stimulation, there are oil production peaks in every producer, after which the oil rate varies considerably from one well to another. As we can see, active producers are all on the eastern side where steam channels into the top water. To improve oil production, wells on the western edge of the model are steam stimulated again during 1981-10-21 to 1981-11-12 and switched to production.

The total oil production rate stays at about 45 m^3/day before 1982-5-7, when again two changes are made to improve recovery. One is to close the upper perforations of the injector and the producers. All perforations in Grosmont D and upper perforations in Grosmont C of the injector are closed. So are the upper perforations in the depleted layers of producers. The other change is to decrease the steam injection rate from 500 m^3/day to 75 m^3/day according to an over-injection calculation. As a result, the total oil rate is raised and stays at a higher level of 100 m^3/day for the following 6 months. After that, it gradually declines to about 10 m^3/day at the end of 5 years' production (Fig.5.4.2.2a).

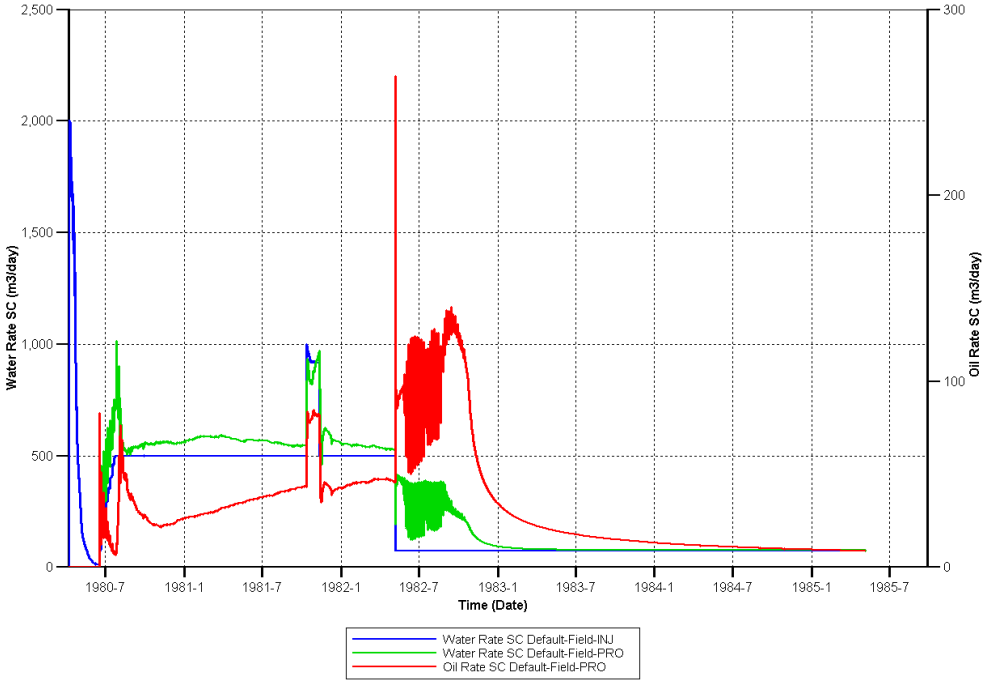

Figure 5.4.2.2a. The steam injection, oil and water production rate curves of the 5-acre nine-spot steamflood Case Y15-2A-1B-1D-1B.

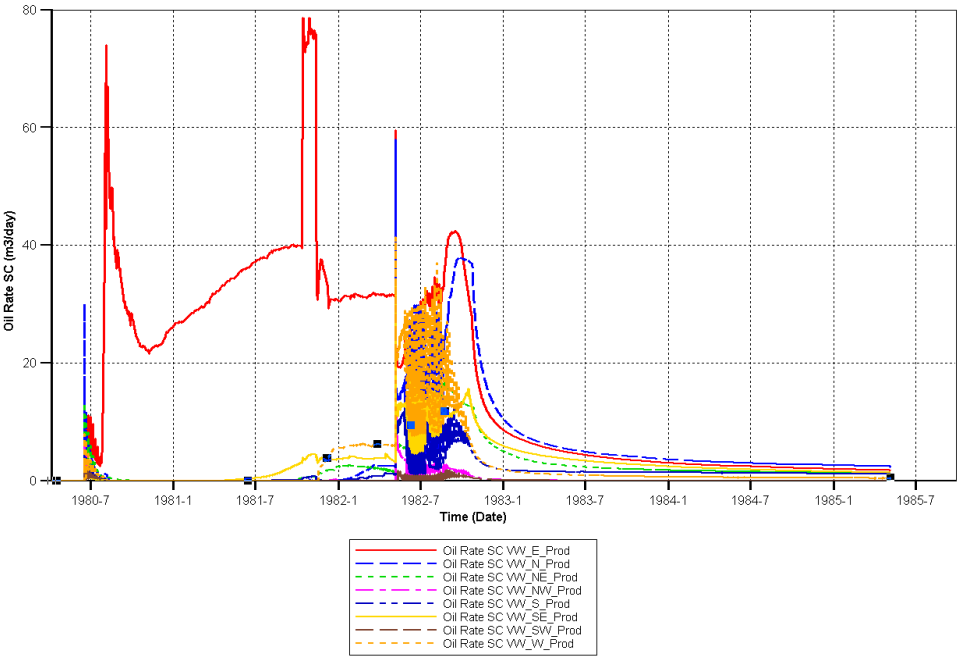

Figure 5.4.2.2b. Oil production rate of each producer of the 5-acre nine-spot steamflood Case Y15-2A-1B-1D-1B.

5.4.2.3 Oil recovery and SOR

For the nine-spot pattern steamflood Case Y15-2A-1B-1D-1B, an SOR of 8 m^3/m^3 and an oil recovery factor of 41% are obtained at the end of the five years' production. The final ratio of the produced enthalpy to injected enthalpy is 0.6. Note that this ratio is already 0.5 at 1982-5-7, before reducing the steam injection rate. The increase of this ratio is slowed down very much after that. If the over-injection calculation was done and the steam injection rate reduced at an earlier time and through more stages, the steam utilization could have been much better and SOR could have been reduced further.

5.4.3 Seven-spot Pattern Steamflood

5.4.3.1 Pattern selection and perforations

A repeated seven-spot pattern has an injector-to-producer ratio of 1:2. It has been used in a number of steamfloods in California, Venezuela, and Alberta. Another feature of a seven-spot pattern is that the wells are equidistant from the injector, so that the flow is closer to radial flow than in any other pattern. At the same time, it should be noted that infill drilling in a seven-spot is more complicated than in a five-spot or nine-spot pattern.

For the present study, two seven-spot configurations were fitted into the model area, as shown in Figs.5.4.3.1a and 1b. In one configuration, the seven-spot principal axis (i.e., I-axis) followed an east-west direction in Case Y16 (Fig. 5.4.3.1a). In the other configuration, the axis was rotated 90 degrees, so that it followed a north-south direction (Fig. 5.4.3.1b). This was done to assess the effect of geology on pattern configuration. Blocks beyond the pattern in both cases were nulled. The resulting patterns had an area of 4.3 acres. The small area led to quick pattern flood-out.

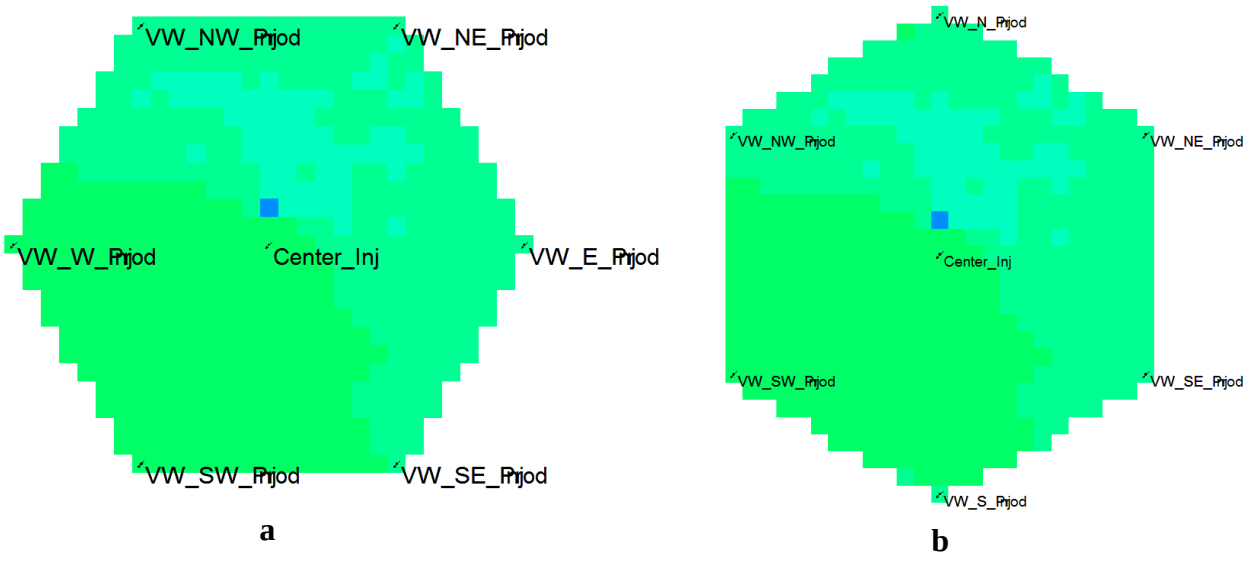

Figure 5.4.3.1. (a) Repeated 4-acre seven-spot pattern of the seven-spot pattern steamflood Case Y16. (b) Repeated 4-acre seven-spot pattern of the seven-spot pattern steamflood Case Y17.

The injectors and producers are perforated both above (Grosmont D member) and below (Grosmont C member) the middle tight streak to contact the largest possible volume of oil. Considering steam override, while the injector is perforated in the entire oil-bearing zones, the producers are perforated near the base of the oil-bearing members (Fig. 5.4.3.2). All simulated processes start from 1980-4-7. In both cases, the injection pressure is 5,000 kPa and the injection rate is initially 500 m^3/day. The producers are steam stimulated at 500 m^3/day, 5,000 kPa during the first 61 days. The initial flowing bottomhole pressure is set at 50 kPa lower than the injector bottomhole pressure at the beginning of production for each producer and gradually reduced with time. As there are two producers supporting one injector in the seven-spot pattern, the liquid production rate is defined as one-half of the injection rate for each producer.

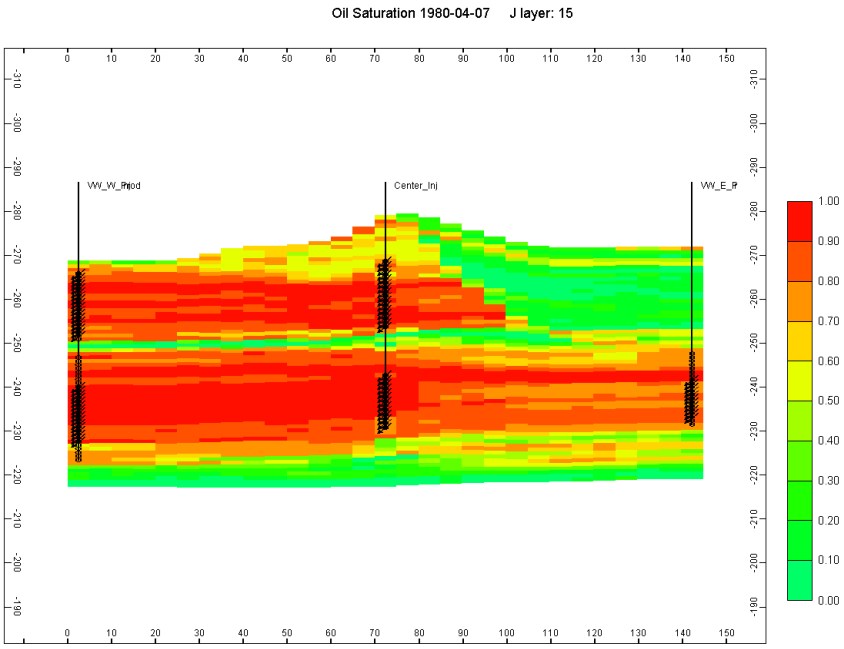

Figure 5.4.3.2. Initial perforation intervals in the centre injector and two producers in the IK cross-section across the injector of the seven-spot steamflood case, Case Y16. The injection perforations in producers are only for the steam stimulation during the first 61 days of the process.

5.4.3.2 Simulation cases

Table 5.4.3.1 shows the SOR and recovery factor for these two cases, with different hexagons. Although the operational parameters are the same, the SOR and recovery factor for Case Y16 are better than for Case Y17. The difference in recovery performance between these two cases gives an idea of how much impact the geology has on the process performance.

Table 5.4.3.1. Oil recovery and steam-oil ratio of the two seven-spot pattern steamflood cases after three year' production.

	Oil Recovery (%)	Steam-oil Ratio
Y16	28	17
Y17	26	19

Restricted by the long CPU time and a limited number of computers, only Y16 was continued further. As can be seen from Fig. 5.4.3.3, after the oil production rate peaks as a result of steam stimulation, the oil rate declines and then gradually increases to about 30 m^3/day as the producers again get connected with the mobile oil.

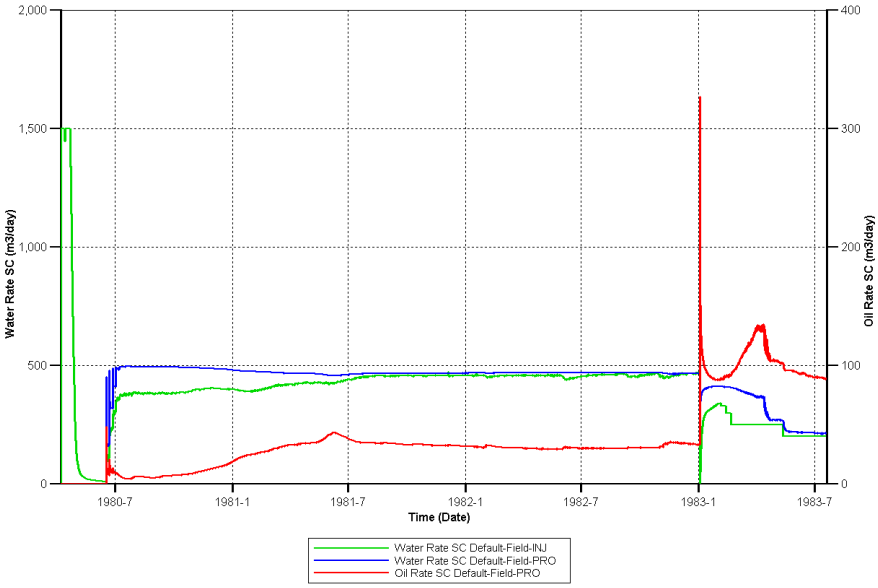

Figure 5.4.3.3. The steam injection, oil and water production rate curves for the 4-acre seven-spot steamflood Case Y16.

Steam override, early steam breakthrough and dominant gravity flow are also observed for the seven-spot pattern steamflood. To improve recovery, again two changes were made from 1983-1-3. One is to close the upper perforations of the injector and producers. All perforations in Grosmont D and upper perforations in Grosmont C of the injector are closed. So are the upper perforations in the depleted layers of producers. The other way is to decrease the steam injection rate from 470 m^3/day on 1983-1-2 to 200 m^3/day on 1983-6-28 through several stages. As a result,

the oil rate is increased to about 100 m^3/day in the following 6 months. This case was terminated on 1983-7-20 after three years' production.

5.4.3.3 Oil recovery and SOR

Although the oil recovery is relatively high, 45%, SOR at the end of three years' production is 10.7 m^3/m^3. The ratio of enthalpy produced to enthalpy injected is 0.6 at the end of production.

5.4.4 Performance Optimization of the Pattern Steamfloods

Under the circumstance that steam override and oil gravity flow are the main fluid flow streams, closing perforations and reducing the steam injection rate at proper times during the process proved to be efficient optimization methods for the pattern steamfloods.

5.4.4.1 Closing perforations with time

Affected by a combination of high vertical fracture permeability and top water on the eastern top, although the injector is perforated through oil intervals, respectively, in Grosmont C and D members, steam flows upward and accumulates at the top of each member. This steam override can be seen from the gas saturation, water fraction of gas and temperature profile of the cross-section across the injector at 1982-3-22 of the five-spot steamflood case, Y8-3F-2C-1G-1J (Figs. 5.4.1.4 a, b, and c in Section 5.4.1.2). As a result, oil is depleted only from the top of each member (Figs. 5.4.1.4 d in Section 5.4.1.2). As we can see from the oil saturation profile, at this moment, oil in Grosmont D member is mostly depleted because steam injected from both members flows upward and accumulates there. However, most of the oil in the lower layers of Grosmont C member is still unrecovered and the temperature there is still low, 20~150℃.

On 1982-3-22, after about two years' production, in order to force steam to go through the lower perforations, injector perforations in the Grosmont D are all closed as well as the upper perforations in the Grosmont C member. Only the lower 40% of the perforation interval is kept open (Fig. 5.4.1.5a in Section 5.4.1.2). Also, perforations in the oil-depleted layers of producers are closed considering that the mobilized oil can flow from the top to the open perforations in the dominant gravity flow and helps to form the steamflood in the not depleted layers (Figs. 5.4.1.5b and c in Section 5.4.1.2).

Case Y8-3F-2C-1G is continued for another 6 months after closing perforations in 1982-3-22 without changing any other parameters. Figure 5.4.4.1 shows the gas saturation, mole fraction of water in gas saturation, temperature and oil saturation distributions 6 months after closing the upper perforations. Compared with that before closing the upper perforations (Figs. 5.4.1.4a, b, and c in Section 5.4.1.2), temperature in the lower layers of Grosmont C member is considerately increased in a large area as more steam goes through there. In the oil rate curve of Case Y8-3F-2C-1G, Fig. 5.4.4.2, there is an oil production rate peak right after closing perforations and the oil rate gradually declines in the following half year and stays at about 60 m^3/day, while it is 50 m^3/day before closing the upper perforations.

The positive effect on oil production by closing upper perforations at a proper time is due to the gravity flow dominance, high vertical fracture permeability and steam channelling to the top water.

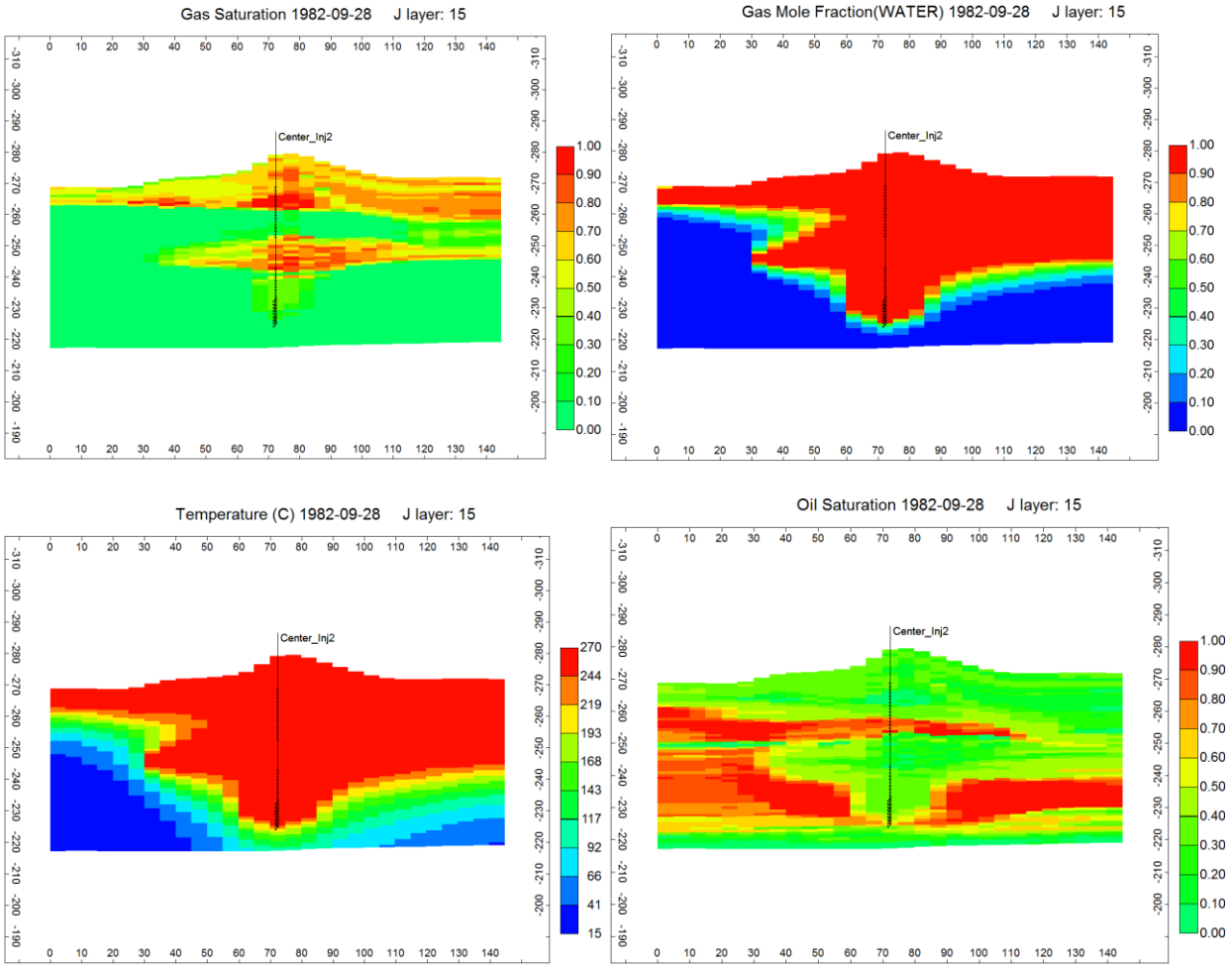

Figure 5.4.4.1a. The gas saturation, mole fraction of water in gas saturation, temperature and oil saturation profile of the cross-section across the centre injector of Case Y8-3F-2C-1G, six months after closing the upper perforations.

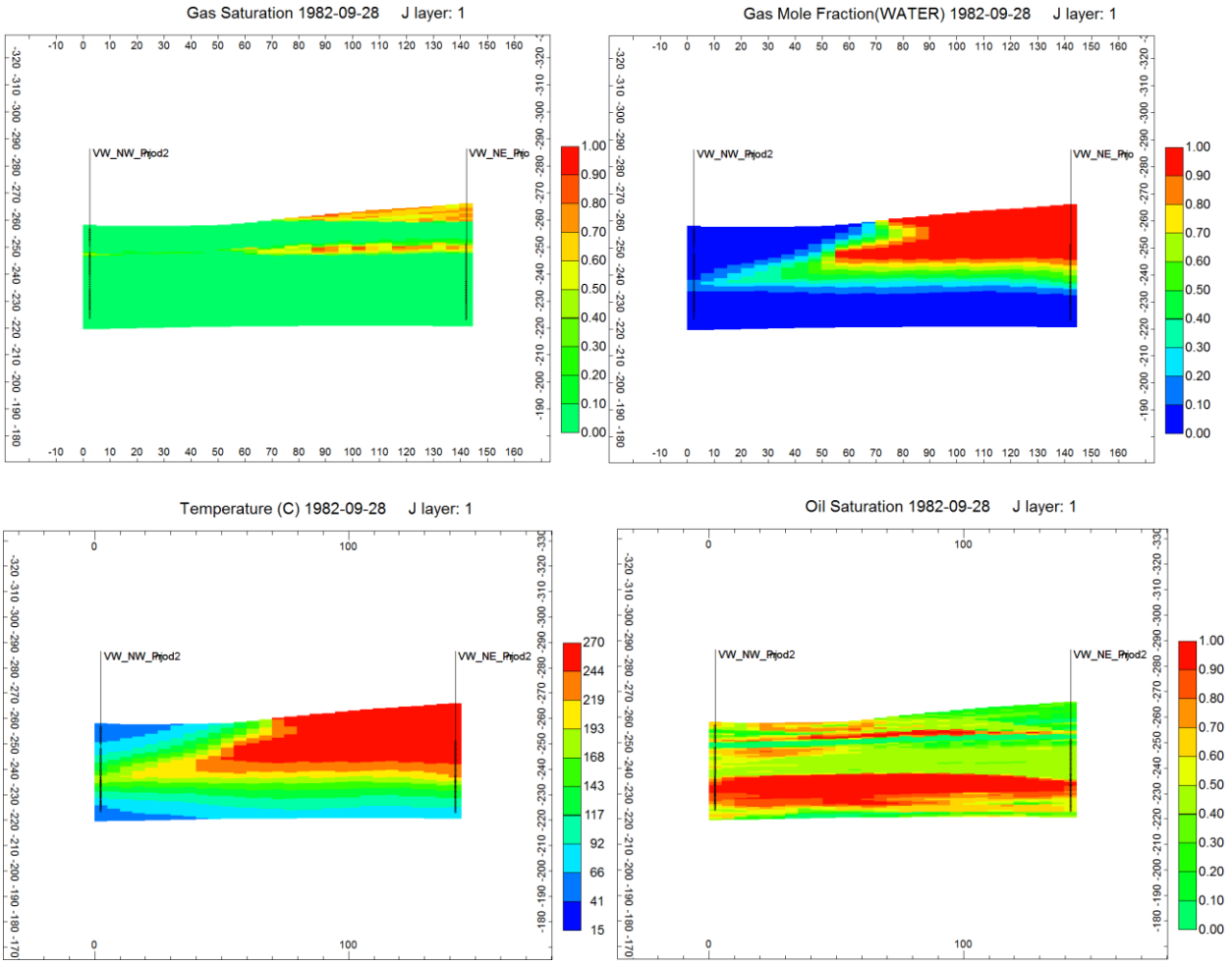

Figure 5.4.4.1b. The gas saturation, mole fraction of water in gas saturation, temperature and oil saturation profile of the cross-section across the producers in the north of Case Y8-3F-2C-1G, six months after closing the upper perforations.

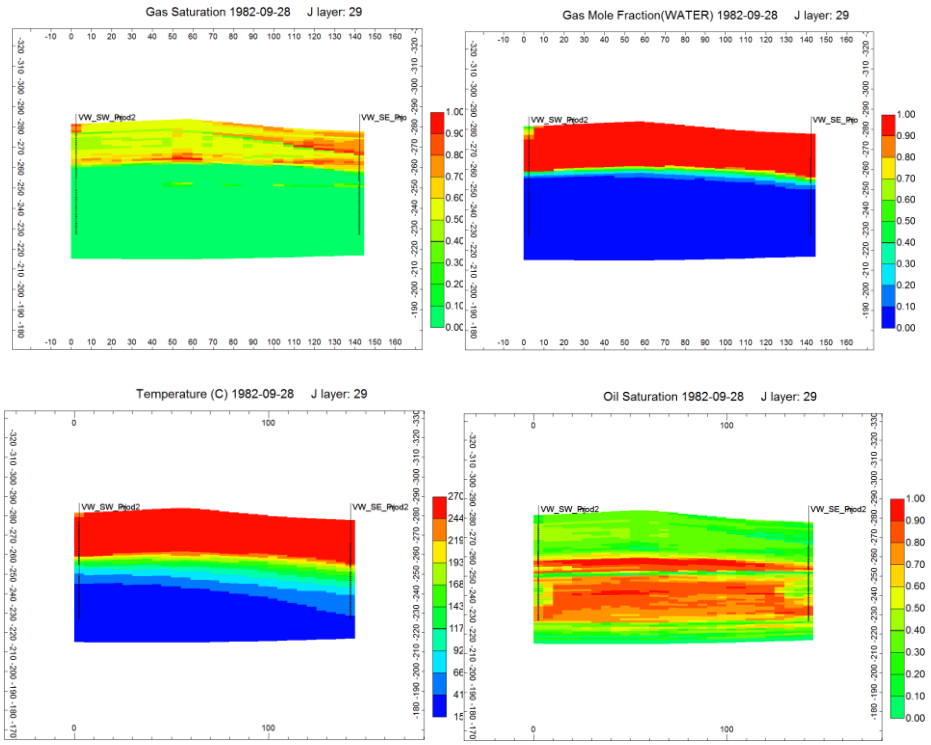

Figure 5.4.4.1c. The gas saturation, mole fraction of water in gas saturation, temperature and oil saturation profile of the cross-section across the producers in the south of Case Y8-3F-2C-1G, six months after closing the upper perforations.

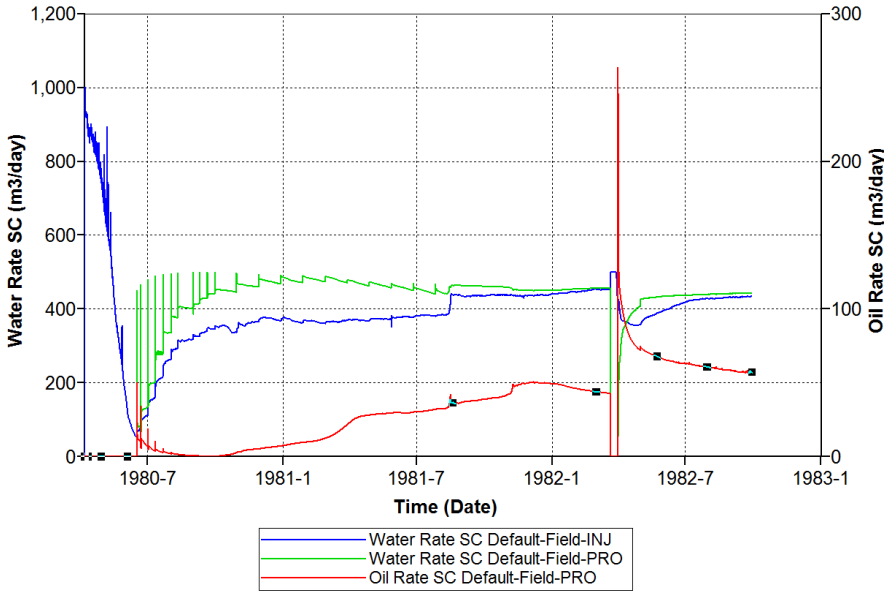

Figure 5.4.4.2. The steam injection, oil and water production rate curves of the 5-acre five-spot steamflood Case Y8-3F-2C-1G.

5.4.4.2 Reducing steam injection rate with time

As described in Sections 5.4.1.2, 5.4.2.2 and 5.4.3.2, for all simulated pattern steamfloods, when the steam injection rate is reduced after about two years' production, the oil production rate does not decrease but remains stable or even increases (Fig. 5.4.1.3a in Section 5.4.1.2, Fig. 5.4.2.2a in Section 5.4.2.2, Fig. 5.4.3.3 in Section 5.4.3.2). One reason is that by the time the steam injection rate is reduced, the cumulative steam injection volume is high and the portion of the formation which can be easily exposed to steam has been sufficiently heated (Table 5.4.4.1). However, steam continues channelling into the large top water zone and is wasted. So it is no longer necessary to inject as much steam as at the beginning. The other reason is the dominant gravity drive mechanism for this reservoir. From Figs. 5.4.4.3, 5.4.4.4 and 5.4.4.5, we can see that the bottomhole pressure of the injector and producers are very close during the whole production period as a result of early steam breakthrough. However, oil continues to be produced through all producers. This indicates the dominant gravity flow. In the process, steam overrides the top of Grosmont C and D members and mobilized oil flows downward to be produced. Therefore, at the moment when a considerable portion of the reservoir is heated, reducing the steam injection rate does not reduce the oil production rate from the gravity flow. However, it may help recovery as it slows down the upward steam stream which counters the downward oil flow.

Table 5.4.4.1. Production time, ratio of steam injection volume to the initial pore volume and the highest formation temperature before reducing steam injection rate of the 5-acre five-spot pattern steamflood Case Y8-3F-2C-1G-1H-1C, 5-acre nine-spot pattern steamflood Case Y15-2A-1B-1D-1B, and 4-acre seven-spot pattern steamflood CaseY16F-4B.

	5-acre five-spot pattern steamflood	5-acre nine-spot pattern steamflood	4-acre seven-spot pattern steamflood
Production time before reducing the steam injection rate	1980-4-7 to 1982-3-22	1980-4-7 to 1982-5-7	1980-4-7 to 1983-1-2
Ratio of steam injection volume to initial pore volume before reducing steam injection rate (%)	1.3	1.9	3.0
Highest temperature in the formation before reducing the steam injection rate (°C)	264	250	264

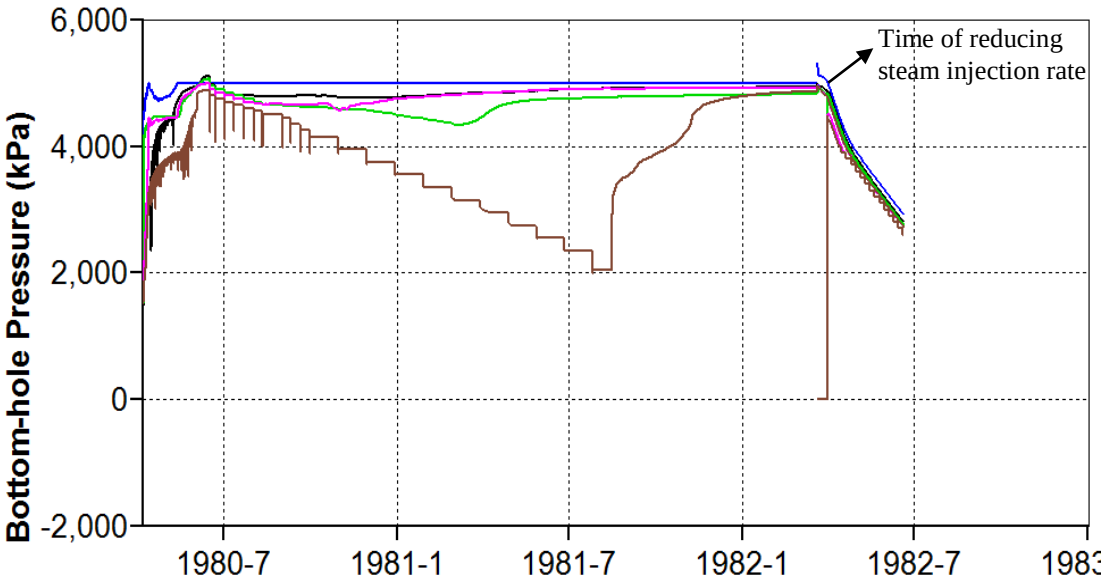

Figure 5.4.4.3. Bottomhole pressure curves of the injector and producers of the 5-acre five-spot steamflood Case Y8-3F-2C-1G. Bottomhole pressure of the centre injector is plotted in blue, the northeast producer in black, the northwest producer in green, the southeast producer in purple, the southwest producer in brown.

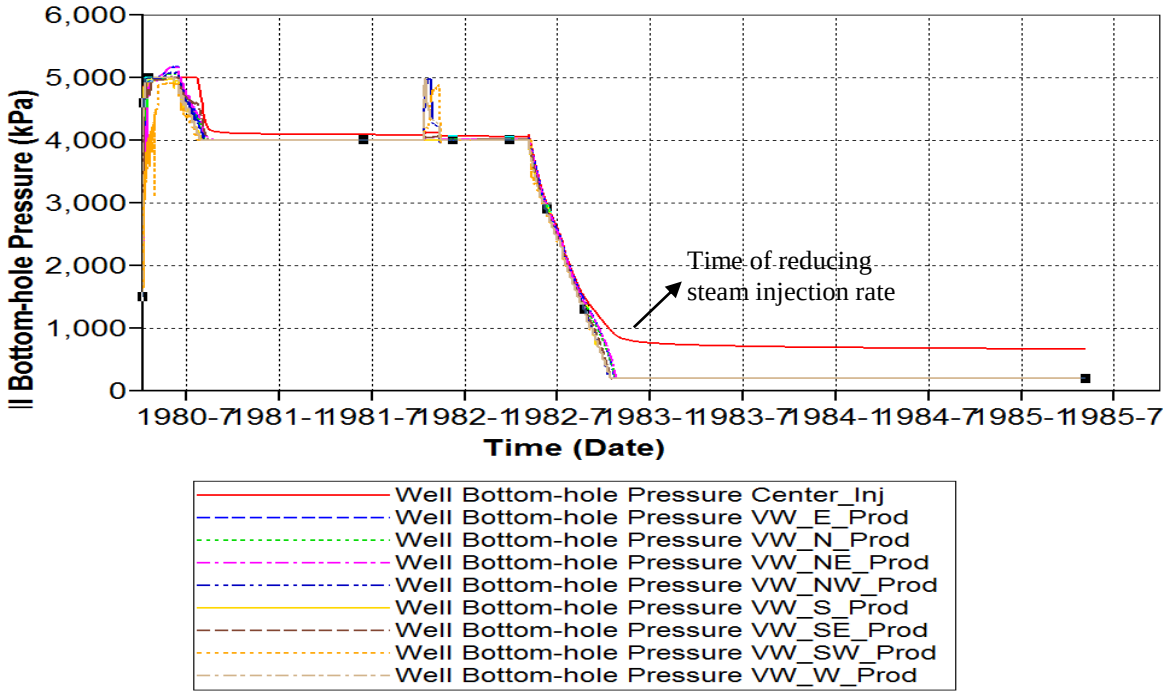

Figure 5.4.4.4. Bottomhole pressure curves of the injector and producers of the 5-acre nine-spot steamflood Case Y15-2A-1B-1D-1B.

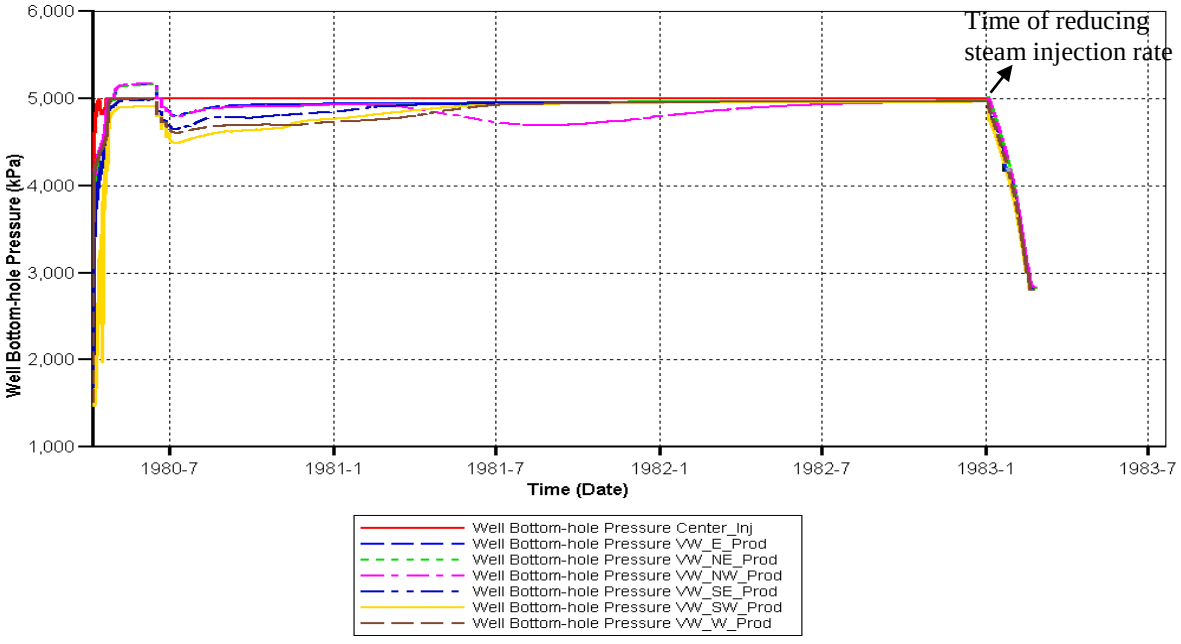

Figure 5.4.4.5. Bottomhole pressure curves of the injector and producers of the 4-acre seven-spot steamflood Case Y16F-4B.

In the steam injection rate reduction calculation used in this study, it is intended that the new steam injection rate should supply enough heat to offset the formation heat loss so that the steam zone volume is maintained. Assuming that heat is lost through conduction from the top of the reservoir (in accordance with the discussion in Section 5.6), the instantaneous heat loss rate during the steamflood process at time t is

$$q = \frac{A \cdot k_{hob}(T_s - T_r)}{\sqrt{\pi\ \alpha\ t}}$$

where t is the time, s;

A is the formation area; in this model, $A = (29 \times 5)^2 = 13625\ m^2$;

f_{st} is the steam quality; in this simulation, f_{st}=0.7;

k_{hob} is the thermal conductivity of the overburden, kW/m· ℃; in this model, $k_{hob} = 1.699 \times 10^{-3}$ kW/m· ℃;

α is thermal diffusivity, m^2/s; in this model, heat capacity of the reservoir rock, M_s=2350 kJ/m^3·℃,

so $\alpha = \frac{k_h}{M_s} = \frac{1.699\times10^{-3}}{2.35\times10^{3}} = 7.2\times10^{-7} m^2/s$.

In order to reduce the steam injection rate just to maintain the steam zone at time t, the latent heat injection rate should equal to the formation heat loss rate:

$$q = i_{st} f_{st} L_v$$

where i_{st} is the steam inejction rate, kg/s.

Therefore, the new steam injection rate at time t is

$$i_{st} = \frac{A \cdot k_{ob}(T_s - T_r)}{f_{st} L_v \sqrt{\pi\alpha t}}$$

Considering the heterogeneity and steam channelling, the new injection rate is arbitrarily increased by 1.5 times, so that the practical steam injection rate used in simulation, i_{st}^{*}, is

$$i_{st}^{*} = 1.5 \times \frac{A \cdot k_{hob}(T_s - T_r)}{f_{st} L_v \sqrt{\pi \alpha t}}$$

The nine-spot pattern steamflood case, Y15-2A-1B-1D-1B, starts on 1980-4-7. Before reducing the steam injection rate on 1982-5-7, the steam rate has been 500 m^3/day with injection pressure of 4,000 kPa. According to the steam tables, the steam saturation temperature T_s and latent heat L_v are 250.3 ℃ and 1712 kJ/kg, respectively. Therefore, the reduced injection rate at this time is

$i_{st}^{*} = 1.5 \times \frac{A \cdot k_{ob}(T_s - T_r)}{f_{st} L_v \sqrt{\pi \alpha t}} = 1.5 \times \frac{13625 \times 1.699 \times 10^{-3} \times (250.3 - 15)}{0.7 \times 1712 \times \sqrt{\pi \times 7.2 \times 10^{-7} \times 760 \times 86400}}$ = 74,602 kg/day=75.0 m^3/day.

The same calculation is done for the five-spot pattern steamflood Case Y8-3F-2C-1G-1J and seven-spot pattern steamflood Case Y16F-2I in the new restart Cases Y8-3F-2C-1G-1H-1C and Y16F-4B. On the day of closing the upper perforations, the new reduced injection rate is determined by the steam injection rate reduction calculation (Table 5.4.4.2). As the steam injection rate is reduced, injection pressure is reduced accordingly. Therefore, the flowing bottomhole pressure constraint of producers must be lowered to continue simulation. Figures 5.4.4.6, 5.4.4.7, and 5.4.4.8 show the water injection and oil, water production curves of the cases for which the steam injection rate is reduced based on the steam injection rate reduction calculation and in cases in which the steam injection rate is not reduced. The restart cases of the five-spot and seven-spot pattern steamfloods are continued for 2-3 months after using i_{st}^{*} , limited by CPU time. Because the steam injection rate is reduced to i_{st}^{*} after closing upper perforations, the difference of oil rates in the i_{st}^{*} cases and the original cases is only due to the effect of reducing the steam rate to i_{st}^{*}. As

seen in Figs. 5.4.4.6, 5.4.4.7, and 5.4.4.8, during the simulated time of all pattern steamfloods, after reducing the steam injection rate to i^*_{st}, the oil rate stays stable or even increases.

Table 5.4.4.2. Steam reduction calculation parameters of of the 5-acre five-spot pattern steamflood Case Y8-3F-2C-1G-1H-1C, 5-acre nine-spot pattern steamflood Case Y15-2A-1B-1D-1B, and 4-acre seven-spot pattern steamflood CaseY16F-4B.

	Production time by the day of steam injection rate reduction, t, day	Steam injection pressure before steam injection rate reduction, p_s, kPa	Steam saturation temperature at p_s, T_s, °C	Steam latent heat at p_s, L_v, kJ/kg	Reduced steam injection rate, i^*_{st}, m^3/day
Case Y8-3F-2C-1G-1H-1C	714	5,000	263.9	1,639	50
Case Y15-2A-1B-1D-1B	760	4,000	250.3	1,712	75
Case Y16F-4B	1,001	5,000	263.9	1,639	50

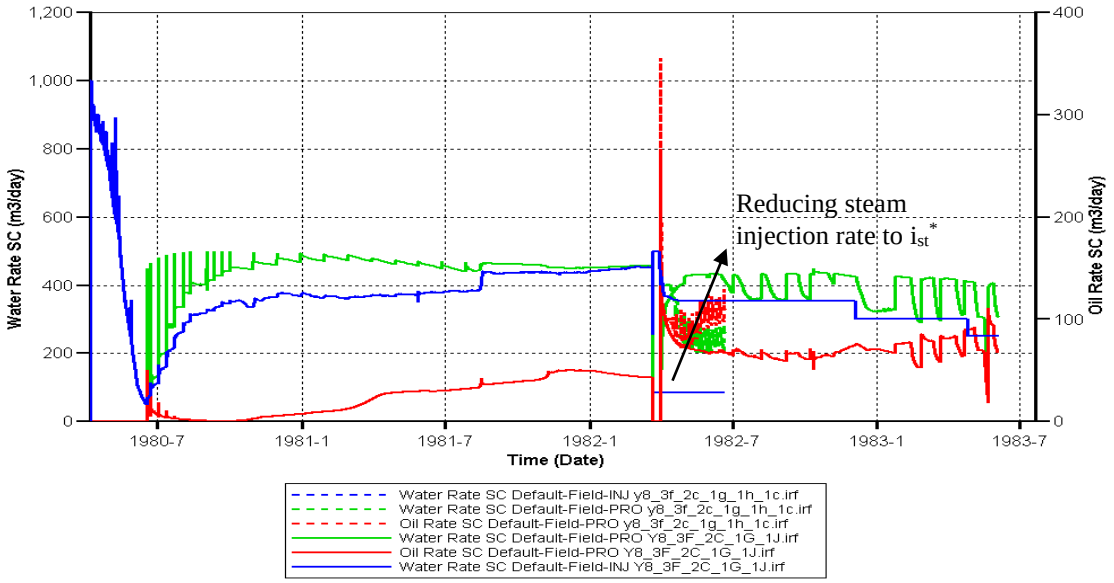

Figure 5.4.4.6. Steam injection (in blue), water (in green) and oil production rate (in red) curves of the five-spot pattern steamflood. Solid lines represent the case with no injection rate reduction; the dotted lines represent the case with steam injection rate reduced to i_{st}^* on 1982-3-22.

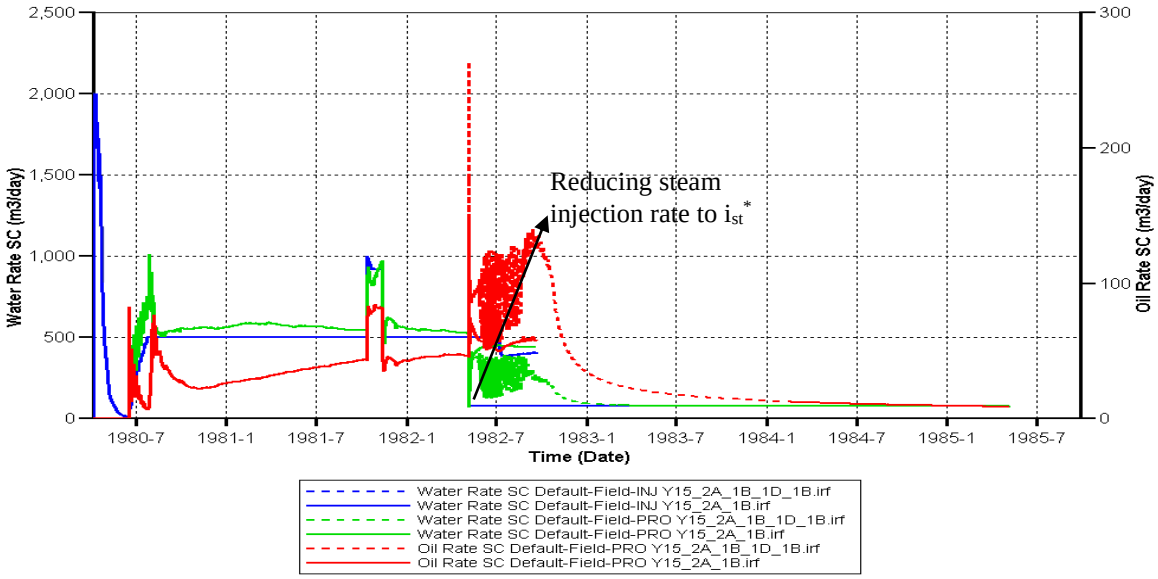

Figure 5.4.4.7. Steam injection (in blue), water (in green) and oil production rate (in red) curves of the nine-spot pattern steamflood. Solid lines represent the case with no injection rate reduction; the dotted lines represent the case with steam injection rate reduced to i_{st}^* on 1982-5-7.

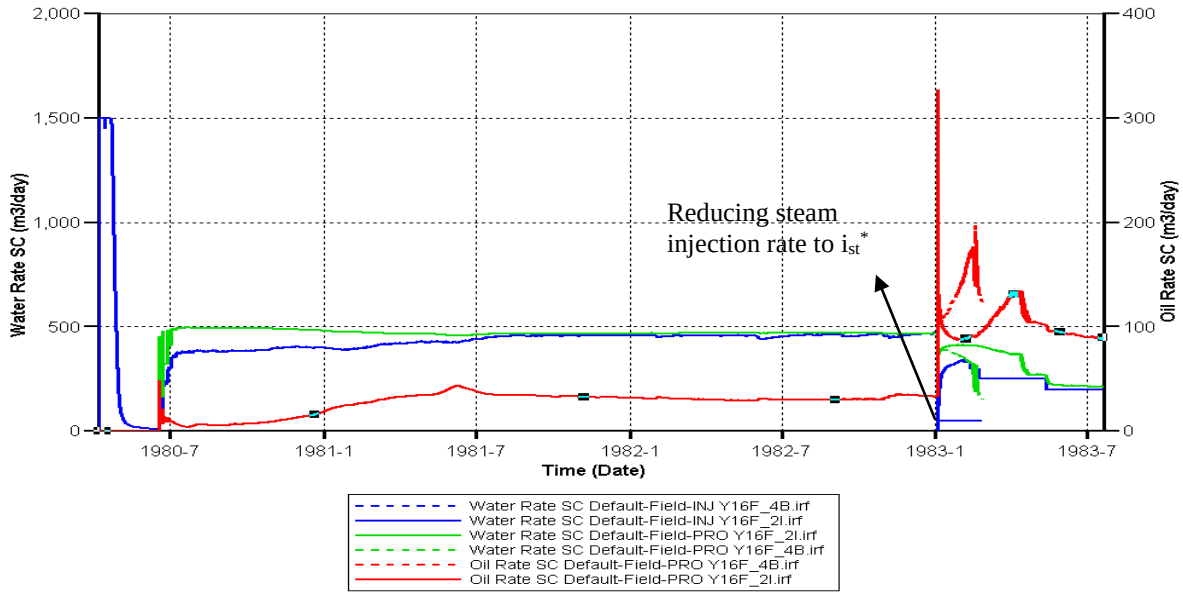

Figure 5.4.4.8. Steam injection (in blue), water (in green) and oil production rate (in red) curves of the seven-spot pattern steamflood. Solid lines represent the case with no injection rate reduction; the dotted lines represent the case with steam injection rate reduced to i_{st}^* on 1983-1-2.

5.4.5 General Comparison of the Five-spot, Seven-spot and Nine-spot Pattern Steamfloods

All pattern drive steamfloods show early steam breakthrough which can be seen from the bottomhole pressure curves giving injection and production pressures (Figs. 5.4.4.3, 5.4.4.4 and 5.4.4.5 in Section 5.4.4.2). On the other hand, because of gravity flow, there is oil production although the pressure difference between the injector and the producer is low. Production can be improved by closing upper perforations in the wells and reducing a steam injection rate at the late stage of the process.

Figure 5.4.5.1 shows the oil production rate curves for the first two years' steamflooding of the three patterns. The oil rate curves for all three steamfloods (Fig. 5.4.5.1) show an oil rate peak at the beginning of the production resulting from steam stimulation. Then the oil rate declines to a very low value and exhibits a low-production transition period. When the mobilized oil again reaches producers and steamflood is developed between the wells, the oil rate gradually increases and remains constant.

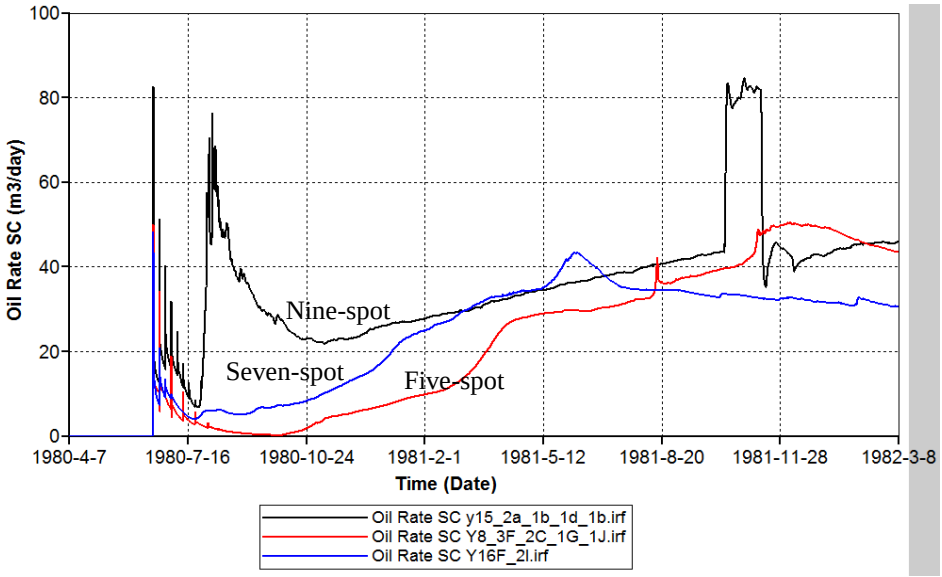

Figure 5.4.5.1. Oil Production rate curve of the five-spot (in red), seven-spot (in blue) and nine-spot (in black) pattern steamflood cases.

The ratio of the number of producers to that of injectors is 1:1, 2:1 and 3:1 for the five-spot, seven-spot and nine-spot steamfloods, respectively. Compared to the five-spot pattern, in spite of more producers, the seven-spot oil rate curve does not show a shorter low-production transition period between the oil rate peaks after steam stimulation and the stable steamflood. Nor is the oil rate in the stable production period of seven-spot steamflood higher than that in the five-spot steamflood process. Thus the seven-spot does not have an obvious advantage. The reason may be that due to the high heterogeneity of this carbonate formation, steam injected from the centre injector does not flow evenly in all directions and the steam zone does not propagate as a radial pattern. Thus the producers placed around the injector do not have the advantage for capturing oil.

Figure 5.4.5.1 shows that, by changing the pattern from five-spot to nine-spot , the low-production transition period between the oil rate peaks after steam stimulation and the stable steamflood is

greatly shortened, showing that the additional wells in the nine-spot pattern help to capture mobilized oil in this heterogeneous reservoir. The oil rate in the stable steamflood period of nine-spot is similar to that for the five-spot, about 50 m^3/day. Therefore, the nine-spot pattern has an advantage only at the beginning of the production, but not as much afterwards.

Among the three patterns, the five-spot seems to be a relatively economical and efficient steamflood pattern. Note that in an actual field where the five-spot patterns are next to each other, oil can be captured inside and outside of a particular pattern and so the effect of formation heterogeneity would be much alleviated.

This comparison further implies that in a highly heterogeneous reservoir, any process demanding a uniform steam zone, e.g., SAGD or seven-spot pattern steamflood, may not achieve optimal performance.

5.5 Unconventional Steamflood Configurations

5.5.1 Well Location and Operation Constraints

A steamflood process consisting of vertical injectors and horizontal producers, VWinj-HWprod, is simulated for this microcosm model of Grosmont reservoir and shows encouraging results. As shown in Fig. 5.5.1, four types of well placements were simulated and listed, together with the corresponding simulation cases.

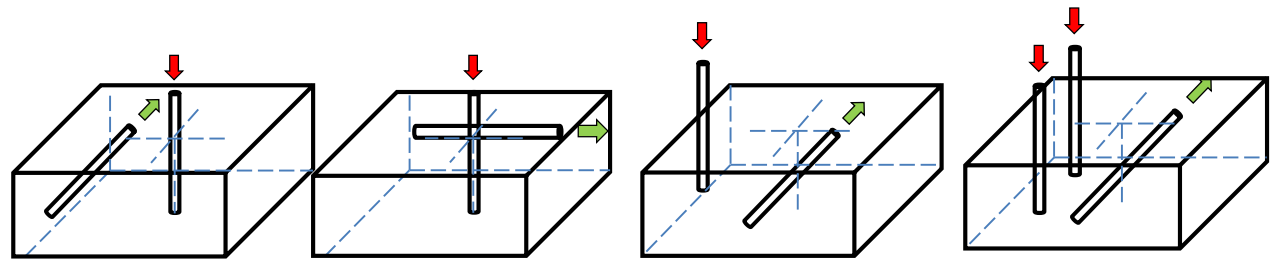

(a) Well Placement Type 1 (b) Well Placement Type 2 (c) Well Placement Type 3 (d) Well Placement Type 4

Figure 5.5.1. Vertical injector, horizontal producer well combinations considered in this study.

All simulations start from 1980-4-7. The horizontal well is given one steam cycle, injecting steam at 500 m^3/day, for the first 60 days before being switched to production. For well placement Types (1), (2) and (3), the steam injection rate into the injector is 100 m^3/day. For well placement Type (4), i.e., Case Moon 4-3C-1, steam is injected from both injectors at 100 m^3/day during the first 450 days and later reduced to 50 m^3/day for each injector.

Simulation results for the four cases are listed in Tables 5.5.1a, b, c, and d. In the following sections, notable features of the vertical well injector-horizontal well producer steamflood are discussed.

(1) One vertical injector at the centre, one N-S horizontal well near the west boundary.

Table 5.5.1a. Well location of the VWinj-HWprod, Type (1).

Case Name	Vertical Injector Location [I,J,K]	Location Layer of Horizontal Producer	Perpendicular Distance between the Injector and Producer (m)
Moon 2A	[15, 15, 35 to 44]	31	40
Moon 4B		48	
Y14		54	60
Y14-1		48	

(2) One vertical injector at centre, one E-W horizontal producer near the north boundary.

Table 5.5.1b. Well location of the VWinj-HWprod, Type (2).

Case Name	Vertical Injector Location [I,J,K]	Location Layer of Horizontal Producer	Perpendicular Distance between the Injector and Producer (m)
Moon 3	[15, 15, 35 to 44]	33	60
QY3		42	

(3) One vertical injector near the west boundary, one N-S horizontal producer near the centre.

Table 5.5.1 c. Well location of the VWinj-HWprod, Type (3).

Case Name	Vertical Injector Location [I,J,K]	Location Layer of Horizontal Producer	Perpendicular Distance etween the Injector and Producer (m)
Moon 4-2D	[3, 15, 35 to 46]	50	40

(4) Two vertical injectors near the west boundary, one N-S horizontal producer near the centre.

Table 5.5.1 d. Well location of the VWinj-HWprod, Type (4).

Case Name	Vertical Injector Location [I,J,K]	Located Layer of Horizontal Producer	Perpendicular Distance between the Injector and Producer (m)
Moon 4-3C-1	Injector 1: [3, 15, 35 to 46] Injector 2: [3, 26, 35 to 46]	50	40

5.5.2 Steam Override

It is to be noted that the injected steam had a strong tendency to override. In all cases, steam reached the topmost layer. An example is given in Fig. 5.5.2, showing the temperature, gas saturation, and mole fraction of water in gas of the topmost Layer 1 for the Case Moon 2A, on 1980-6-7, the last day of the horizontal well steam stimulation. Although all the well perforations are in the oil interval below the middle tight streak (i.e., Grosmont C member), from the consistency of temperature, gas saturation, and mole fraction of water in gas, it is confirmed that

steam arrives at the top layer from the beginning of production. The severe steam override is a result of the high vertical permeability and leads to high heat loss from the top.

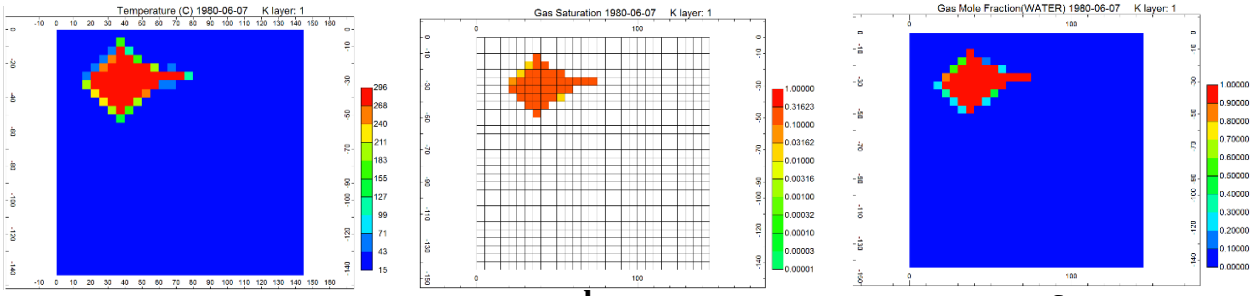

Figure 5.2.2. Temperature (a), gas saturation (b) and mole fraction of water in gas (c) distribution of the topmost layer of the VWinj-HWprod Case Moon2a.

5.5.3 Steam Directional Flow

As the formation properties in the carbonate are highly heterogeneous, steam preferentially flows to the more permeable regions. Therefore, although in all cases of well placement Types (1), (2), and (3), the vertical injector is placed perpendicular to the centre of the horizontal producer, steam zones form only between the injector and a certain portion of the horizontal well producer near which the formation permeability is higher. For example, in Case Moon4-3C-1, the formation permeability near the heel of the horizontal well is higher than that near the toe (Fig. 5.5.3a). As a result, it is shown in the temperature distribution of the IJ plane across the horizontal well that steam preferentially flows towards the heel of the horizontal well (Fig. 5.5.3c). Even until the end of the five years' production, there is still no steam over one-third of well length near the horizontal well heel (Fig. 5.5.3b). The same can been seen in Case Moon 4b, in which most of the oil is also drained from the formation near the heel of the horizontal well producer where the permeability is higher, although the initial oil saturation is equally high along the producer well length.

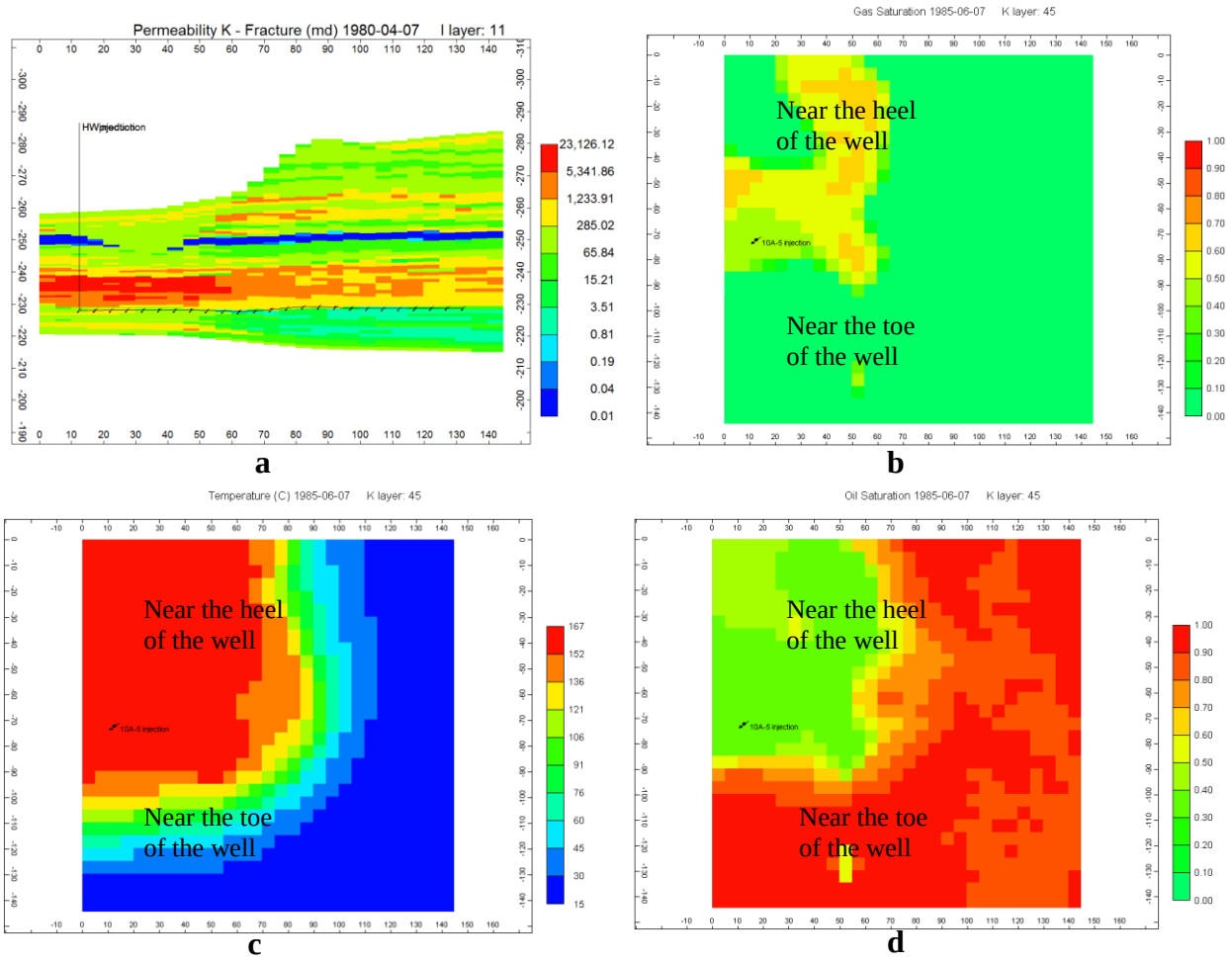

Figure 5.5.3. (a) Facture vertical permeability of the JK cross-section across the horizontal producer of the VWinj-HWprod Case Moon4-2D. (b) Gas saturation in the IJ plane 5m above the horizontal producer at the end of production of the VWinj-HWprod steamflood Case Moon4-2D. (c) Temperature distribution in the IJ plane 5m above the horizontal producer at the end of production of the VWinj-HWprod steamflood Case Moon4-2D. (d) Oil saturation distribution in the IJ plane 5m above the horizontal producer at the end of production of the VWinj-HWprod steamflood Case Moon4-2D.

5.5.4 Effect of the Gravity Flow

As shown in Table 5.5.1a, in Cases Moon 4B and Moon 2A, the injector is placed in the middle of the model and perforated in the same layer in Grosmont C member. In the Case Moon 4B, the

horizontal producer is placed in Layer 48 below the injection perforations while in Case Moon 2A, it is in layer 31 above the injection perforations.

From the oil saturation distribution across the horizontal producer for the two cases, it is seen that the oil desaturation zone is largely above the horizontal well producer (Fig. 5.5.4). Besides, there is more oil drained from the formation near the heel as it is a more permeable region to which steam preferentially flows. In the undepleted layers below the horizontal well, the oil viscosity at the end of production is fairly low, 80~200 cP, but the oil remains unproduced. As included in Table 5.1 in Section 5.1, given the same production time and steam injection volume, the recovery factor of Case Moon 4B (producer below the injection perforations) is much higher than that of Case Moon 2A (producer above the injection perforations), and SOR is lower. Therefore, gravity drainage is also the dominant drive mechanism of the VWinj-HWprod steamflood. The horizontal producer should be placed at the base of the oil-bearing formation member to capture more mobilized oil, except that some stand-off is necessary if the bottom water is present.

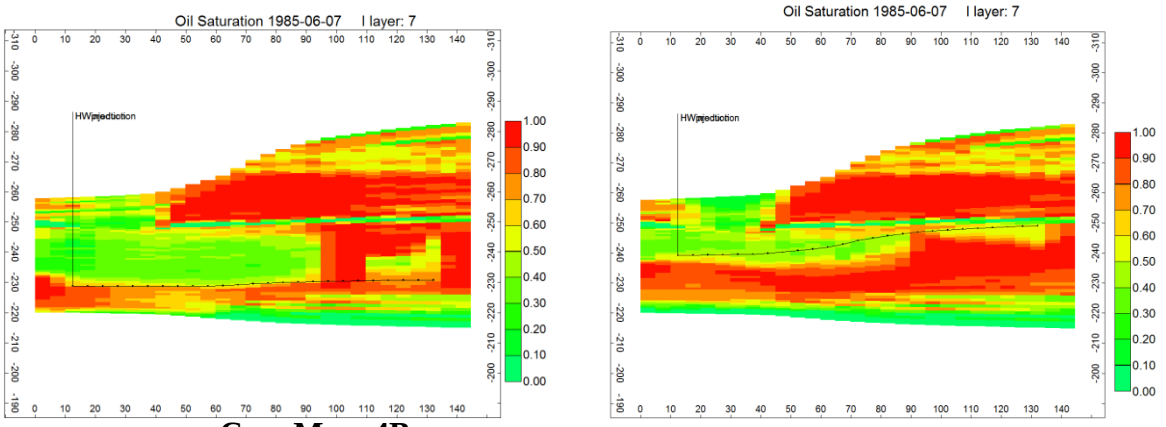

a. Case Moon4B **b. Case Moon2A**

Figure 5.5.4. (a) Oil saturation distribution of the JK cross-section across the horizontal producer of the VWinj-HWprod Case Moon4B. (b) Oil saturation distribution of the JK cross-section across the horizontal producer of the VWinj-HWprod Case Moon2A.

5.5.5 Advantage of the Vertical Well Injector in Expanding Steam Zone

As discussed in the previous sections, in all the cases simulated with one vertical injector, i.e., well placement Type (1), (2), and (3), steam preferentially flows towards the more permeable region between the injector and the producer, so that the less permeable area in between is not much drained although the oil saturation is high. As shown in Fig. 5.5.3a in Section 5.5.3, in the Case Moon 4-2D, as the formation permeability near the well heel is higher than that near the toe, most of the oil is drained from the northwest portion of the model (Fig. 5.5.3d). In order to distribute steam more evenly and enlarge the drainage area, in Case Moon4-3C-1, another vertical injector, Injector 2, is placed in the southwest corner, targeting the formation near the toe of the horizontal producer where oil saturation is as high as that near the heel (Fig. 5.5.5). The location of the horizontal well is the same with that in Case Moon4-2. Both the vertical injectors and the horizontal producer are perforated in the oil-bearing intervals of the Grosmont C member. Steam

is injected into both injectors at 100 m^3/day for the first 450 days and then reduced to 50 m^3/day for each injector.

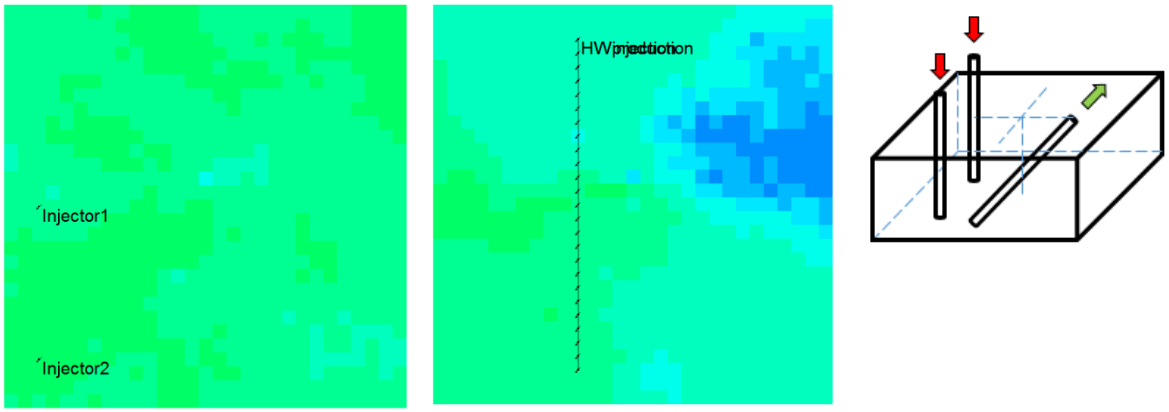

Figure 5.5.5. Location of the two vertical injectors shown in Layer 46 of the VWinj-HWprod steamflood Case Moon4-3c-1; Location of the horizontal producer in Layer 50 of the VWinj-HWprod steamflood Case Moon4-3c-1; Well configuration schematic of the VWinj-HWprod steamflood Case Moon4-3c-1.

For Case Moon4-3C-1, Fig. 5.5.6a shows the temperature distribution in the cross-section across the horizontal producer at the end of production; Figures 5.5.6b and 5.5.6c show the gas saturation, and mole fraction of water in gas, i.e., steam, in an IJ plane 5 m above the horizontal well at the end of production; Figure 5.5.6d shows the oil saturation distribution in the IJ plane 5 m above the horizontal well at the end of production. Compared to the other vertical well injector-horizontal well producer steamflood cases, although the total steam injection rate is the same for most of the five years' production time, the additional vertical injector efficiently targets the low permeability region, helping to create more uniform steam distribution and enlarging the drainage area, thus resulting in the optimal recovery factor and SOR.

Given the area limitation of this microcosm of Grosmont formation, Case Moon4-3C-1 is an example to show the effectiveness of a vertical injector in expanding a uniform steam zone over this highly heterogeneous reservoir and most of this is due to the fact that a vertical injector can efficiently target any low permeability, high oil saturation area. Therefore, in the large scale field operation, the optimal well configuration of the vertical injector-horizontal producer steamflood does not have to follow any repeated pattern but covers the less permeable, high oil saturation region within the vertical injector network.

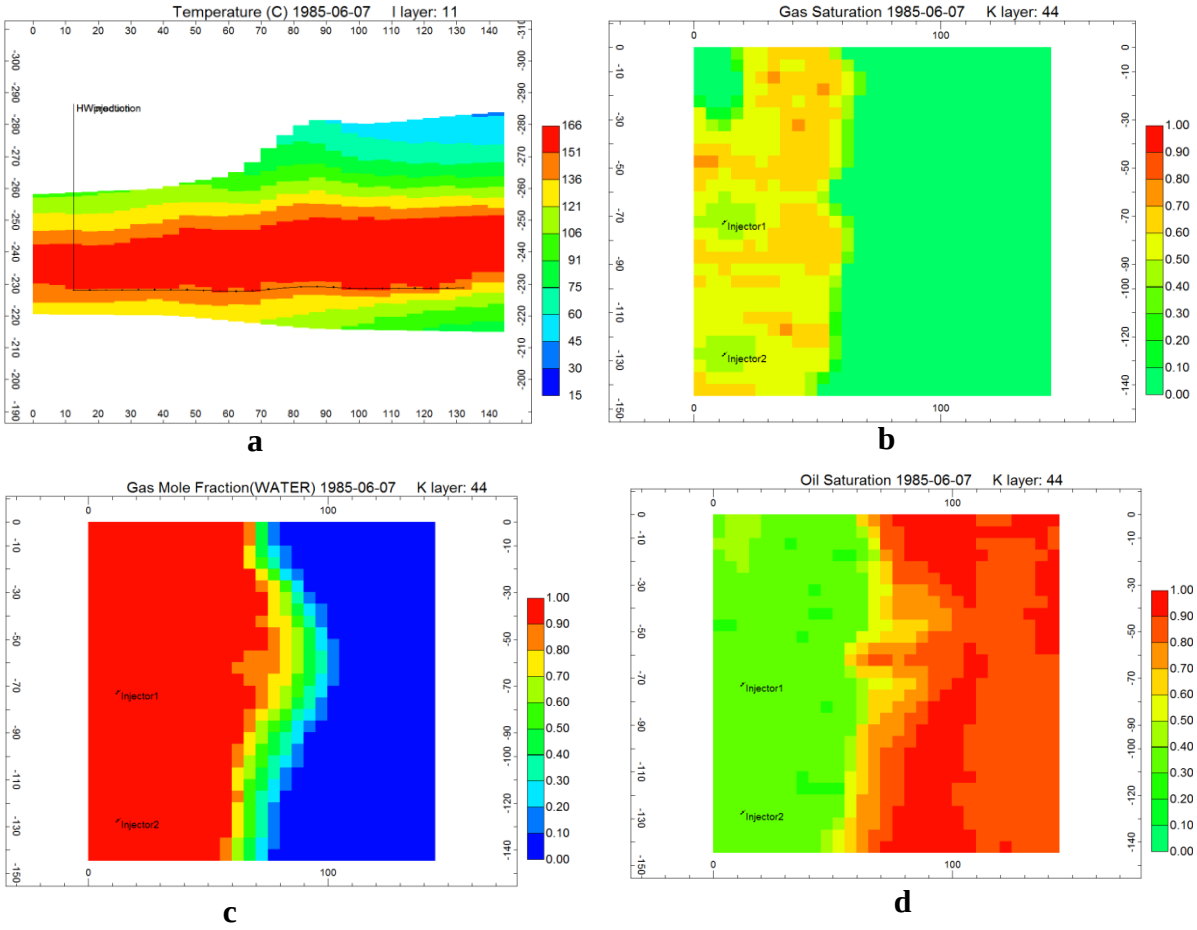

Figure 5.5.6. (a) Temperature distribution in the cross-section across the horizontal producer at the end of production of the VWinj-HWprod steamflood Case Moon 4-3C-1. (b) Gas saturation in the IJ plane 5m above the horizontal producer at the end of production of the VWinj-HWprod steamflood Case Moon 4-3C-1. (c) Mole fraction of water in gas saturation in the IJ plane 5m above the horizontal producer at the end of production of the VWinj-HWprod steamflood Case Moon 4-3C-1. (d) Oil saturation distribution in the IJ plane 5m above the horizontal producer at the end of production of the VWinj-HWprod steamflood Case Moon 4-3C-1.

5.5.6 Faster Oil Recovery than the Horizontal Well CSS

Comparing the Case Moon4-3C-1 to the best horizontal well CSS Case Q5-2, the vertical injector-horizontal producer steamflood gives the same recovery performance in a much shorter time. Case Q5-2 is the best horizontal well CSS case, for which steam is injected also in the west side of the model. The comparison is based on the same cumulative steam injection volume. The cumulative steam injection volume at the end of the best horizontal well CSS case, Case Q5-2, is 181,499 m^3, and the time when the VWinj-HWprod Case Moon4-3C-1 reached the same cumulative steam injection volume is 1983-1-17. Therefore, the steam zone, drainage area, SOR and oil production on 1983-1-17 of the Case Moon4-3C-1 are used to compare with those at the end of Case Q5-2. As can be seen from Fig. 5.5.6 of this section and Figs. 5.2.2.6 and 5.2.2.7 in Section 5.2.2.4, although for both cases, the steam is injected in the west side of the model, the steam zone and drainage area of the horizontal well CSS Case Q5-2 are mainly in the northwest corner, whereas the whole formation along the horizontal producer is adequately heated and drained in the VWinj-HWprod Case Moon4-3C-1. Table 5.5.2 shows the process time, SOR and recovery factor of the two cases. Given the same cumulative steam injection volume, the SOR and recovery factor of the two processes are the same. However, the VWinj-HWprod steamflood achieves the same recovery 21 months earlier than the horizontal well CSS.

Table 5.5.2. SOR and recovery factor of the single horizontal well CSS Case Q5-2 at the end of production and those of the vertical injector-horizontal producer steamflood Case Moon4-3c-1 given the same cumulative steam injection volume.

Process Type	Schematic	Case Number	SOR (m^3/m^3)	Recovery Factor (%)	Cumulative Steam Injection Volume	Simulated Time (Years)
HWCSS		Q5-2	7.0	18.3	181,499	1980-4-7 ~ 1984-10-2
VWinj-HWprod Steamflood		Moon4-3c-1	7.0	18.0	181,499	1980-4-7 ~ 1983-1-17

As described in Section 5.2.2.4 (the horizontal well CSS), when steam is injected through a horizontal well, although the well can penetrate the formation over a larger distance, steam continues to migrate to the same high permeability region. Although the formation oil saturation is generally high, the drainage area is restricted to only the more permeable area. By contrast, a vertical steam injector has the flexibility to target any high oil saturation region regardless of the difference in the local formation properties.

5.5.7 Comparison with the Pattern Steamfloods

As described in Section 5.4.4.2, for all the pattern steamfloods simulated for this reservoir, bottomhole pressures of the injectors and producers become close from the very early stage of the process indicating early steam breakthrough caused by the formation heterogeneity. Figure 5.5.7 shows the injection and production pressure curves of four VWinj-HWprod simulation cases, one from each well placement type. Unlike the pattern steamfloods, a stable pressure difference is maintained between the bottomhole pressure of the injector and the producer during the VWinj-HWprod process, so that there is no steam breakthrough. Compared with the vertical producers in the conventional pattern steamfloods, the horizontal producer placed near the base of the oil-

bearing intervals effectively delays steam breakthrough in view of the overwhelming upward steam flow. Therefore, in addition to gravity drainage, VWinj-HWprod arrangement makes use of viscous drive as an additional drive mechanism.

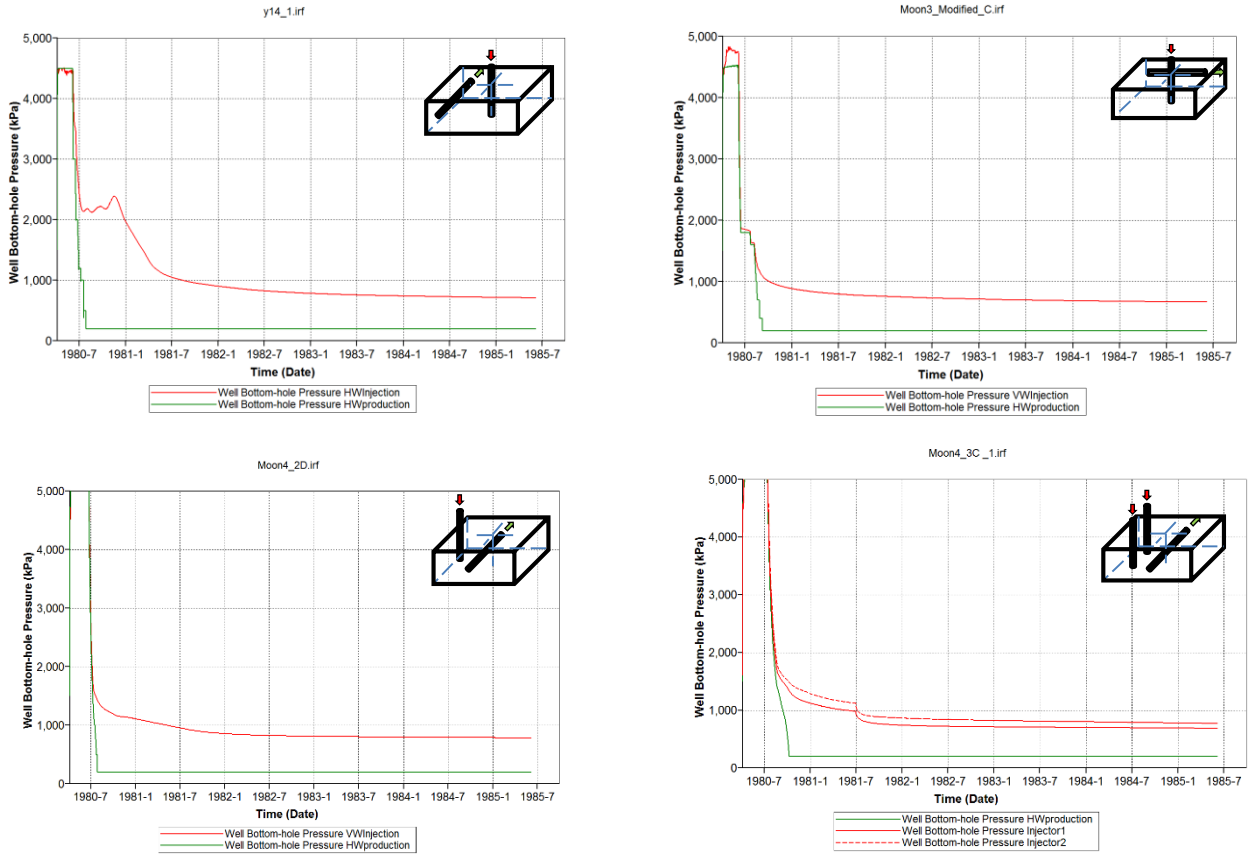

Figure 5.5.7. Injection and production bottomhole pressures of VWinj-HWprod steamflood Cases Y14-1, Moon3C, Moon4-2D and Moon4-3C-1, one from each well placement type.

Furthermore, comparing the VWinj-HWprod steamflood Case Moon4-3C-1 with the nine-spot pattern steamflood Case Y15-2A-1B-1D-1B which is the best optimized pattern steamflood case, the VWinj-HWprod steamflood shows a lower SOR and a comparable oil recovery factor, especially considering the fact that it only targets the Grosmont C member while the wells in the pattern steamfloods cases are perforated in both Grosmont C and D members.

5.5.8 Effect of Well Distance

As included in Table 5.5.1 a, in Case Moon 4B, the horizontal producer is placed 40 m away from the centre vertical injector in Layer 48; in Case Y14-1, the horizontal well producer is placed in the same layer but laterally further from the centre injector; in Case Y14, the horizontal producer is placed both laterally and vertically farther from the centre injector, in Layer 54. Both Cases Moon 4B and Y14-1 were simulated for five years' production while Case Y14 was conducted only for three years' simulation because of the restriction on CPU time (Table 5.1). As shown by the dashed line in Fig. 5.5.9, after some peaks as a result of initial steam stimulation, the oil production rate of Case Y14-1 exhibits a low-production transition period and then steadily rises to a new peak. The low-production transition period occurs because steam injected from the centre injector does not preferentially flow towards the horizontal producer but to the top water zone in the east (Fig. 5.5.8a). However, as the steam zone expands with time, the connection between the injector and the producer is re-established (Fig. 5.5.8b) and the oil rate increases again. For Case Moon 4B, there is no low-production transition period in the oil production rate curve (dotted line in Fig. 5.5.9) because the well distance between the injector and the producer is the shortest. For Case Y14, the oil production rate curve (solid line in Fig. 5.5.9) includes the longest low-production transition period because the well distance is the longest. However, the final cumulative oil production for the three cases is similar. Even in Case Y14 with the longest well distance, oil production increase rapidly after the low-production transition period and shows a tendency to catch up with the highest rate for Case Moon4. This is also evident from the SOR and oil recovery for the three cases in Table 5.1. The oil recovery and SOR in the two five-year-production Cases Moon4B and Y14-1 are almost the same although well distances are different;

within three years Case Y14 has enough time to offset the long low-production transition period and gives a recovery performance quite close to that of the other two. Therefore, because it combines the advantage of vertical injector in expanding the steam zone and the advantage of the horizontal producer in capturing oil gravity flow, the production performance of the VWinj-HWprod steamflood does not vary with well distance, which makes it a potentially economical choice.

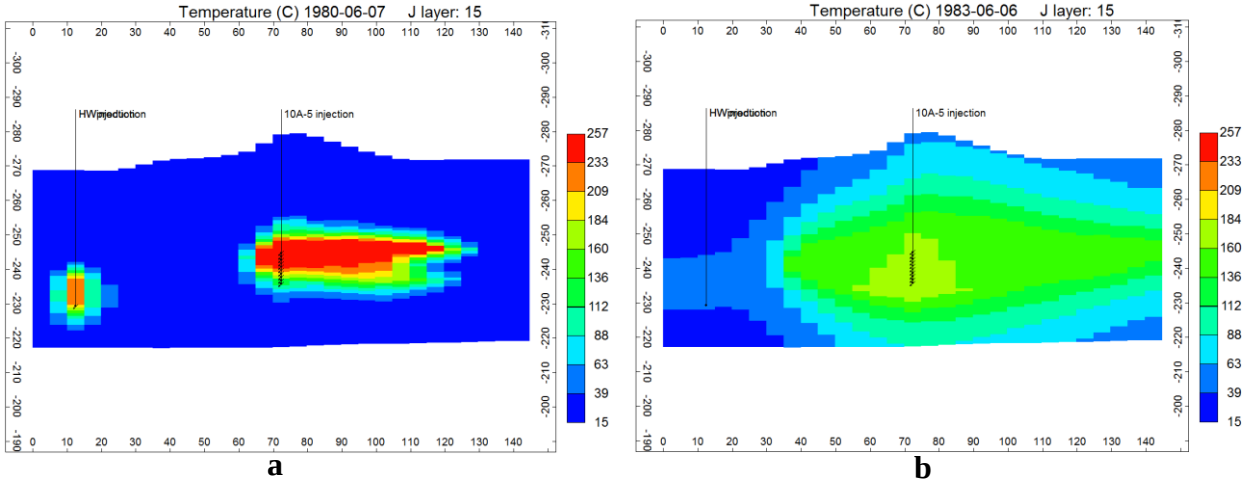

Figure 5.5.8. (a) Temperature distribution of the cross-section across the injector and the producer of the VWinj-HWprod steamflood Case Y14-1 at the early stage of production when there is little connection between the injector and the producer as a result of steam channelling into the top water. (b) Temperature distribution of the cross-section across the injector and the producer of the VWinj-HWprod steamflood Case Y14-1 at the mid stage of production when there connection between the injector and the producer is re-established.

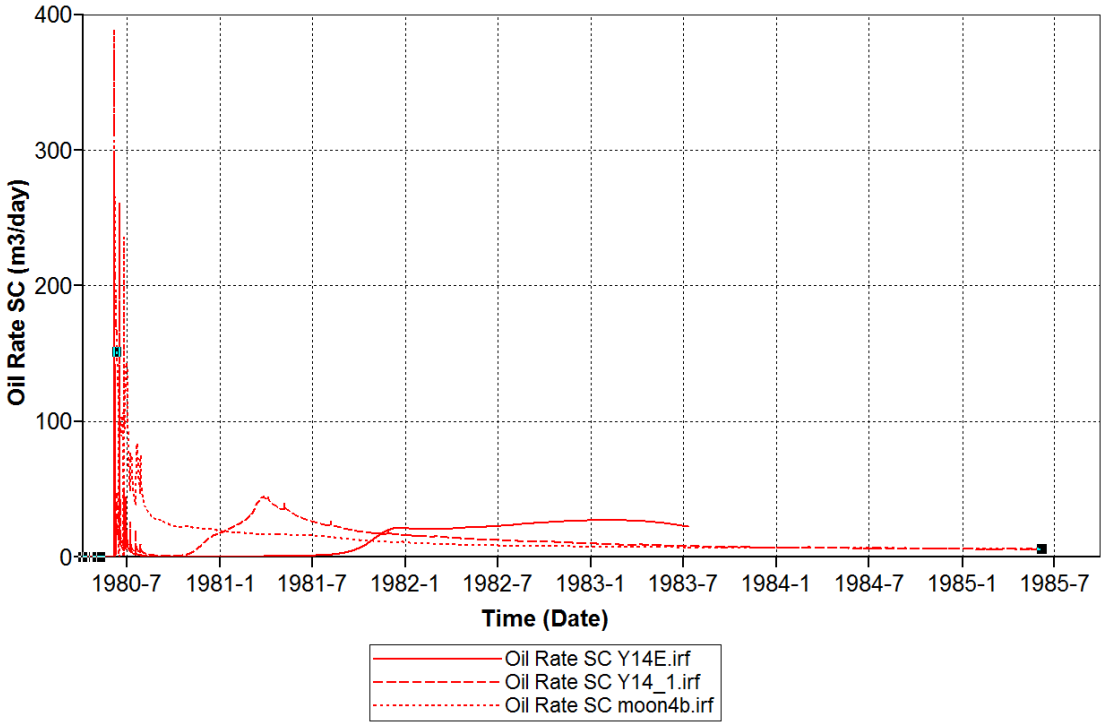

Figure 5.5.9. Oil production rate of the VWinj-HWprod steamflood Cases Moon 4B, Y14-1 and Y14.

5.6 Heat Loss Analysis

Given the thermal properties and average geometric parameters of this model, a variation of the classical Marx-Langenheim model, derived in Appendix A, can be used to estimate the cumulative heat loss at a certain time of steamflood, which can also be derived from the simulation output. Comparison of the cumulative heat loss from the simulation results and that based on the derivation in this study (Appendix A) provides an insight into fluid flow during steam injection in this reservoir.

For any time t, there are three outputs from CMG STARS, cumulative enthalpy injected, cumulative enthalpy produced and cumulative enthalpy in place. As the enthalpy parameters are

based on the same reference temperature, cumulative heat loss is the balance of these three parameters. So the simulated cumulative heat loss at time t, $H_{L,s}(t)$, is

$H_{L,s}(t)$ = Cumulative Enthalpy Injected (t) - Cumulative Enthalpy Produced (t) - Cumulative Enthalpy in Place.

The cumulative heat loss can also be obtained from the analytical Marx-Langenheim model for a homogeneous formation. According to the Marx-Langenheim equation (Marx et al. 1959), given the formation thickness, h, thermal conductivity of the overburden and underburden rocks, k_{hob}, heat capacity of the overburden and underburden rocks, M_{ob}, and the reservoir rocks M_s, the fraction of cumulative heat loss at time t, $Q_{loss,ML}$, is

$$Q_{loss,ML} = 1 - \frac{F_1}{t_D}$$

where $t_D = \frac{4k_{hob}M_{ob}t}{M_s^2 h^2}$, and $F_1 = e^{t_D}\operatorname{erfc}\sqrt{t_D} + 2\sqrt{\frac{t_D}{\pi}} - 1$

Then the cumulative heat loss at time t, $H_{L,ML}(t)$, is given by

$H_{L,ML}(t)$ = Cumulative Enthalpy Injected $(t) \times Q_{loss,ML}$

In this model, the average thickness h=53.35 m, k_{hob}=1.7 $\times 10^{-3}$ kW/m $\cdot$ ℃, $M_{ob} = 2350$ kJ/ $m^3 \cdot$ ℃, $M_s = 2347$ kJ/$m^3 \cdot$ ℃ .

For the three-year production period for the five-spot pattern steamflood Case, Y8-3F-2C-1G-1J, cumulative heat loss is calculated at selected times according to the simulation result and Marx-

Langenheim equation, respectively, and is plotted against time in the same figure, Fig. 5.6.1, for comparison. The same is done for the five-year production, nine-spot pattern steamflood Case Y15-2a-1b-1d, Fig. 5.6.2.

Figure 5.6.1 and 5.6.2 show that the simulation cumulative heat loss curve (black) does not agree much with the Marx-Langenheim cumulative heat loss curve (purple). After the first two years' production, the Marx-Langenheim cumulative heat loss curve exceeds the simulation result and the difference grows with time.

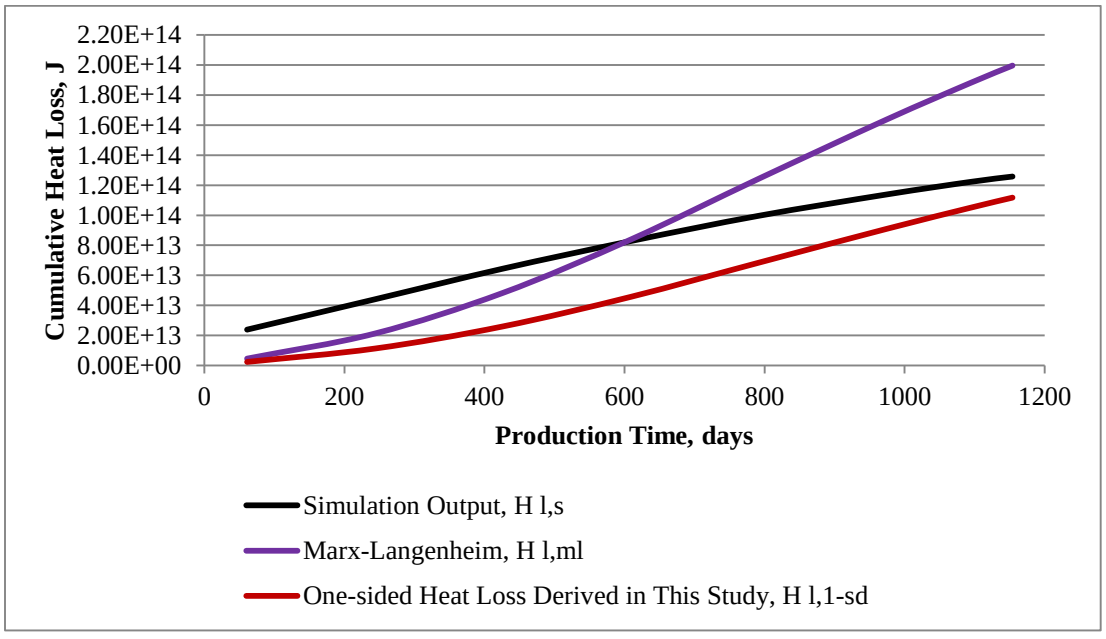

Figure 5.6.1. Simulated cumulative heat loss, cumulative heat loss calculated from the Marx-Langenheim equation and one-sided heat loss equation for the five-spot pattern steamflood Case Y8-3F-2C-1G-1J.

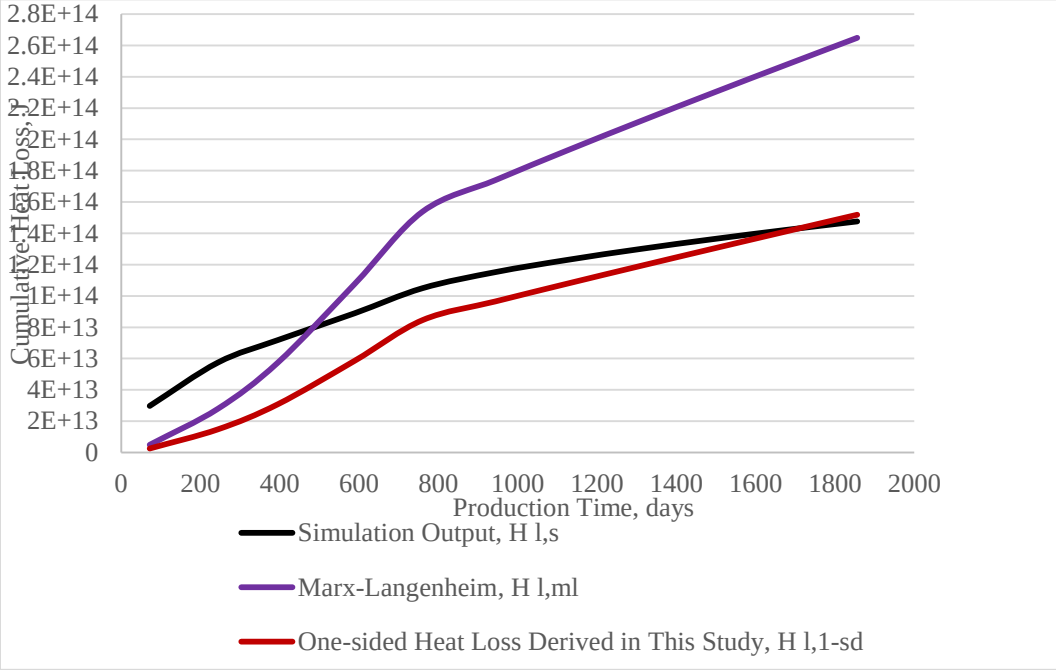

Figure 5.6.2. Simulated cumulative heat loss, cumulative heat loss calculated from Marx-Langenheim equation and one-sided heat loss equation for the nine-spot pattern steamflood Case Y15-2A-1B-1D-1B.

The reason for the disagreement between these two curves is that the Marx-Langenheim model assumes simultaneous heat loss to the formation overburden and underburden, while during a steamflood with strong steam override, heat is mostly lost from the overburden. As we can see from the temperature profile of both cases (Figs. 5.6.3, 5.6.4, 5.6.5, and 5.6.6), steam override occurs from the very beginning of the process and, till the end, the bottom of the formation is still close to the initial reservoir temperature. For this reason, the equation considering only one-sided heat loss is derived as a limiting case (see Appendix A). When strong steam override occurs, heat loss is principally from the top of the formation, and the segregated steam condensate serves to "insulate" the lower part of the formation. According to the one-sided heat loss equation derived, the cumulative heat loss as a fraction of the of cumulative heat injected at time t, $Q_{loss,\ 1\text{-}sd}$, is

$$Q_{loss,1\text{-}sd} = 1 - \frac{F_1}{t_D}$$

where $t_D = \frac{k_{hob} M_{ob} t}{M_s^2 h^2}$, and $F_1 = e^{t_D} \operatorname{erfc}\sqrt{t_D} + 2\sqrt{\frac{t_D}{\pi}} - 1$

Then the cumulative heat loss at time t, $H_{L,\,1\text{-}sd}(t)$, is given by

$H_{L,\,1\text{-}sd}(t)$ = Cumulative Enthalpy Injected (t) $\times$ $Q_{loss,1-sd}$.

In Figs.5.6.1 and 5.6.2, cumulative heat loss based on the one-sided heat loss equation, $H_{L,\,1\text{-}sd}(t)$, is plotted in red. As can be seen, the $H_{L,\,1\text{-}sd}(t)$ curve and the simulated cumulative heat loss curve, $H_{L,\,s}(t)$, have similar curvatures and are closer. $H_{L,\,s}$ is larger than $H_{L,1\text{-}sd}$ at the beginning but the two curves gets closer with time. This is because steam migrates to the top at an early stage, so that the heat loss is much higher than in the analytical model at the beginning (Figs. 5.6.3b and 5.6.5b).

Instead of the original Marx-Langenheim equation, the one-sided heat loss equation derived here gives a better estimation of the cumulative heat loss, which is consistent with the fact of the overwhelming upward steam flow. The one-sided heat loss equation may underestimate the heat loss at the early stage as a result of early steam override but this error gets smaller with time.

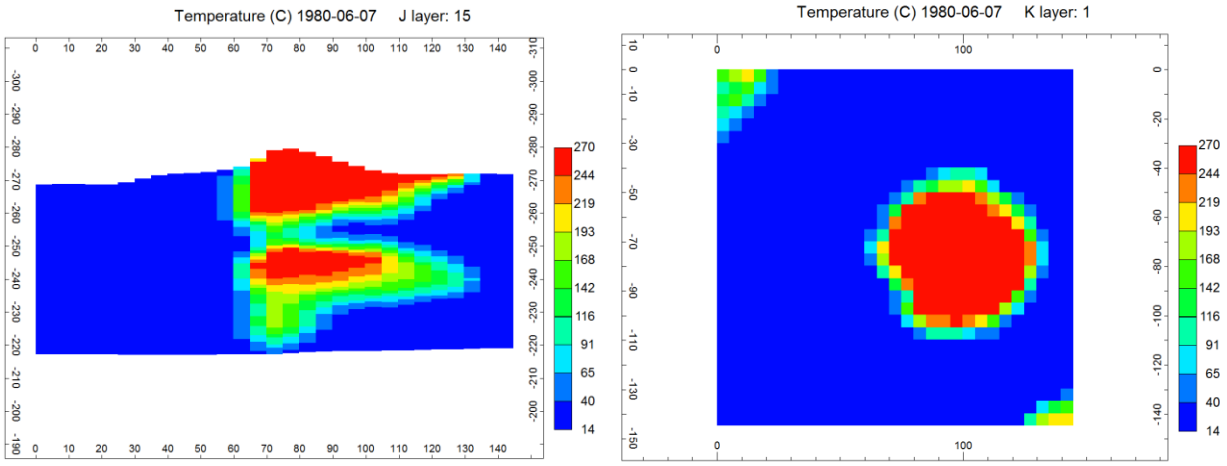

a **b**

Figure 5.6.3. (a) Temperature profile of the IK cross-section across the centre injector of the five-spot pattern steamflood Case Y8-3F-2C-1G-1J. At the very early stage of this process, the end of the second month, strong steam override occurs. (b) Temperature profile of the top layer of the five-spot pattern steamflood Case Y8-3F-2C-1G-1J. At the very early stage of this process, the end of the second month, strong steam override occurs.

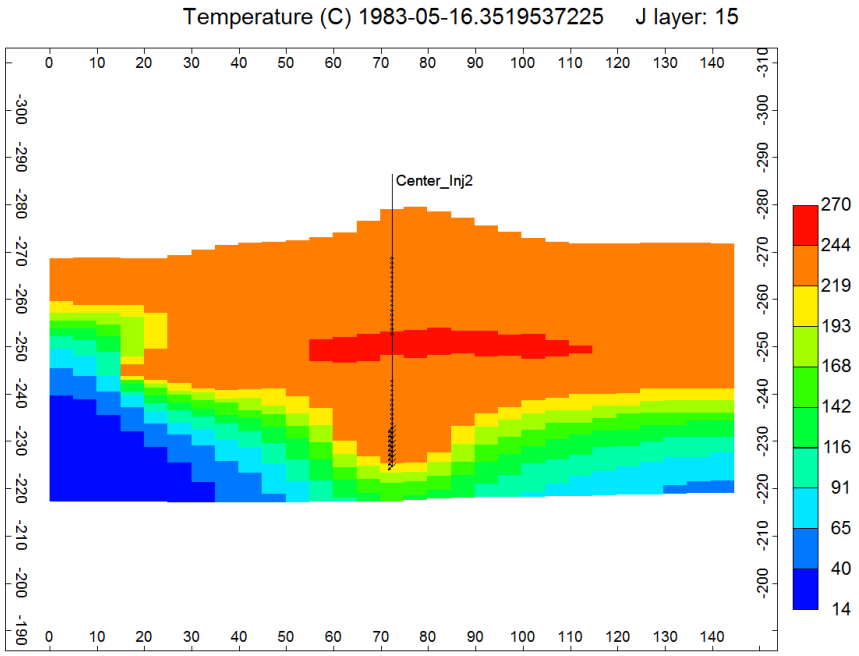

Figure 5.6.4. Temperature profile of the IK cross-section across the centre injector of the five-spot pattern steamflood Case Y8-3F-2C-1G-1J. At the end of the three-year production, the temperature at the bottom of the reservoir is much lower at than the top. A considerable portion of the bottom is still close to the initial reservoir temperature.

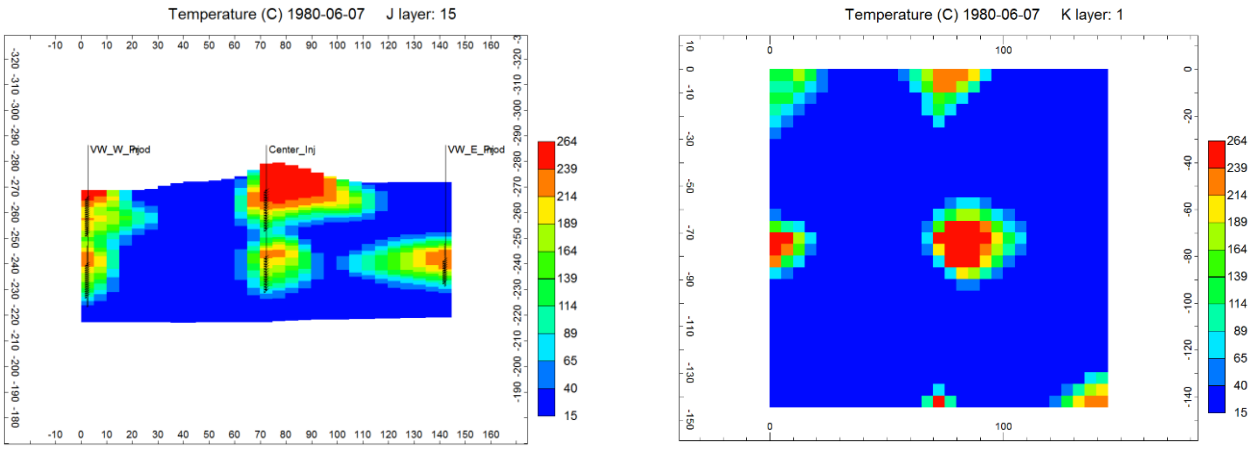

a **b**

Figure 5.6.5. (a) Temperature profile of the IK cross-section across the centre injector of the nine-spot pattern steamflood Case Y15-2A-1B-1D-1B. At the very early stage of this process, the end of the second month, strong steam override occurs. (b) Temperature profile of the top layer of the nine-spot pattern steamflood Case Y15-2A-1B-1D-1B. At the very early stage of this process, the end of the second month, strong steam override occurs.

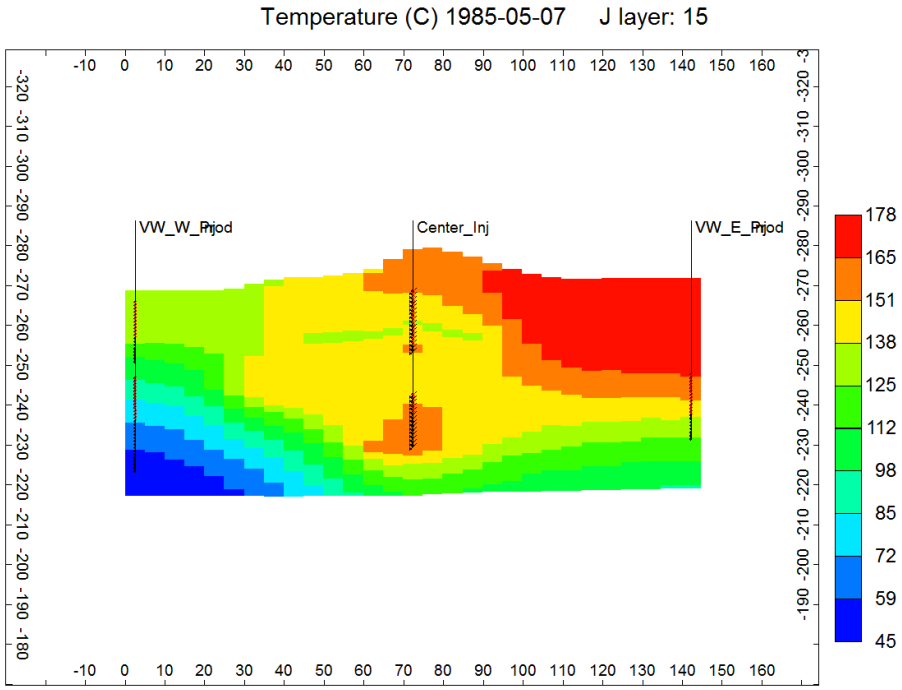

Figure 5.6.6. Temperature profile of the IK cross-section across the centre injector of the nine-spot pattern steamflood Case Y15-2A-1B-1D-1B. At the end of the five-year production, the temperature at the bottom of the reservoir is much lower than at the top. A considerable portion of the bottom is still close to the initial reservoir temperature.

5.7 Steamflood Residual Oil Saturation Analysis

According to the classical Marx-Langenheim and Mandl-Volek models, formation heating by steam injection is based on the concept of a constant steam temperature T_s into a porous medium at temperature T_r. Assuming a constant formation thickness h, as shown in Fig. 5.7.1, at a certain time t_1, the steam zone volume is V_{s1}; as steam injection continues, this volume is increased by ΔV_{s2} at time t_2, by ΔV_{s3} at time t_3, and so on. Between a certain time period, t_{n-1} to t_n, the steam zone increases by a volume ΔV_{sn}. According to the Marx-Langenheim and Mandl-Volek equations (Farouq Ali 2013), given the average formation thickness, the rock and fluid thermal properties, the incremental steam volume ΔV_{sn} formed during time t_{n-1} to t_n is given by

$$\Delta V_{sn}(t) = \frac{Q_i M_s h^2}{4k_{hob}M_{ob}(T_s - T_r)}\left[F_1(t_n) - F_1(t_{n-1})\right] \quad (t \le t_c)$$

$$\Delta V_{sn}(t) = \frac{Q_i M_s h^2}{4k_{hob}M_{ob}(T_s - T_r)}\left[F_3(t_n) - F_3(t_{n-1})\right] \quad (t > t_c)$$

where

$$F_1 = e^{t_D}\mathrm{erfc}\sqrt{t_D} + 2\sqrt{\frac{t_D}{\pi}} - 1,$$

$$F_3 = e^{t_D}\mathrm{erfc}\sqrt{t_D} + 2\sqrt{\frac{t_D}{\pi}} - 1 - \sqrt{\frac{t_D - t_{Dc}}{\pi}}\left\{\left[1 + \frac{f_{st}L_v}{c_w(T_s - T_r)}\right]^{-1} + \left(\frac{t_D - t_{Dc} - 3}{3}\right)e^{t_D}\mathrm{erfc}\sqrt{t_D} - \frac{t_D - t_{Dc}}{3\sqrt{\pi t_D}}\right\},$$

$$t_c = \frac{M_s^2 h^2 t_{Dc}}{4k_{hob}M_{ob}},$$

$$F_{2c} = e^{t_{Dc}}\mathrm{erfc}\sqrt{t_{Dc}} = \left[1 + \frac{f_{st}L_v}{c_w(T_s - T_r)}\right]^{-1},$$

and the average heat injection rate is $\bar{Q}_{i,n} = \bar{i}_{st,n}\left[h_w + f_{st}L_v - c_w T_r\right]$

.

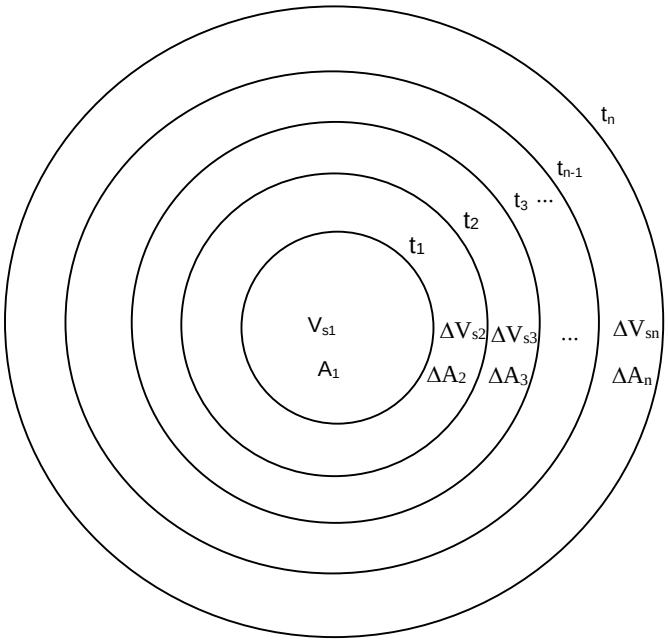

Figure 5.7.1. Plan view of a growing steam zone (the incremental areas do not have to be circular).

In this model, $k_{hob}= 1.7 \times 10^{-3}$ kW/m · ℃, $M_{ob} = 2350$ kJ/m³ · ℃, $M_s = 2347$kJ/m³ · ℃, T_r=15℃, steam quality f_{st}=0.7, T_s, h_w, and L_v are the steam saturation temperature, hot water enthalpy at steam saturation temperature, and the steam latent heat corresponding to the average steam injection pressure from time t_{n-1} to t_n, respectively, and $\bar{i}_{st,n}$ is the average steam injection rate during t_{n-1} to t_n.

Assuming that the oil production from the time interval t_{n-1} to t_n, $\Delta N_{p,n}$, comes from the corresponding incremental steam volume $\Delta V_{s,n}$, the residual oil saturation of $\Delta V_{s,n}$ at time t_n, $S_{orst,n}$ is given by

$$S_{orst,n} = S_{oi} - \frac{\Delta N_{p,n}}{\Delta V_{s,n} \cdot \emptyset}$$

$\Delta N_{p,n}$ can be obtained from simulation output as the difference of cumulative oil production at time t_{n-1} and t_n. Given the initial pore volume of 205,287 m^3, the initial oil in place of 140,848 m^3, the bulk volume of $(29 \times 5)^2 \times 53.35 = 1.12 \times 10^6\ m^3$, the average porosity and initial oil saturation of the model are calculated as $\phi = 18.3\%$ and S_{oi}=68.6%. Note that the S_{oi}=68.6% used here is the average porosity value in terms of the whole grid including top, middle and bottom water zones. Therefore it appears to be lower than that included in Table 2.2.1.

For example, during the last year, 1984-6-7 to 1985-6-7, of the five-year production vertical well injector-horizontal well producer steamflood Case, Moon 4-3C-1, oil production $\Delta N_{p,1985-6-7}$ is the difference of the simulation output cumulative oil production of these two days:

$\Delta N_{p,1985-6-7} = N_{p,1985-6-7} - N_{p,1984-6-7}$= 30,987.1-28,692.4=2,294.7 m^3

The average steam injection rate during this time is

$$\bar{i}_{st,n} = \frac{\text{Cumulative water injection}_{1985-6-7} - \text{Cumulative water injection}_{1984-6-7}}{365}$$

$$= 100\ \text{m}^3/\text{day} = 1.157\ \text{kg/s}$$

From the injection pressure curve (Fig. 5.5.7), the average injection pressure in this period is 800 kPa. Accordingly, $T_s = 170.4\ ℃$, $L_v = 2047\ \frac{kJ}{kg}$, and $h_w = 720.9\ \frac{kJ}{kg}$.

Substituting the simulation output and thermal properties into the Marx-Langenheim, Mandl-Volek equations, the steam zone formed during 1984-6-7 to 1985-6-7 is $\Delta V_{s,1985-6-7} =$ 183,847.4 m^3, and the residual oil saturation in this incremental steam zone is $S_{orst,1985-6-7} =$ 61.8%.

The same is done for $S_{orst,1984-6-7}$, $S_{orst,1983-6-7}$, $S_{orst,1982-6-7}$, and $S_{orst,1981-6-7}$ and the results are shown in Table 5.7.1

Table 5.7.1. Steam zone incremental volume and corresponding residual oil saturation in every year of the vertical well injector-horizontal well producer steamflood Case, Moon 4-3C-1. (Initial oil saturation 68.8%)

Time Interval	Steam Zone Increase (m^3)	Residual Oil Saturation in the Incremental Steam Zone (%)
1980-4-7 ~ 1981-6-7	350,272	38.3
1981-6-8 ~ 1982-6-7	197,605	57.8
1982-6-8 ~ 1983-6-7	184,322	61.2
1983-6-8 ~ 1984-6-7	184,796	61.5
1984-6-8 ~ 1985-6-7	183,847	61.8

Table 5.7.1 shows that as the production time gets longer, the residual oil saturation in the incremental steam volume increases. This indicates that at the steam front, there is actually hot water flow. The result of this analysis corresponds to the theory that as production time gets longer, the steamflood passes into a hot waterflood which is not as efficient as steam in displacing oil. However, note that Case Moon4-3C-1 is an element of the vertical well injector-horizontal well producer configuration in a microcosm of the Grosmont reservoir. At the field scale, hot waterflood may be delayed as there is heat support from the neighbouring wells.

5.8 Heat Production via Steam Production

The steam production rate can be estimated using the basic theory. Under reservoir conditions, steam is produced from the well with gas. Assuming that the gas production rate is V_g m^3/day and the steam rate is q_{st} kg/day, according to Dalton's partial pressure law,

$$\frac{q_{st}/M_{w,st}}{V_g/M_v} = \frac{p_s}{p_{bh}-p_s} \quad (5.8.1)$$

where $M_{w,st}$ is the molecular weight of steam, 18 g/mole; M_v is the molecular volume of gas, which is 22.4 L/mole assuming it is an ideal gas at standard conditions; p_{bh} is the producer bottomhole pressure available from the simulation output; p_s is the partial pressure of steam, which is steam saturation pressure at the producer bottomhole temperature, T_{bh}.

Given the producer bottomhole temperature T_{bh}, the steam saturation pressure p_s (MPa) and steam specific volume V_s (m^3/kg) can be calculated using the formulas below (Farouq Ali, 2013):

$T_{bh} = 179.81 p_s^{0.2376}$

$V_s = 0.19228 p_s^{-0.9588}$

Thus the volumetric steam production rate in volume is $q'_{st} = q_{st} \cdot V_s$.

For example, for the horizontal well CSS case, Q5-2J, on the first day of the fifth cycle, 1983-7-2, the gas production rate is 129 m^3/day, the average producer bottomhole temperature is 192 °C and the producer bottomhole pressure is 5,088 kPa. Substituting these values into the equations above, the steam production rate is calculated, q'_{st}=5 m^3/day. The same calculation is done for another five days of the same cycle. As we can see that at the beginning of production of a HWCSS cycle, steam production rate is high and takes a large proportion of the water production. This is because that water flashes into steam with the sudden pressure drop when the process is switched from soak to production (Table 5.8.1).

Table 5.8.1. Estimated steam production rate at different times of the fifth cycle of the horizontal well CSS Case Q5-2J.

Simulation Output				Estimation through Analytical Methods
Date	Water Production Rate (m^3/day)	Gas Production Rate (m^3/day)	Well Bottomhole Pressure (kPa)	Steam Production Rate (m^3/day)
1983-7-2	7.3	129.2	5,088.8	5.31
1983-8-5	176.2	19.0	3,279.5	1.23
1983-9-4	180.4	16.6	2,413.0	1.44
1983-11-3	184.3	9.6	1,603.7	1.38
1984-1-2	185.6	8.1	1,360.8	1.38

5.9 General Evaluation of the Simulated Processes and the Recommended Solution

Given the high fracture vertical permeability, steam override and oil gravity flow are the dominant phenomena for all processes simulated and described above. During any steam injection process for this formation, steam preferentially flows upwards and overrides the top of the formation members; the mobilized oil flows downward by gravity drainage. Therefore, a horizontal production well has the advantage of capturing more oil than a vertical well, which is evident from the comparison of the simulated vertical well CSS and horizontal well CSS (Section 5.2.3).

Because of the permeability contrast of the dolomite dominated matrix and the secondary porosity system (fracture and vugs) of the Grosmont carbonate reservoir, steam chamber does not form as well as it does during SAGD for oil sands. For this reason, SAGD does not have an advantage over HWCSS in capturing oil gravity flow, as discussed in Section5.3.5.

The heterogeneous carbonate formation properties and fracture network make the steam zone growth uneven in all processes. As a result, any process demanding a uniform steam zone, e.g.,

SAGD or seven-spot pattern steamfloods, may not achieve the optimal performance. Also, based on the simulation of horizontal well CSS, when steam is injected through a long horizontal well, steam continues to migrate to the region of high permeability cycle after cycle, so the steam zone is formed in the same drainage area. By contrast, a vertical injector has the flexibility of targeting any high oil saturation region regardless of the difference in local formation properties. This is why the pattern steamfloods generally have a large drainage area and large recovery factor. However, the high formation heterogeneity leads to early steam breakthrough in the vertical injector-vertical producer arrangements of pattern steamfloods.

An efficient steam injection process for this reservoir should allow for steam override, make use of the oil gravity flow, offer flexibility of injection well location to distribute steam more evenly, and avoid early steam breakthrough. The vertical injector-horizontal producer configuration proposed in this study combines the advantage of a vertical injector in expanding the drainage area against the formation heterogeneity and the advantage of a horizontal producer in capturing the oil from gravity flow. The horizontal well producer is placed offset from the vertical well injector so that the upward steam flow does not encounter the downward oil gravity flow in the same path. In the vertical injector-horizontal producer configuration, the horizontal producer is placed at the base of the oil-bearing intervals of formation member to capture the oil; the vertical injector provides the flexibility to target specific regions in this heterogeneous reservoir, thus achieving a more uniform steam zone, a larger drainage area and optimum steam utilization. For this reason, it shows a more uniform steam zone and a larger sweep area than the horizontal well CSS, leading to faster oil recovery, as discussed in Section 5.5.6. Therefore, even considering the possible optimization of the horizontal well CSS with flow control devices, the proposed VWinj-HWprod

steamflood shows more potential to be a robust solution for the Grosmont reservoir. Under the circumstance of the overwhelming upward steam flow, the horizontal producer placed near the base of the oil-bearing interval effectively delays steam breakthrough, which is an advantage over the conventional pattern steamfloods. Also, as described in Section 5.5.7 and 5.5.8, it is as productive as the conventional pattern steamflood but has higher thermal efficiency and its recovery performance is less affected by well distance.

Therefore, given this microcosm of Grosmont model which consists of the Grosmont C and D members and the discontinuous marl layer in between, with high vertical fracture permeability and severe petrophysical property heterogeneity, the vertical injector-horizontal producer steamflood is the recommended solution. Note that given the high initial oil viscosity, the horizontal producer of a VWinj-HWprod steamflood must be initially steam-stimulated to build communication with the vertical injector. There is flexibility in terms of the initial steam cycles before the VWinj-HWprod steamflood. The optimization methods used in this work aiming at tackling the steam override problem for the pattern steamfloods, closing upper perforations and reducing the steam injection rate at a proper time, also apply to the VWinj-HWprod steamflood to enhance the steam utilization and recovery performance. The other scenario is that the VWinj-HWprod steamflood can be used as a follow-up process of HWCSS. As mentioned in Sections 5.2.3, 5.2.2.5, and 5.3.5, HWCSS has advantage in capturing oil gravity flow but the drainage area is often limited to the more permeable area along the well. When the cycle oil production HWCSS shows decline, it may be the time to drill vertical well injector in the less depleted oil bearing zones and switch the process to the VWinj-HWprod steamflood. The cost of steam and wells and the total revenue of Case Moon4-3c-1, the VWinj-HWprod steamflood with two vertical well injector and one

horizontal well producer, was calculated. Based on the current market price, assuming the bitumen price of $50/bbl and gas price of $3/MScf, the cost of steam and wells is 34% to 42% of the total revenue.

5.10 CPU Time for the Simulations

Table 5.10.1 shows the CPU times for typical cases. CPU time is generally very long and gets longer with an increase in the number of wells and more complex saturation changes. As mentioned in Sections 5.2.2.3 and 5.3.4, Cases Q5-2-1 and SAGD-3 are simulated in the model with the fracture system removed; otherwise, they are identical to the horizontal well CSS Case Q5-2 and the SAGD Case SAGD, respectively. The dramatic CPU time decrease from simulations in the model with fractures to those in the model without fractures, i.e., from 960 hours for Case Q5-2 to 1 hour for Case Q5-2-1 and from 18 hours for Case SAGD to 1 hour for Case SAGD-3, shows the extremely large CPU time demanded by the dual porosity/dual permeability model compared with the single porosity model. Experiments were also done to downsize the model by combining adjacent layers. The result shows that by reducing the number of grid blocks by half, the CPU time can be reduced by 4 times. However, as the deviation between the simulation result from the downsized model and that from the original model was considered unacceptable, the downsized model was not used in this study.

Table 5.10.1. CPU time of selected simulation cases.

Process Type	Schematic	Case Number	CPU Time (Hours)
Single Vertical Well CSS	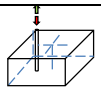	Q6	40
Single Horizontal Well CSS		Q5-2	960
Single Horizontal Well CSS		Q5	489
SAGD		SAGD	18
5-acre Five-spot Steamflood		Y8-3F-2C-1G-1J	2,432
4-acre Seven-spot Steamflood	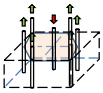	Y16-2I	1,839
5-acre Nine-spot Steamflood		Y15-2A-1B-1D-1B	2,000
Vertical Injector-Horizontal Producer Steamflood		Moon4-3c-1	136
Single Horizontal Well CSS (Without the Fracture System)		Q5-2-1	1
SAGD (Without the Fracture System)		SAGD-3	1

Chapter 6: CONCLUSIONS

This study is based on 40 numerical simulations (25 are reported here) and mathematical analysis of the results obtained for an element of the Grosmont formation. The model includes all of the major features of this reservoir, such as fractures, water zones, highly variable petrophysical properties, high bitumen viscosity, and a middle tight streak with discontinuity. Numerical simulations consisted of single well (vertical or horizontal) cyclic steam stimulation, steamflooding using five-spot, seven-spot, and nine-spot patterns, and unconventional steamflooding scheme using vertical injectors and a horizontal producer. The steam injection rate and perforation interval were varied in a few simulations to increase the recovery factor, and reduce the steam-oil ratio. Selected simulation results were analyzed using classical methods. The CPU time for each case was 10 to 100 ***days***, limiting the number of simulations.

The conclusions derived are presented in two groups: general conclusions for bitumen recovery from the Grosmont carbonate formation, and specific conclusions for the geological model used.

The following conclusions are general for steam injection in the Grosmont formation:

1. Given the very high oil viscosity (1 to $10x10^6$ cP at 15°C) and the low matrix permeability in the Grosmont formation, the presence of fractures is crucial for achieving a high enough steam injectivity and well productivity in spite of the initial cyclic steam stimulation of the producers, which is an integral part of any steam-based process. When fractures were removed in this study, steam injectivity decreased drastically.

2. As vertical and subvertical fractures are present, severe steam override may occur, and at the same time, oil production may be mostly by gravity flow. The chosen steam injection process must allow for these effects. The best arrangement for this situation is a combination of vertical injectors and a horizontal producer, with injection interval control.

3. Water sands may occur at the top, bottom, or middle of the formation, so well placement must minimize the migration of steam into the water zones, and also the flow of water into the producers. This can be partially achieved by opening and closing the perforations at appropriate times.

The following specific conclusions refer to the Grosmont model used in the simulation of steam injection processes. As noted in the discussion, the elemental model consists of the Grosmont C and D members with the discontinuous marl layer in between, with the high vertical fracture permeability and severe heterogeneity of petrophysical properties.

1. The high fracture vertical permeability leads to very early steam override, promoting gravity drainage of the oil into the producing wells. Early steam breakthrough occurs in pattern steamfloods (five-spot, seven-spot, and nine-spot), as a result of high fracture vertical permeability and high formation heterogeneity.

2. The combination of the extremely heterogeneous formation properties and complex fracture network leads to uneven steam zone growth and a limited drainage area, which adversely affected the recovery performance of the steam injection processes, including SAGD, seven-spot pattern steamflood and horizontal well CSS.

3. Compared to the conventional steam injection processes simulated, viz. cyclic steam stimulation (vertical or horizontal wells), SAGD, and steamflooding (using five-spot, seven-spot, and nine-spot patterns), the vertical injector-horizontal producer steamflood provides the opportunity to achieve the most uniform heating of the formation and maximum drainage area, to capture the oil gravity flow and to delay steam breakthrough.

4. The steam-oil ratio was high in most of the cases studied, even though the oil recovery was high. For the same cumulative steam injection volume, aiming at recovering the same portion of the formation away from the top water, the vertical well injector-horizontal well producer steamflood gave the same recovery performance (a steam-oil ratio of 7.0 m^3/m^3 and recovery of 18.0%), 21 months earlier than the horizontal well CSS.

5. Given any of the steamflooding schemes tested, the steam injection rate and the injection perforations as well as the production perforations can be modified to minimize the steam-oil ratio, as demonstrated in the three cases. Such optimization is important for the successful exploitation of the Grosmont resource.

6. A mathematical analysis of selected simulation results, including the derivation and application of the analytical one-sided heat loss equation, provided valuable insight into the recovery process and possible ways to improve the performance.

Chapter 7: RECOMMENDATIONS FOR FUTURE WORK

The following recommendations refer to a suitable geological model of the Grosmont reservoir, consisting of typical formation characteristics, such as fractures, tight zones, and water sands.

1. The pattern floods carried out in this work utilized geometrically symmetric five-spot, seven-spot, and nine-spot patterns, with the injection well at the centre. Simulations could be carried out with an off-centre injection well, where the well is located to compensate for the local heterogeneities. The injection well could even be deviated.

2. Location of the injection and production intervals, defined by perforations and their modification in time, is an important part of performance optimization. Many more scenarios can be developed for this purpose, especially in the horizontal producers.

3. Steam override, steam production, migration into water zones, gravity flow of bitumen, and flow dynamics in the horizontal well are amenable to analytical treatment, and could be an extension of this work.

References

Alvarez, J. 2014. Re-examination of Previous AOSTRA Pilot Tests: Grosmont Formation Experience. Presentation at the SPE Unlocking Alberta's Carbonate Reservoirs Workshop, Calgary, September 16-17.

Buschkuehle, B. E., Hein, F. J., and Grobe, M. 2007. An Overview of the Geology of the Upper Devonian Grosmont Carbonate Bitumen Deposit, Northern Alberta, Canada. Natural Resources Research, 16 (1): 3-15.

Buschkuehle, B. E. and Grobe, M. Geology of the Upper Devonian Grosmont Carbonate Bitumen Deposit, Northern Alberta, Canada. Alberta Energy & Utilities Board, Alberta Geological Survey.

Cimolai, M.P., Solanki, S. C., and Edmunds, N. R. 2010. Passive Reservoir Heating for Improved Bitumen Recovery. Journal of Canadian Petroleum Technology. 49 (11) 30-42.

Clark, H. and Jimenez, T. 2014. Summary of Shell Grosmont Pilot. Presentation at the SPE Unlocking Alberta's Carbonate Reservoirs Workshop, Calgary, September 16-17.

Edmunds, N., Barrett, K., Solanki, S., Cimolai, and M., Wong, A. 2009. Prospects for Commercial Bitumen Recovery from the Grosmont Carbonate, Alberta. Journal of Canadian Petroleum Technology, 48 (9): 26-32.

Ezeuko, C.C., and Gates, I.D. 2013. Simulation Analysis of Steam-Based EOR using MultiObjects Grosmont Models. Paper SPE 165484 presented at the SPE Heavy Oil Conference Canada, Calgary, 11-13 June.

Ezeuko, C.C., Kallos M.S., and Gates, I.D. 2013. Object Characterization and Simulation of Thermal Recovery from Karstified, Brecciated and Fractured Bitumen Carbonate Reservoirs. Paper IPTC 16860 presented at the International Petroleum Technology Conference, Beijing, 26-28 March.

Ezeuko, C.C., Wang, J., Kallos, M. S., and Gates, I. D. 2012. Towards the Development of Bitumen Carbonates: An Integrated Analysis of Grosmont Steam Pilots. Oil & Gas Science and Technology.

Farouq Ali, S. M. 2013. Practical Heavy Oil Recovery.

Hosseininejad, M., Yang, D., and MacDonald, J. 2014. Thermal Recovery of Bitumen From the Grosmont Carbonate Formation-Part 1: The Saleski Pilot. Journal of Canadian Petroleum Technology.

Husky Oil Operations Limited, 2013, Application for Husky Oil Operations Limited Saleski Thermal Experimental Project, Alberta Energy Regulator.

Jiang, Q., Yuan, J., Russel-Houston, J., Thornton, B., and Squires, A. 2010. Evaluation of Recovery Technologies for the Grosmont Carbonate Reservoirs. Journal of Canadian Petroleum Technology, 49 (5): 56-64.

Machel, H. G., Borrero, M. L., Dembicki, E., Huebscher, H., Ping, L., and Zhao, Y. 2012. The Grosmont: a complex dolomitized, fractured and karstified heavy oil reservoir in a Devonian carbonate-evaporite platform. GeoConvention.

Machel, H. G., Borrero, M. L., Dembicki, E., Huebscher, H., Ping, L., and Zhao, Y. 2012. Advances in Carbonate Exploration and Recovery Analysis. 370: 49-81.

Marx, J.W., and Langenheim, R.H. 1959. Reservoir Heating by Hot Fluid Injection. *Petroleum Transactions,* **216**:312-365

Novak, J., Edmunds, N., and Cimolai, M. 2007. A History Match of CSS Recovery in the Grosmont. Paper 2007-154 presented at the Petroleum Society's 8th Canadian International Petroleum Conference (58th Annual Technical Meeting), Calgary, 12–14, June.

Qi, J. and Yuan, J. 2013. History Matching Grosmont C Carbonate Thermal Production Performance. Paper SPE 16560 presented at the SPE Heavy Oil Conference Canada, Calgary, 11-13 June.

Qin, K., 2014. 40 Months of the Saleski Pilot History: Observations and Evolving Understanding of Thermal Operations in the Grosmont Part, Calgary, 16-17 September.

Russel-Houston J., and Gray, K. 2014. Paleokarst in the Grosmont Formation and reservoir implications, Saleski, Alberta, Canada. Interpretation, 2 (3): 29-50.

Yang, D., Hosseininejad, M., and Brand, S. 2014. Thermal Recovery of Bitumen From the Grosmont Carbonate Formation-Part 2: Pilot Interpretation and Development Strategy. Journal of Canadian Petroleum Technology.

Yuan, J., Jiang, Q., Russel-Houston, J., Thornton, B. and Putnam, P. 2010. Evolving Recovery Technologies Directed Towards Commercial Development of the Grosmont Carbonate Reservoirs. Paper SPE 137941 presented at the Canadian Unconventional Resources & International Petroleum Conferences, Calgary, 19-21 October.

APPENDIX A

Derivation for the Equation of Heat Loss from only the Formation Top (or only the Formation Bottom) during Steamflood

This derivation of the heat loss equation considers heat loss to only the overburden of the formation during steamflood. The same derivation and equation apply to the heat loss from only the underburden of the formation. The original Marx-Langenheim derivation is not given in any paper; therefore, this derivation of a special case is given in full detail.

Formation heating by steam injection into a porous medium, in this case, is based upon the concept of a constant temperature equal to the steam temperature T_s into a rock at temperature T_r. At some time t_1, the heated area (assuming a constant formation thickness, h m) is A_1. As steam injection is continued, this area increases by an amount ΔA_2 at time t_2, by ΔA_3 at time t_3, and so on. As a result, the original area A_1 loses heat for time 0 to t_3, and the incremental area ΔA_3 loses heat from time t_2 to t_3.

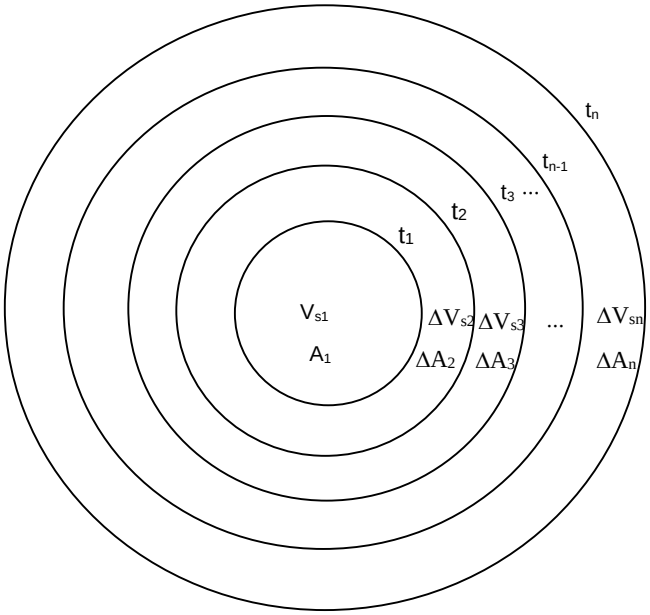

Figure A.1 Plan view of a growing steam zone.

It is, thus, clear that the total heat loss to the formations above and below must take into account this difference in the time periods over which heat loss from the various incremental areas occurs. Consider some incremental area ΔA, which is created at time u. If we are computing heat loss till the end of the time t, then the total heat loss from all such areas will be given the integral

$$1 \cdot \int_0^{A(t)} f\left(t-u\right) \Delta A \tag{A1}$$

where f(t) is the function giving the heat loss per unit time per unit area, A(t) is the total area heated at the end of time t, and the multiplier 1 accounts for the fact that heat loss occurs from only the formation top (or only the formation bottom).

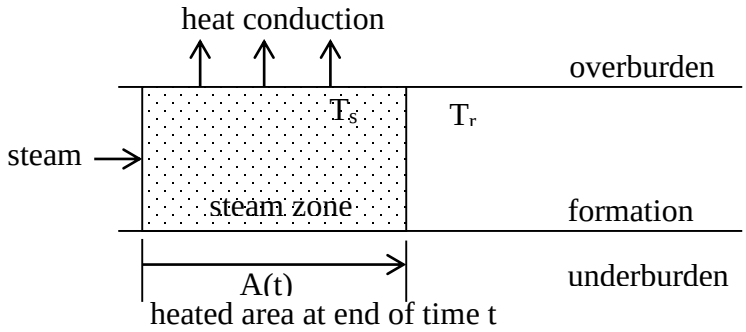

Figure A.2 Heat loss to the overburden in a cross-section of a growing steam zone.

Consider that the flow of heat into the overburden (or underburden) is strictly linear in the vertical direction. Imagine the formation top maintained at the steam zone temperature T_s, conducting heat into the infinite medium above.

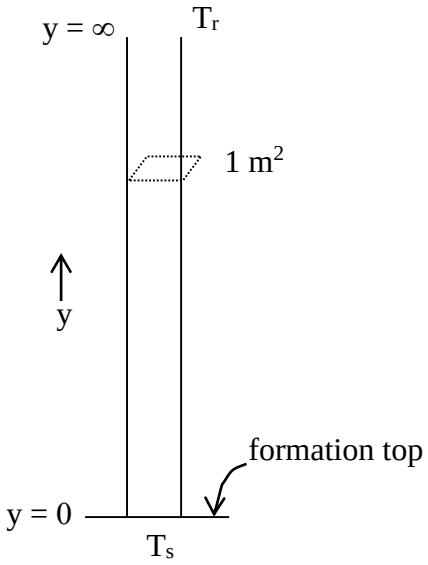

Figure A.3 Schematics of temperature distribution in the 1D linear heat conduction

The distance between a certain point in the overburden to the formation top is y m. Take the coordinate y=0 at the formation top. At the other end, take $y=\infty$, and imagine that this end is constantly maintained at the original formation temperature of T_r. Let the cross- sectional area of

this vertical slice be 1 m^2. Then the conductive heat transport into this semi-infinite medium is described by the equation

$$\frac{\partial^2 T}{\partial y^2} = \frac{1}{\alpha}\frac{\partial T}{\partial t} \tag{A2}$$

where T is temperature in °C,

y is in m,

t is in s,

and α is thermal diffusivity of the overburden (or underburden), in m^2/s.

$$\alpha = \frac{k_{hob}}{M_{ob}}$$

where k_{hob} is the thermal conductivity of the overburden (or underberden) in kW/m·°C and M_{ob} is the volumetric heat capacity of the overburden (or underberden) in $kJ/m^3 \cdot °C$.

The desired solution will have the form

$$T = T(y,t). \tag{A3}$$

The boundary conditions are $T = T(0,t) = T_s, T = T(\infty,t) = T_r.$ (A4)

The initial condition is $T = T(y,0) = T_r \qquad 0 \le y < \infty.$ (A5)

To solve the above problem, first take the Laplace transform of Eq. (A2) with respect to t, thus obtaining an ordinary differential equation containing a single independent variable y:

$$s\bar{T}(y,s) - T(y,0) = \alpha \frac{d^2\bar{T}(y,s)}{dy^2} \tag{A6}$$

where $\bar{T}(y,s)$ is the transformed temperature. We shall write it as $\bar{T}$ for brevity.

Now, $T(y,0)=T_r$ from Eq. (A5), so that Equation (A6) becomes:

$$\frac{d^2\bar{T}}{dy^2} - \frac{s}{\alpha}\bar{T} = -\frac{T_r}{\alpha} \tag{A7}$$

This is an ordinary differential equation, the auxiliary equation for which is

$$m^2 - \frac{s}{\alpha} = 0,$$

which gives $m_1 = \sqrt{\frac{s}{\alpha}}$ and $m_2 = -\sqrt{\frac{s}{\alpha}}$ as the roots.

Thus the complimentary function becomes

$$\bar{T} = C_1 e^{y\sqrt{\frac{s}{\alpha}}} + C_2 e^{-y\sqrt{\frac{s}{\alpha}}}, \tag{A8}$$

where C_1 and C_2 are arbitrary constants.

To obtain the particular integral, consider a function such as

$$\bar{T} = Ay + B. \tag{A9}$$

This must satisfy the differential Equation (A7).

Substitute Eq. (A9) into Eq. (A7):

$$0 - \frac{s}{\alpha}(Ay + B) = -\frac{T_r}{\alpha}. \tag{A10}$$

Equate like powers of y,

$$-\frac{s}{\alpha}A = 0, \qquad -\frac{s}{\alpha}B = -\frac{T_r}{\alpha}$$

where $A=0$ and $B = \frac{T_r}{s}$.

Thus the general solution of Eq. (A7) becomes

$$\bar{T}(y,s) = C_1 e^{y\sqrt{\frac{s}{\alpha}}} + C_2 e^{-y\sqrt{\frac{s}{\alpha}}} + \frac{T_r}{s}. \tag{A11}$$

Taking the transforms of the boundary conditions Eq. (A3) and (A4), we have

$$\bar{T}(0,t)=\frac{T_s}{s}, \quad \bar{T}(\infty,t)=\frac{T_r}{s}. \tag{A12}$$

These can be substituted in Eq. (A11) to obtain the constants C_1 and C_2, so that C_1 = 0 and $C_2=\frac{T_s-T_r}{s}$. The solution Eq. (A11) then becomes

$$\bar{T}(y,s)=\frac{T_r}{s}+\frac{T_s-T_r}{s}e^{-y\sqrt{\frac{s}{\alpha}}}. \tag{A13}$$

Now, in order to get back to t, take the inverse transform, using the Laplace transform table

$$\mathcal{L}(C)=\frac{C}{s}, \text{ and } \mathcal{L}\left(erfc\frac{k}{2\sqrt{t}}\right)=\frac{1}{s}e^{-k\sqrt{s}}.$$

Therefore, Eq. (A13) becomes

$$T(y,t)=T_r+(T_s-T_r)erfc\frac{y}{2\sqrt{\alpha t}}, \tag{A14}$$

where *erfc* is the complementary error function, given by

$$erfc(x)=1-erf(x)=1-\frac{2}{\sqrt{\pi}}\int_0^x e^{-t^2}dt \tag{A15}$$

Substituting Eq. (A15) in Eq. (A14), a temperature distribution equation of the 1D linear heat transfer model is

$$T(y,t)=T_s-(T_s-T_r)erf\frac{y}{2\sqrt{\alpha t}}. \tag{A16}$$

To evaluate the heat loss rate per unit area at this surface, use Fourier's equation of heat conduction:

$$f(t)=-k_{hob}\left.\frac{\partial T}{\partial y}\right|_{y=0} \tag{A17}$$

From Eq. (A16),

$$\frac{\partial T}{\partial y} = -\frac{2}{\sqrt{\pi}} \frac{T_s - T_r}{2\sqrt{\alpha t}} e^{-\frac{y^2}{4\alpha t}} \tag{A18}$$

Using $erfc(x) = 1 - erf(x) = 1 - \frac{2}{\sqrt{\pi}} \int_0^x e^{-t^2} dt$ and

putting y=0 in Eq. (A18), we have from Eq. (A17):

$$f(t) = -k_{hob} \left. \frac{\partial T}{\partial y} \right|_{y=0} = \frac{k_{hob}(T_s - T_r)}{\sqrt{\pi \alpha t}}. \tag{A19}$$

Referring to Eq. (A1), the heat balance on an incremental per unit time basis is: At time t, (Heat injected per unit time)=(Heat lost per unit time)+(Heat used to heat the rock per unit time) or

$$Q_i = 1 \cdot \int_0^{A(t)} f(t-u) dA + M_s h (T_s - T_r) \frac{dA}{dt} \tag{A20}$$

where Q_i is the heat injection rate in kJ/s, M_s is the formation heat capacity in kJ/$m^3 \cdot$℃, and h is the formation thickness in m. The multiplier 1 accounts for the fact that heat loss occurs from only the formation top (or formation bottom). Substituting for $f(t)$, we have

$$Q_i = \frac{k_{hob}(T_s - T_r)}{\sqrt{\pi \alpha}} \int_0^t \frac{1}{\sqrt{t-u}} \frac{dA}{du} du + M_s h (T_s - T_r) \frac{dA}{dt} \tag{A21}$$

where the variable of integration is changed from A to u, i.e., time.

Letting $C_1 = \frac{k_{hob}(T_s - T_r)}{\sqrt{\pi \alpha}}$ and $C_2 = M_s h (T_s - T_r)$, Eq. (A21) becomes

$$Q_i = C_1 \int_0^t \frac{1}{\sqrt{t-u}} \frac{dA}{du} du + C_2 \frac{dA}{dt}. \tag{A22}$$

Recalling that

$$\mathcal{L}\left\{ \int_0^t f(u) g(t-u) du \right\} = \bar{f}(s) . \bar{g}(s)$$

and considering that $f(u) \to \frac{dA}{du}$ and $g(u) \to \frac{1}{\sqrt{u}}$, take the Laplace transform of Eq. (A22),

$$\frac{Q_i}{s} = C_1 \cdot \mathcal{L}\left(\frac{1}{\sqrt{t}}\right) \cdot \mathcal{L}\left(\frac{dA}{dt}\right) + C_2 \cdot \mathcal{L}\left(\frac{dA}{dt}\right)$$

$$= C_1\sqrt{\frac{\pi}{s}}.\left(s\bar{A}(s) - A(0)\right) + C_2\left(s\bar{A}(s) - A(0)\right)$$

where $\bar{A}(s)$ is the Laplace transform of $\bar{A}(t)$. Take the heated area $A(t) = 0$ at *t*=0, and simplify:

$$\bar{A}(s) = \frac{Q_i}{\sqrt{\pi}C_1 s^{\frac{3}{2}} + C_2 s^2} = Q_i \cdot \frac{C_2}{\pi C_1^2} \cdot \frac{\left(\frac{\sqrt{\pi}C_1}{C_2}\right)^2 - 0^2}{\sqrt{s}\left(s - 0^2\right)\left(\frac{C_1\sqrt{\pi}}{C_2} + \sqrt{s}\right)}, \tag{A23}$$

which can be inverted using the Laplace transform table:

$$\mathcal{L}\left[\frac{b^2 - a^2}{\sqrt{s}\left(s - a^2\right)\left(\sqrt{s} + b\right)}\right] = e^{a^2 t}\left[\frac{b}{a} erf\left(a\sqrt{t}\right) - 1\right] + e^{b^2 t}\left[erfc\ b\sqrt{t}\right]$$

where *a*=0 and $b = \frac{\sqrt{\pi}C_1}{C_2}$ for expression (A24).

In order to evaluate the inverse transform, the limit of the right-hand side for *a*=0 must be obtained.

Using an asymptotic expansion for *erf*, we have

$$erf\left(a\sqrt{t}\right) = \frac{2}{\sqrt{\pi}} \sum_{n=0}^{\infty} (-1)^n \frac{a^{2n+1} t^{\frac{2n+1}{2}}}{(2n+1)n!}$$

which gives

$$\lim_{a \to 0} \frac{1}{a} erf\left(a\sqrt{t}\right) = \lim_{a \to 0} \frac{2}{\sqrt{\pi}}\left[\sqrt{t} - \text{terms containing } a\right] \tag{A25}$$

Thus the inverse transform of $\bar{A}(s)$ becomes

$$A(t) = Q_i \cdot \frac{C_2}{\pi C_1^2}\left\{\left[\frac{\sqrt{\pi}C_1}{C_2}\cdot\frac{2\sqrt{t}}{\sqrt{\pi}} - 1\right] + e^{\left(\frac{\sqrt{\pi}C_1}{C_2}\right)^2 t} erfc\,\frac{\sqrt{\pi}C_1}{C_2}\sqrt{t}\right\}. \quad \text{(A26)}$$

Substituting for C_1 and C_2 and simplifying, we have the final expression:

$$A(t) = \frac{Q_i h M_s}{k_{hob} M_{ob}\left(T_s - T_r\right)}\left[e^{t_D} erfc\sqrt{t_D} + \frac{2\sqrt{t_D}}{\sqrt{\pi}} - 1\right], \quad \text{(A27)}$$

Multiplying Eq. (27) by h, the steam zone volume considering one-sided heat loss becomes:

$$V_s(t) = \frac{Q_i M_s h^2}{k_{hob} M_{ob}\left(T_s - T_r\right)}\left[e^{t_D} erfc\sqrt{t_D} + \frac{2\sqrt{t_D}}{\sqrt{\pi}} - 1\right] \quad \text{(A28)}$$

where $t_D = \frac{k_{hob} M_{ob} t}{M_s{}^2 h^2}$ and $V_s(t)$ is the steam zone formed at time t.

The ratio of the cumulative heat loss to the cumulative heat injected at time t, $Q_{loss,1\text{-}ML}$, is

$$Q_{loss,1\text{-}ML} = \frac{\text{Cumulative Heat Injected} - \text{Heat Accumulated}}{\text{Cumulative Heat Injected}} = \frac{Q_i \cdot t - V_s M_s\left(T_s - T_r\right)}{Q_i \cdot t} = 1 - \frac{F_1}{t_D} \quad \text{(A29)}$$

where $F_1 = e^{t_D} erfc\sqrt{t_D} + 2\sqrt{\frac{t_D}{\pi}} - 1$.

(The original Marx-Langenheim equation for a steam zone volume considering simultaneous heat loss from the formation top and bottom is

$$V_s(t) = \frac{Q_i M_s h^2}{4 k_{hob} M_{ob}\left(T_s - T_r\right)}\left[e^{t_D} erfc\sqrt{t_D} + \frac{2\sqrt{t_D}}{\sqrt{\pi}} - 1\right]$$, where $t_D = \frac{4 k_{hob} M_{ob} t}{M_s{}^2 h^2}$.)